2008-2009 Design and Fabrication of a SAE Baja Race Vehicle

A Major Qualifying Project Report
Submitted to the Faculty of
WORCESTER POLYTECHNIC INSTITUTE
In partial fulfillment of the requirements for the
Degree of Bachelor of Science

By:

_____
Derek Britton

_____
Jessy Cusack

_____
Alex Forti

_____
Patrick Goodrich

_____
Zachary Lagadinos

_____
Benjamin Lessard

_____
Wayne Partington

_____
Ethan Wyman

Date: April 29,2009

_____
Kenneth Stafford, Advisor

_____
James Van De Ven, Advisor

_____
Torbjorn Bergstrom, Advisor

Table of Contents

List of Figures

List of Tables

Introduction

The Baja Collegiate Design Series is a competition run annually by the Society of Automotive Engineers. The Baja competition was introduced in 1976 and only ten teams competed, WPI being one of them. After 1976 WPI did not enter again until 2007. The Baja series has grown, over time, to holding three regional competitions in North America and other around the world. In the 2009 competition, WPI will compete in Wisconsin against 120 teams from all around the world. This competition will include a maneuverability test, an acceleration test, a mud bog, a hitch pull, and an endurance race. These races and tests include a harsh terrain that the car has to endure for four hours.

In addition to holding up to the harsh off-road terrain, the car has to be designed to be lightweight and inexpensive. The car is not only judged on the performance or completion of the race, but there is a cost report as well as an engineering design report. The car has to conform to all of the rules stated in the SAE's rulebook. The reason for the lightweight constraint is the limited power produced by the engine that is required by the rules. Briggs and Stratton sponsors the competition and each team receives the same ten horsepower engine. This field-leveling engine is what drives most of the design specifications.

The Baja Collegiate Design Series objective follows the curriculum for a great Major Qualifying Project. Its purpose is to bring students into a real world engineering scenario and have these students work in teams to obtain funding, design, fabricate, test, promote, and compete in the tests and races against other teams of students, all the while staying within the strict rules. The project has driven us all to take what we have learned in the classrooms and apply it to the project that we chose as our MQP. Throughout the MQP many challenges arose; managing our time, budgeting, managing three teams, relationships with suppliers, and asking for further guidance from other students and professors were among the many that we encountered.

The 2007 team was very successful for the first year back. They took home Rookie of the Year and placed high in the design and endurance events. This is why we have taken in to account the amount of analysis they did and have incorporated some of their successful designs into our car. The work on the 2009 WPI SAE Baja Vehicle was a completely new car intended to participate in the last competition for the 2009 season. The new design incorporates some new

ideas that have never been tried for a WPI team and some that haven't been seen at a competition. With extensive research in these innovative ideas, and through testing after the fabrication and assembly, we will be confident to accomplish our goal of completing and placing well in the endurance race.

Design Goals

When starting this project, there were certain goals that were set. These goals were set based on SAE Baja Competition rules, obstacles seen throughout the course, pre-build testing, successful past iterations, and intuition. Below is a table of the design parameters of this year's Baja vehicle.

Wheelbase:	64"
Track Width:	60", 58" (Front, Rear)
Suspension Travel:	7" up, 5"down F&R
Ground Clearance:	12"
Weight:	350
Chassis:	Space Frame
Wheels/Tires:	Custom 17" Aluminum Rims, 25" Motocross Type Tires
Drive train:	Two Stage Chain and Sprocket Reduction
Tubing:	Heat Treated AISI 4130
Front Suspension Type:	Unequal Length Double A-arm
Rear Suspension Type:	Independent Links with Stressed Axle
Front Steering:	Camber Inducing Front Knuckles

Table 1: Design Parameter Table

The dimensions of the chassis and suspension sizes have outside parameters set by the rules. In Section 20.2.1 Maximum Vehicle Dimensions it states "Width: 162 cm (64 inches) at the widest point with the wheels pointing forward at static ride height." Using this as a maximum point along with driver measurements, drivetrain fitment, overall vehicle size, and considerations from the 2007 vehicle, the decisions for the wheelbase goal and the track width were made. The track width is offset front to rear in order to increase the chance of breaking the rear end loose while cornering to increase maneuverability.

The suspension travel of 7 inches of up travel and 5 inches of droop from ride height was used because of considerations in the 2007 vehicle as well as ground clearance and track width parameters. Looking at the course at Wisconsin as well as looking at common obstacles in any off-road application we decided to put the ride height at twelve inches. This will give us sufficient height to overcome any common obstacle seen in an off-road scenario.

In the competition, the motor is a large limiting factor because of the lack of power output. Taking this into account, the chassis was designed to be as lightweight as possible while maintaining rigidity when experiencing large stresses. The first goal set for the chassis was weight. To decide our goal we looked at the 2007 vehicle and decided what we could do to lighten the chassis. It was decided that we could bring the car down to 350 pounds. The next goal was what type of chassis would achieve this lightweight. Originally, the thought was that we were able to build a monocoque chassis using carbon fiber body paneling. Through analysis of the feasibility of a chassis such as this, we decided that a space frame, tubular build would be a more desirable chassis. Analysis was also done to ensure that the use of AISI 4130 tube steel would be sufficient.

Examination of media from other teams and from decisions made in the 2007 vehicle it was decided that an A-arm link suspension would be best for the front. Through discussions on advantages and disadvantages of different types of rear suspensions during team meetings, it was decided that a similar double A-arm rear suspension would be made. One of the designs of our car that sets us apart is that our rear suspension has no separate lower control arm because the rear drive axle is used as the rear control arm. This was decided to lighten the car and raise the ground clearance in the rear.

High ride heights and the camber induced steering drove the selection of the motocross wheels and tires. Using tires that are the size of motocross tires allows the ride height to be twelve inches at the center of the car as well as along the entire lower control arms in the front. The tires also are designed to corner on edge instead of vertically. This is taken care of by the design of the knuckle which, in the design goals, was set to camber the tire as the driver turned the steering wheel.

Chassis

This section details the design features of the vehicle's chassis. The chassis serves many critical functions that include linking the powertrain, control, and suspension systems together. The driver must also be comfortable in order to operate the vehicle effectively, thus driver ergonomics and safety take precedence. Mounting points and the overall frame geometry are crucial design considerations that affect desired characteristics such as the weight distribution and suspension operation. The chassis must also be resilient enough to endure all of the loads imposed upon it yet maintain a lightweight.

The team used the previously designed chassis as a knowledge base and benchmark for many of the design considerations this year and thus much of the material property data and design processes were referenced. This was necessary because of a severe lack of materials testing data available for AISI4130 as well as to effectively continue the iterative process of SAE Baja vehicle design. All of the previously employed design considerations and features from 2007 were thoroughly researched and reviewed against available competition data, experience, and newly publish test data that were not present during that initial design period. Because of these efforts, the team made many improvements and while the chassis this year is a completely original design, many tried and true elements were carried through in the design process thus increasing the overall vehicle quality and likelihood for success in SAE Baja competitions.

Ergonomics

One of the major design criterium that was used in the design of the chassis is the idea of driver ergonomics. Ergonomics is the study of how to layout and design the driver controls and safety features of the car according to the needs of the driver in order to optimize human well being and overall system performance in a given situation. For the application of Baja, it was necessary to create a driver envelope that would not only fit the planned drivers, but allow comfort, safety, and stability to the driver for a period of time of up to 2 hours. This time period was chosen so that one driver could complete at least half of the endurance competition without becoming tired or uncomfortable, while still remaining safely within the vehicle. The ideal driver that has been determined for this car is a person roughly 6 feet tall and weighing around 165 pounds. This driver's envelope is the cornerstone of our design and answers many of the questions that the group had about the design of the vehicle. Some of the major ergonomic

factors that were taken into consideration were the seat location and inclination, the location of the steering wheel, the design of the foot box area so that the driver will be able to properly operate the vehicle in all driving scenarios, and most importantly to comply with all the rules and regulations that were set forth in the 2009 Baja SAE competition rulebook.

To allow for proper movement of the drivers feet to control the gas and brake pedal, the foot box was designed to be as small as possible while allowing the driver the proper amount of space to operate the controls safely. In an investigation of the 95^{th} percentile man, it was found that the average man with shoes on has a foot width of roughly 4.5 inches. Because of these parameters, the final dimensions of the foot box were chosen to be 7 inches wide at the bottom and left relatively open at the top to allow each of our competition drivers to drive comfortably as well as allowing our other drivers to safely fit in the car for testing. The size and shape of the foot box also allowed for an optimum placement of the brake pedal and assembly low and between the lower frame members maintaining a low center of gravity. This was performed by a plate that integrated the brake pedal, master cylinders, as well as the gas pedal. By having the brake pedal and gas pedal integrated and properly spaced, it allows the driver of the car to operate the pedals by the use of one or both feet, depending on the preference of the driver. The brake pedal and assembly was also extensively designed in order to maximize driver efficiency in a normal as well as panic braking scenario.

The next area of the driver envelope that was investigated was the location of the steering wheel within the cockpit. The location of the steering wheel must be within a comfortable distance of the driver's chest to prevent either driver interference or overextending of the arms. If the driver's arms are over extended, the muscles in the arms will tire more rapidly as well as decreasing the amount of force that the driver can put into the wheel, which could lead to problems in an emergency situation. However, if the wheel is placed too close to the driver then the driver may not be able to exit the car within the required time of five seconds, even with the addition of a quick release steering wheel. Through a great deal of ergonomic research and physical testing, it was determined that the ideal location would be approximately 19.5 inches forward from the bottom of the rear roll hoop and 20 inches up from the lower frame members. This location will give the driver sufficient advantage to apply force to the wheel as well as allowing space for the driver to exit. Another rule that must be taken into account when designing the steering system is that the driver's wrists are attached to the steering wheel with

safety straps. This has a major influence on the type of mechanism that is used to relay driver input to the steering by limiting the angle that the wheel can be turned. If the wheel must be turned more than 90 degrees to reach the lock on the steering mechanism, and the driver is unable to adjust their hands, than this will create an extremely uncomfortable angle as well as increase the possibility of injury should an accident happen at full lock.

The final ergonomic parameter that was considered was the location and inclination of the driver's seat. The seat is crucial to supplying enough support to the driver's back to allow him to stay upright with a clear view of the track ahead, to apply the proper forces to the gas and brake pedals, and support the shift in the driver's weight while cornering or landing from a jump. To properly determine the inclination of the seat a great deal of research was done both online and by a trial and error approach with many members of the team being tested. In the search that was conducted electronically, the typical answer was anywhere from 10-20 degrees was the standard used in the automobile industry with a great deal of emphasis on adjustability being a very important feature for driver comfort. With this basic information, a physical test was conducted with a few members of the team and it was found that roughly 20 degrees of inclination was comfortable for those tested and was chosen. In addition to the seat back and inclination, aluminum bolsters are necessary in order to deal with the cornering forces that will be seen during the operation of the vehicle.

Although driver comfort sometimes is overstepped or thought of last, if we are to meet our goal of performing well and completing the endurance race in good standing, than ergonomics must be considered. Good ergonomics will allow the driver to drive quickly and comfortably avoiding unnecessary stoppage throughout the endurance race.

Seat

In designing the chassis, a major consideration was the size, shape, location, and inclination of the seat. Once the seat envelope was determined, the design of the seat began. In the previous car, an aluminum seat was used. This seat was chosen by the previous team for many reasons such as size, cost, and time of manufacturing. After looking over the chassis and applying our design objectives, it was found that the seat could be a possible place where a significant amount of weight could be lost. The first design that was considered was a basic aluminum seat much like the seat that was used in the previous car. This design was proven to

be strong and well suited to the application. In an examination of the design for this year's seat, it was found that the aluminum design was much too heavy for the car at 10.25 lbs. After this discovery was made, the next option that was considered was an alternate, lightweight material.

Roughly the same design was considered using carbon fiber in an attempt to reduce the weight of the seat. This design, while successful in reducing the weight and handling any and all loads, dramatically increased the cost and manufacturing time of the seat. The third and final design that was considered and ultimately chosen was the idea of a sling seat. A sling seat is very much like a hammock in the essence that it is made of a cloth material and is slung between two preexisting chassis members, so no other members need to be added. For our application the seat will be created from 3 pieces of cloth that will be stitched together and then tensioned with four seatbelt style cinch straps attached to preexisting chassis members. This design will increase the versatility and comfort of the seat while simultaneously reducing the weight. The cloth portion of the seat must be made out of a strong, yet lightweight material that will be able to handle the most extreme loading cases such as cornering and most prominently a landing scenario. There are many different materials that meet the necessary specifications such as high tensile strength cinch straps for trailers and boat slings, as well as many other woven and non-woven materials. After examining many different materials in terms of strength, weight, and cost, the decision was made to go with a carbon-kevlar epoxy laminate material that is most commonly used for sail making. This material will make up the majority of the seat and will be easily adjusted to the proper angle and height by the way the material is stitched as well as the before mentioned cinch straps. In addition to the sling portion of the seat, an aluminum bolster is necessary to further restrain the driver during a cornering scenario. Although this small aluminum bolster is necessary, the overall weight of the seat will be much less than that of the initial all aluminum seat. This seat design incorporates all of the major design criteria that were used in the rest of the car such as comfort, support, lightweight, and most importantly safety.

Materials

Two materials were considered during the chassis design: steel and aluminum. The chassis built in 2007 was constructed from steel and performed exceptionally well in three SAE competitions. However, because one of the main vehicle design considerations made by the team

this year was lightweight and the previous years' chassis was quite heavy, we were unsure if steel was the most appropriate material choice.

Steel is a ubiquitous material choice for in mass produced chassis, custom auto racing roll cages, and other SAE Baja car frames because of its high strength, low cost, and high weldability. Steel is very responsive to thermal processing which provides for a higher strength to weight ratio and thus less material is required for construction. Aluminum is used by Audi in some of their mass production vehicle chassis and has also been employed by Porsche in the construction of endurance race car frames. While aluminum does have a very high strength to weight ratio, it is inevitably susceptible to fatigue failure and has poor weldability.

Design considerations aside, the driving factor behind chassis material selection were the SAE competition vehicle regulations. Section 31.5 of the official 2009 Baja SAE Rule Book states that "the material used for the entire required roll cage members specified in 31.2.1 must, at minimum, be either circular steel tubing with an outside diameter of 2.5 cm (1 inch) and a wall thickness of 3.05 mm (.120 inch) and a carbon content of at least 0.18% **OR** steel members with at least equal bending stiffness and bending strength to 1018 steel having a circular cross section with a 2.54 cm (1 inch) outer diameter and a wall thickness of 3.05 mm (.120 inch). " This ruling left the team with two options that were to either manufacture the roll cage from steel and the rest of the frame from aluminum or to make the entire chassis using steel. The slight increase in weight from an all steel chassis far outweighed the difficulty of reliably attaching a steel roll cage to an aluminum frame, thus the team chose to use steel. The steel chassis also has many other benefits including lower cost, higher safety factors, better manufacturability, and increased reliability.

After the base material had been selected, the team then had to choose which alloy would best suit the vehicle requirements. The SAE Rule Book uses AISI 1018 steel properties as a base for many of their required strength and stiffness equivalencies, so this alloy was considered first. 1018 is a very common alloy that is cheap and readily available in multiple geometries and wall thicknesses. A maximum carbon content of .30% is required for good weldability, so the low carbon content of .18% in the 1018 steel was acceptable (Kou 2003). However, because of its low carbon content and lack of other alloying elements, 1018 did not have the superior hardenability that other iron alloys like 4130 and 4140 possess. AISI 4130 had all of the same alloying elements as 4140, but a slightly lower carbon content of .30% provides for good

weldability as well as decent hardenability. Also, 4130 is a very popular steel that is easy to obtain for a reasonable price. Therefore, the material that the team chose to use was AISI 4130.

Thermal Processing

With the material chosen, it was necessary to ensure that the frame would perform would in a predictable and reliable manner after construction. In order to achieve this, a uniform material property throughout the entire chassis was necessary and accomplished through thermal processing. The entire process included stress relief, heat treat, quench and temper. Another requirement to obtain a homogeneous material property was the use of pure 4130 filler rod during fabrication. Bodycote again provided sponsorship for this service as a gift in kind, and thus all of the material data and specifications were recycled from 2007 after consulting with the company professionals and getting confirmation that the documentation was still relevant.

With the 2007 chassis having survived three competitions, a slight redesign, and countless roll overs, the real value of heat treating became clear to the team. Because of the thermal processing, heat affected zones from welding were not a concern. Consistent material properties were crucial for the frame to endure the imposed loads and perform accordingly with how it was designed. Heat treating allowed us to utilize the full potential of the material characteristics, specifically by designing for higher yield strength and fatigue limit, because a desired hardness was able to be specified and achieved. Thus, the heat treat directly contributed to increased safety factors, greater driver safety, and a lighter weight frame.

The heat treating process begins by placing the chassis in an oven and heating it above the austenitization temperature which is approximately 1550 degrees Fahrenheit. In this step, the ferrite stage transmogrifies into the austenite stage and the carbides become fully dissolved into the mixture. Next, the structure is cooled very rapidly in order to form a fine microstructure primarily consisting of martensite; the more rapidly the material is cooled the finer the martensite structure will be. While cooling the structure rapidly is necessary to achieve a fully martensitic microstructure, care must be taken to ensure that the quench does not happen too quickly because cracking or localized part deformations can occur. Because the quenching process can only cool about 1/8in to 3/8in thick material effectively enough to form a 100% martensitic structure, the 1/16in thick tube frame is ideal for this process. Finally the chassis is re-heated to between 150-1200 degrees Fahrenheit and held there for as long as it takes the material to reach the desired

hardness. The hardness vs. temper time relationship is derived from the I-T diagram which is illustrated in Figure 89 (Appendix A: Thermal Processing). The temper allows the grain size of the microstructure to grow and the martensite begins to decompose into bainite, a much harder and tougher formation. Also, the presence of other alloying elements such as Cr and Mo can very drastically affect how the material responds to the temper and thus improve the hardenability. This improvement is achieved because they delay the nucleation rate of bainite in the material, resist softening, and lessen creep. (Unterwiser 1984)

In order to determine the optimal hardness to specify for heat treating, the relationship between hardness and fatigue limit was examined. Figure 1 illustrates this relationship.

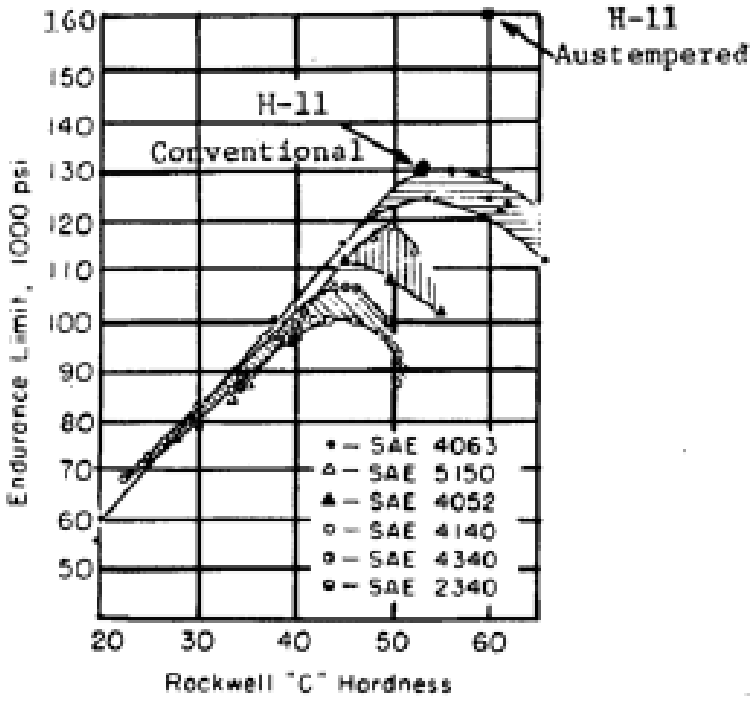

Figure 1: Endurance Limit vs. Hardness (Krauss 1990)

While the actual curve for 4130 is not present in Figure 1, it can be assumed that it would follow very close to the same curve as 4140. This is because they both contain the same alloying elements and only slightly differ in carbon content. The chemical compositions are shown in Figure 2.

Designation or trade name	Composition, weight %					
	C	Mn	Si	Cr	Ni	Mo
4130	0.28 - 0.33	0.40 - 0.60	0.20 - 0.35	0.80 - 1.10	...	0.15 - 0.25
4140	0.38 - 0.43	0.75 - 1.00	0.20 - 0.35	0.80 - 1.10	...	0.15 - 0.25
4340	0.38 - 0.43	0.60 - 0.80	0.20 - 0.35	0.70 - 0.90	1.65 - 2.00	0.20 - 0.30

Figure 2: Steel Chemical Compositions

The discrepancy in carbon content primarily affects the temper specifications, which will be discussed later in the section, but it also has a slight impact on the hardness vs. fatigue limit affiliation. However, due to the lack of test data available for 4130 it was impossible to look up precisely how much discrepancy exists between 4140 and 4130 for the relationship seen in Figure 1. Therefore, it was necessary to draw upon the listed data in order to speculate how much of a divergence may exist. Figure 3 exhibits the difference in engineering stress-strain for 4140 and 4130 samples tempered under the same conditions. Because the 4130 sample has a lower yield strength in comparison to the 4140 sample, it can be concluded that a lower temperature is needed to temper lower carbon steels in order reach the same hardness and strength as higher carbon steels. (Totten 1997)

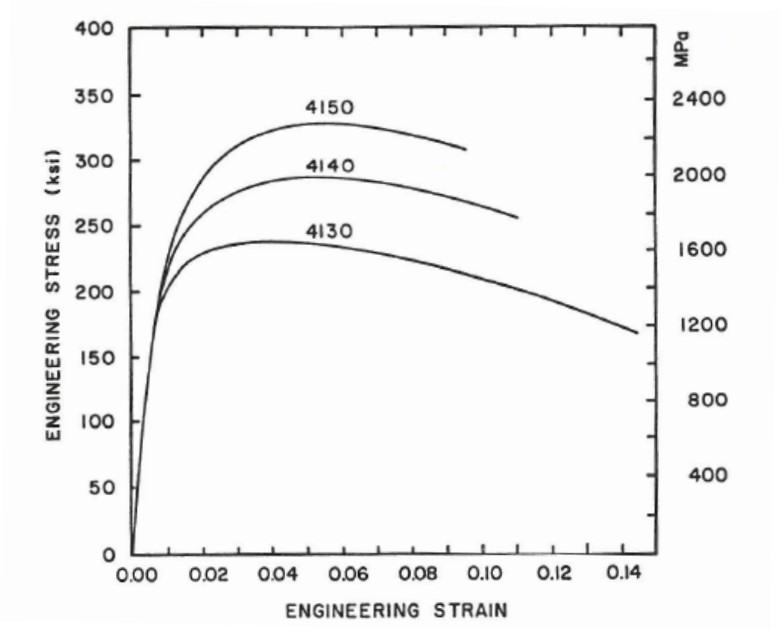

Figure 3: Engineering stress-strain curves for 4130 and 4140 quenched and tempered at 150 degrees C

As a result, the team determined a 10% discrepancy between the displayed 4140 and un-listed 4130 curves in Figure 1was appropriate. When we apply this discrepancy to the 4140 curve, the maximum hardenability of 4130 is approximately 41 Rockwell C. Some ductility and compliance are required in the chassis in order to prevent a brittle failure due to excessive notch sensitivity, thus the optimal hardness was determined to be 35 Rockwell C which would yield a fatigue limit of about 85ksi. Due to manufacturing limitations at Bodycote the minimum tolerance achievable was +/- 1, so the final chassis hardness was specified to be 35 +0/-2 Rockwell.

Ideally the quench would be performed in a salt bath because of the superior heat transfer properties, but the Bodycote facility did not possess this capability. Instead, a heated oil bath at 200 degrees F was setup and used to quench the frame; this was the same method utilized in 2007 because a salt bath was unavailable at that time as well. The temper process was specified to occur at 1000 degrees F and last for two hours. The final theoretical result of the thermal processing would give a yield strength of 120ksi-145ksi and an elongation of 13%-21%, thus providing ample resilience and abating any major notch sensitivity issues. The material properties data resulting from this temper specification can be seen in Appendix A.

Stress Analysis

In order to ensure the structural integrity of the chassis and driver safety through the rigors of competition, a 3D mathematical model of the frame was created and then tested using finite element analysis software. The finite-difference computational simulation created by the 2007 team was modified and utilized to calculate damper loads for predicted jump landing heights. In addition to ensuring chassis integrity, the FEA analysis was also utilized to refine the frame stiffness and minimize the overall weight.

Load Scenario Determination

Before attempting to calculate the input loads, it was necessary to determine what kind of obstacles would be encountered during vehicle operation. This was done by reviewing test and competition videos of other SAE Baja vehicles on the internet as well as driving the 2008 vehicle. This allowed the team to get a very broad sense of what terrain the vehicle would be required to overcome. The vehicles were regularly seen going off of jumps and landing from six

or more vertical feet in the air. Given the repeated success and toughness of the old car which was designed for 5000 six foot landings, it was determined to use similar criteria.

Due to the increased fatigue limit over the previous chassis', which was the result of specifying a greater hardness from thermal processing, the maximum level of allowable average stress imposed on chassis was increased almost 73%. This was determined by examining a graph of fatigue cycles vs. stress which can be seen in Figure 4. One major element for this graph is the applied stress ratio factor which was assumed to be zero. This was because the 2007 calculations yielded the ratio to be negligible (.042) and this year's chassis will experience the exact same environmental conditions.

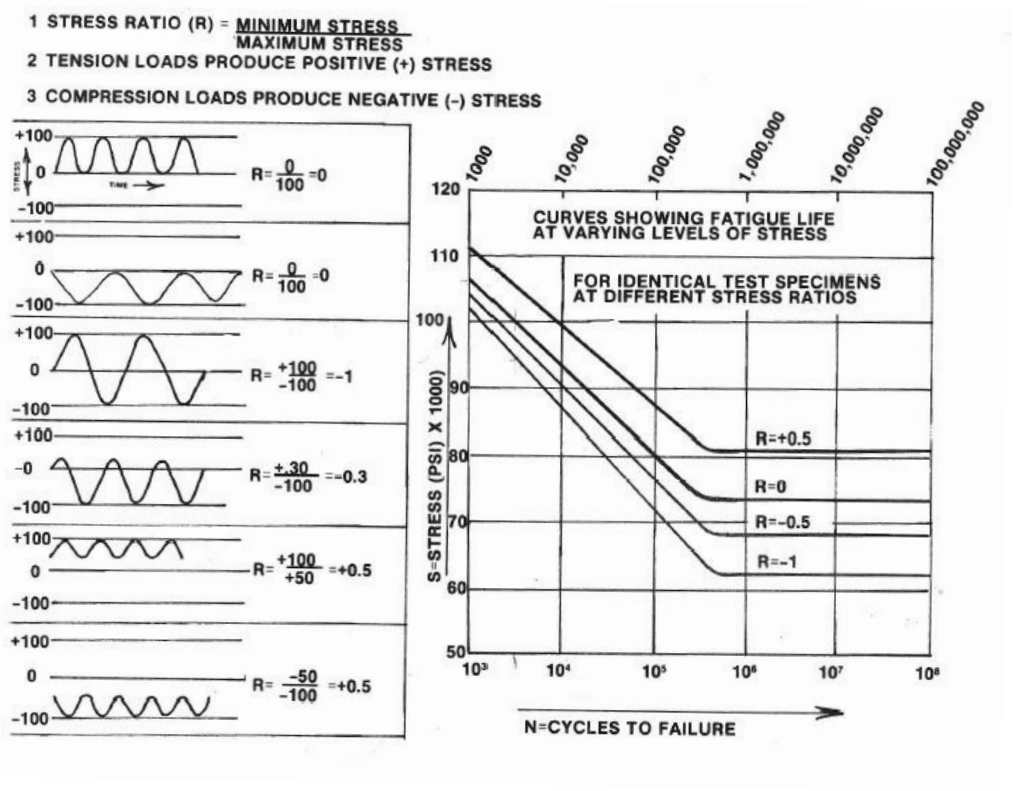

Figure 4: Fatigue Cycles vs. Imposed Average Stress (Smith 1984)

In addition to the stress ratio factor the team also applied a correction factor to the overall stress limit in order to confirm the validity of the previously determined fatigue strength. The team used the same correction factor criteria as in 2007, but the magnitudes were varied based upon insight gained through testing of the old vehicle. The correction factors can be seen in Table 2.

Correction Factor	Magnitude
Load	0.95
Reliability	0.95
Temperature	1
Quality	0.9
Surface	0.8
Size	0.95
Total:	0.617

Table 2: Stress Limit Correction Factors

It is important to note that the largest variation between the 2007 correction factors and the ones used by the current cars design team were load, reliability and surface. This is because we felt as though the predicted loads were calculated accurately, the materials and processes used in manufacturing were correct and appropriate, and the surface finish was consistent because of pre-powder coating preparation. When this correction factor was applied to the median predicted yield strength after heat treat (133Ksi), the result was a fatigue limit of 82Ksi. This result varies from the original fatigue limit by 4% and therefore is considered to be accurate. Thus, the final vehicle life was designed to withstand 5000 six foot jumps by not allowing the average stresses in the chassis to exceed a cycle fatigue limit of 85Ksi. Furthermore, it was determined that the 3G side load used in the 2007 design was also a relevant and necessary loading scenario in case the car should be drifting sideways around a corner and have either the front or rear outside wheel come into contact with a rock or tree. Finally, it was deemed appropriate to include a one wheel landing scenario as reviewing multiple test videos revealed that many jumps are uneven and cause the vehicles that launch of them to roll in the air and land un-evenly on one side. The one wheel landing and 3G side loading were thought of as worst case scenarios and therefore the resulting peak design stresses are limited by the yield strength instead of the fatigue limit.

Input Load Determination

The utilization of a finite difference computational model allowed for maximum precision when calculating the damper loads that would be fed into the chassis. The 2007 team designed the math model by using MatLAB to simulate the effect of a six foot landing with coil over dampers. Because the code was engineered so well, we were only required to change five input variables which specified the force vs. velocity and force vs. compression relationships of the air spring damper the team specified for use on this year's vehicle. The modified code is shown in Appendix B: Input Load Determination. The equation for force vs. compression was not provided by the manufacturer, so it was necessary to re-plot the given graph by sampling data points and generating an equation of best fit. The equation that was produced was a sixth degree polynomial and while it had a miniscule deviation of $R^2=1$, it was too unwieldy to implement in the MatLAB code. Hence, a simpler supplementary power equation with an order of 3.5 was developed and used to estimate the damper response. The original force vs. compression graph can be seen in Appendix B and the re-processed data can be seen in Figure 5.

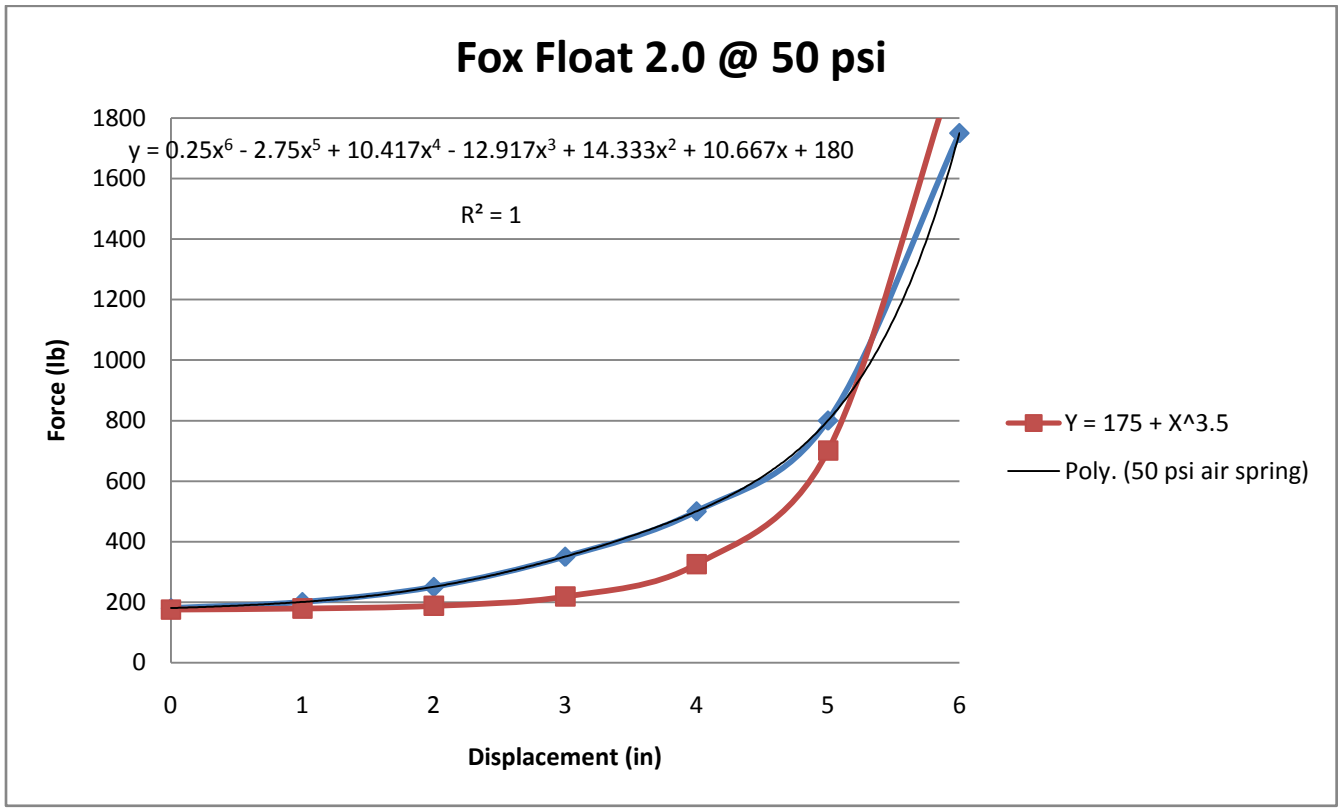

Figure 5: Fox Float 2.0 50psi Force vs. Displacement

The slope for the force vs. velocity on compression and rebound were calculated from the damper specifications provided by Fox Inc and can also be seen in Appendix B. After the MatLAB program was run, the resultant maximum damper load and the corresponding position were fed into a suspension model created with WorkingModel in order to decompose the individual control arm loads. It is important to note that the control arms were included into the model to simulate their compliance and to also further reduce the complexity of additional load decomposition through varying amounts of control arm angulation. The final chassis input loads for the different loading scenarios can be seen in Tables 3, 4, 5, and 6.

Front Jump Landing	
Load Application Point	Magnitude (lb)
Damper	-2100
Lower Control Arm - Forward Member	1200
Lower Control Arm - Rearward Member	1200

Table 3: Front Jump Landing Scenario

Rear Jump Landing	
Load Application Point	Magnitude (lb)
Damper	-2100
Control Arm - Forward Member	500
Lower Control Arm - Rearward Member	1900

Table 4: Rear Jump Landing Scenario

3G Front Cornering Load	
Load Application Point	Magnitude (lb)
Upper Control Arm - Forward Member	-1875
Upper Control Arm - Rearward Member	-1875
Lower Control Arm - Forward Member	866
Lower Control Arm - Rearward Member	866

Table 5: 3G Front Cornering Load

3G Rear Cornering Load	
Load Application Point	Magnitude (lb)
Axel	-1500
Control Arm - Rearward Member	-3200
Control Arm - Forward Member	-550

Table 6: 3G Rear Cornering Load

Finite Element Analysis

The 3D chassis model was created using SolidWorks and the FEA was performed using the complementary software package COSMOSWorks. All analyses were run using a Beam Mesh which partitions the annular frame members into tiny sections and then calculates the load distribution and resulting stresses. The beam mesh is a very convenient feature of COSMOSWorks because the calculation time is very short and it allows for multiple iterations very quickly; however the team suspects that because of its short run time the COSMOSWorks analysis may not have been as accurate as one conducted in a more heavy duty solver such as ABAQUS. In order to account for and minimize the possible inaccuracies, the mesh size was refined as small as possible. The boundary conditions for the chassis simulations were defined by constraining all suspension mounts opposite to the end being loaded. This was to ensure a worst case loading scenario by providing the largest possible lever arm between the reaction and load points. Constraining the frame at the center of mass was also considered, but this method would

incur additional unrealistic stress concentrations due to the unrealistic associations the software would assume between frame nodes and the CM. The CM constraint would influence load propagation to occur relative to one point instead of a section of members at the opposite end of the vehicle and thus the calculated displacements and stresses would be inaccurate. As mentioned before, the control arms were included into the model and the loads were input at nodes perpendicular to ends of the members. The constraint and loading methods can be seen in Figure 6.

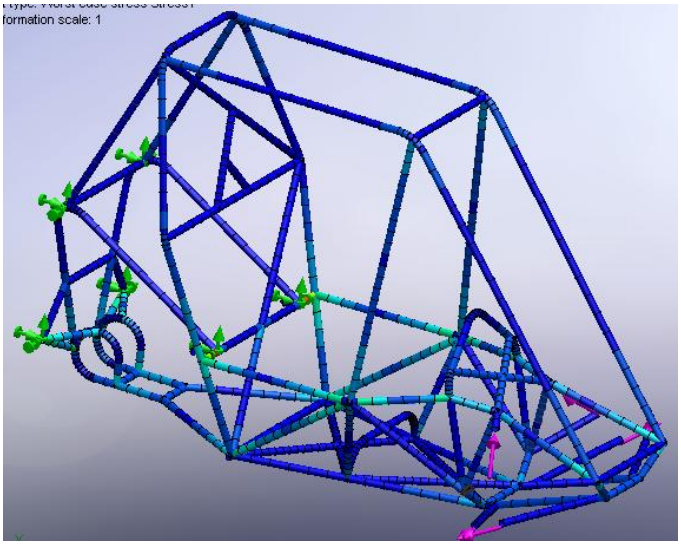

Figure 6: FEA Constraint and Loading Methods

The final step was to run the simulations and optimize the frame geometry and tube size. The final FEA results can be seen in Table 1 and the screenshots are contained in Appendix C: FEA Results.

Load Scenario	Peak Stress (Ksi)	Peak Displacement (in)
Front Jump Landing	65	0.63
Rear Jump Landing	77	0.56
Front One Wheel Landing	115	0.42
Rear One Wheel Landing	90	0.81

Front 3G Side Load	75	0.62
Rear 3G Side Load	82	0.70

Table 7: Chassis FEA Results

It is important to note that the listed values in Table 7 may differ from the maximum values that are pictured in the screen shots. The peak displacement discrepancies are a result of the included suspension members because in some loading scenarios they may experience a greater overall deflection than the chassis members. Therefore, the maximum chassis member deflections were probed and listed in Table 7. The peak stress discrepancies are a result of stress concentrations produced by inaccurate node geometry and therefore imprecise stress distributions. These analysis inaccuracies are intrinsic to the beam mesh, software restraint, and solution methods utilized by COSMOSWorks and are therefore believed to be highly inflated from what would actually occur. In cases where these untrue peak stresses occurred, the highest average probed stress was taken to be true. The most problematic analyses were the rear one wheel landing and rear jump landing. In these scenarios the loads propagated from the rear of the chassis to the front and large stress concentrations developed at the bends in the side impact and front damper mount members. These stress concentrations were a result of the curved geometry inciting a large stack up error in the nodal stress calculations and were accounted for by probing average surrounding values. Even though the nodal stress concentrations were considered to be an erroneous part of the finite element analysis, during construction the nodes where these singularities occurred were heavily reinforced with gussets to ensure that a catastrophic failure would not occur.

Another important factor to discuss is the lack of correlation between peak stresses and displacement. That is to say that peak stresses do not always occur at the location of a peak geometrical displacement. This is because the peak displacement often occurs far away from the restraint points due to the incremental displacement of intermediate frame members, essentially a result of stack up. Frame member displacements vary widely depending on their length, shape, and resultant load vector. For example, if a long member is placed in bending such that it acts like a cantilever, the results will yield a relatively large displacement at the unrestrained end, but the member may not experience any high resultant stresses. The areas of peak stress often occur

at very stiff joints. This is because the non-compliant joints must resist the imposed load to effectively transmit it throughout the surrounding chassis members. Thus the joints become point stresses and can result in massive stress concentrations that are often times not present in the actual system being modeled. The lack of correlation between displacement and peak stresses realization was important because it provided insight into frame member allocation and allowed the team to better refine the overall chassis stiffness matrices thus maintaining an even load distribution.

Chassis Optimization

Chassis optimization was concurrent to the finite element analysis and served to optimize the safety, stiffness, stress distribution, and weight of the frame.

Tube Size Selection

In order to optimize the tubular structure, specific tubes or areas were focused on during each FEA simulation. The SAE rule book and driver envelope specifications (ergonomics) dictated the placement of many of the main structural tubes, so the bulk of refinement occurred with tube size, wall thickness, and location of bracing members. During each analysis, the areas of high stress were concentrated on and alleviated by adding bracing members to tune the stiffness and re-distribute load to other areas. Additionally, the tube size and wall thicknesses were adjusted until they were all uniformly stressed. This was a difficult process because as the chassis was optimized for one loading scenario, the changes made affected the stress distributions in the other load cases. Accordingly, the front and rear jump landing load scenarios were accounted for first by ensuring the maximum resultant stresses were below the fatigue limit of 85Ksi. Next, the worst case load scenarios were designed for by increasing the tube size until the maximum stresses were below the minimal predicted yield stress of 120Ksi. The final resulting tube sizes and their use throughout the chassis can be seen in Figure 7.

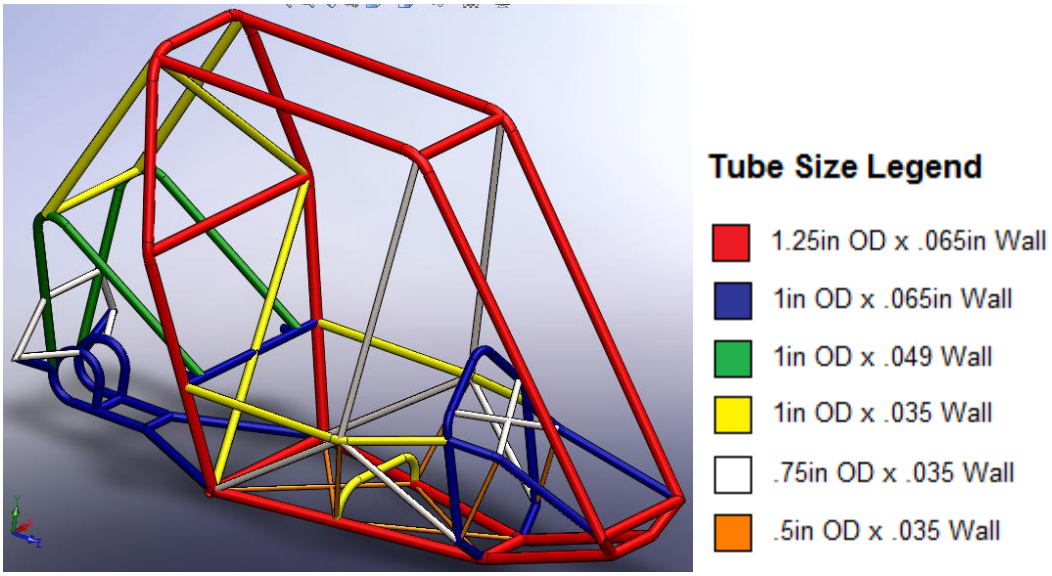

Figure 7: Tube Size Distribution

Weight

The final chassis computer model weighed 64.6lb's which was a 3.2% increase in weight from the final 2007 computer model design, but was acceptable because this frame was designed to directly withstand lateral loading at the rear drive train hoops. The 2007 vehicle employed a trailing arm design that transmitted the lateral loads through the rear roll hoop lower lateral cross member, a design which requires less support structure behind the firewall and thus results in a lighter chassis. However, the current chassis design allowed for a weight reduction in the rear suspension and drive train components which adequately compensated for the additional frame weight and resulted in an overall lower vehicle weight.

Geometry

The general frame geometry as well as individual tube geometries were given considerable design consideration to throughout the chassis optimization process. The overall frame size was minimized as much as possible in order to reduce weight. The firewall area was designed to meet the SAE rule book specification 31.2.2 which states it must be greater than 29 inches wide at 27 inches high measured vertically from the driver's seat, but was designed to taper off at the top and bottom in order to minimize the surface area and thus reduce wind drag. A space frame design approach was employed during the positioning of all structural frame

members such that they are primarily loaded in tension or compression and thus maximizing their effectiveness in force resolution. The final chassis geometry can be seen in Figure 7.

Specific tube geometries such as the front and rear damper mounts were designed to best handle the loads that would be imposed upon them. The curved hoop geometry of the rear damper mount member was modeled after the typical shock tower design found in many desert buggy designs. The intention is to resolve the immediate damper force in the one member such that only smaller bracing members are required for additional stiffness. The hoop design places both sides of the damper mount member in tension and thus requires a tube with less cross sectional area to resolve the load. The front damper mount was designed to feed loads directly into the front hoop, a shape that is both strong and rigid. Arches are a common geometry in structural design because they distribute point loads very well through hoop stress and thus were incorporated into the chassis design. The front hoop design was incorporated effectively and can be confirmed through the FEA displacement result for the front one wheel landing. The maximum displacement had a magnitude of .42 inches and occurred at the top of the hoop which indicates a very high torsional stiffness throughout the entire vehicle, but especially in the front end.

Strengthening Mechanisms

In an attempt to alleviate stress concentrations resulting from chassis geometry as well as improve the frame's torsional stiffness, several strengthening mechanisms were incorporated into the design. These included the use of dimple dies on sheet steel, gusseting at nodes, stressed body panels, and skid plating.

Flared Holes

The first strengthening method incorporated into the chassis was the use of flared holes which are also called dimple dies. Dimple dies were investigated by the 2007 team and heavily incorporated into both the 2007 and 2008 vehicle designs. The dimple die is a flared hole or pattern of flared holes made in a piece of sheet metal. They act to increase the second area moment of inertia in the piece of sheet metal and also reduce weight; both of these qualities combine to effectively improve the stiffness, buckling resistance, and strength to weight ratio. The team reviewed the research and performance put forth from 2007 on flared holes and found

the results to be positive, thus dimple dies were added to the current chassis wherever possible. An example of where flared holes were incorporated can be seen in below.

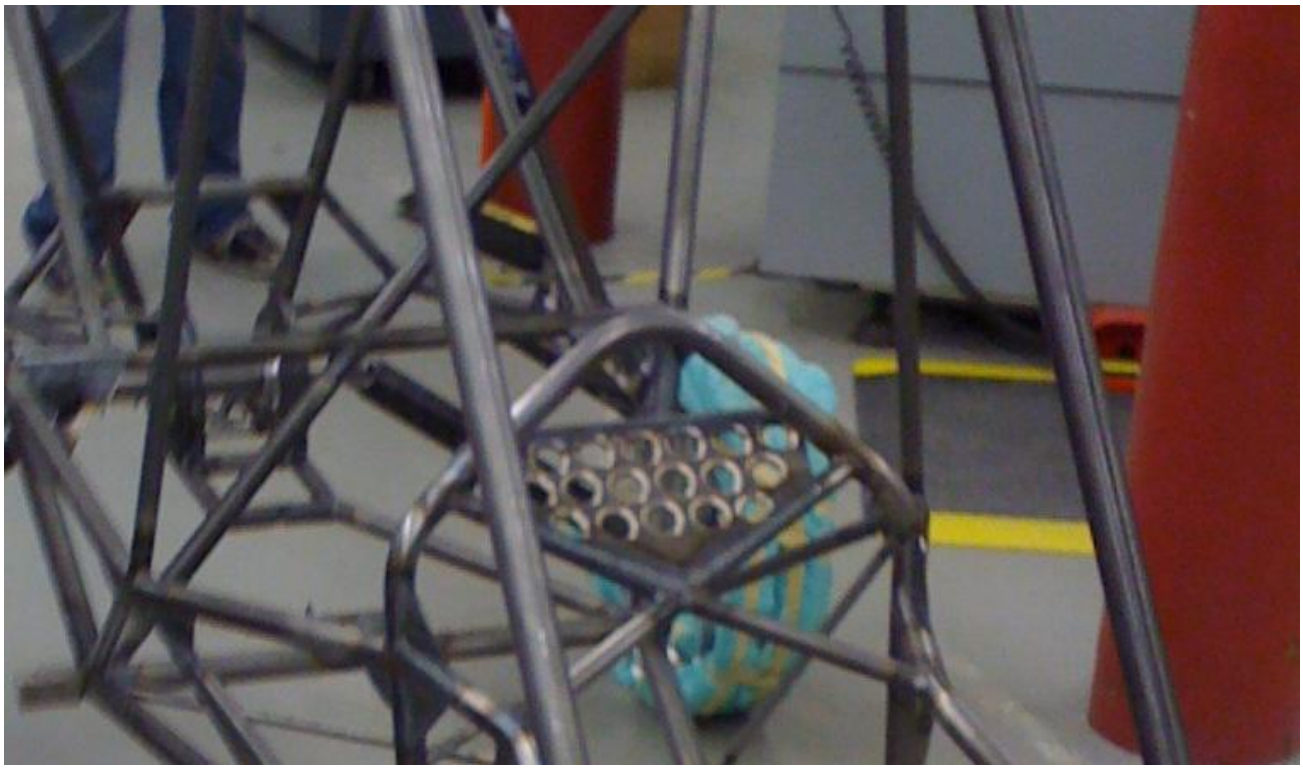

Figure 8: Flared Hole Steering Column Mount

The steering column mounting plate was a piece of .049 inches thick sheet steel that spanned a large area. The addition of dimple dies to the sheet provided for adequate torsional stiffness such that it would undergo minimal deflections when steering loads were applied. The panels' weight was also reduced by 58%.

Gussets

The team also assessed the research done in 2007 on gusset theory. Gussets are pieces of sheet steel that are welded tangential to two tubes intersecting at a node. They reduce nodal stresses by distributing load farther down the intersecting members. Per the 2007 gusset theory evaluation .0325in to .049in thick sheet was used to manufacture the gussets, they were placed on the outer tangent of the intersecting tubes, and finally all structural gussets were between 3 and 4 inches long. The research from 2007 also concluded that gussets are most effective when placed in tension, so they were added to joints that required bracing and in such a way that they

would be loaded in this manner. Also, a relief hole was added to center of all gussets in order to reduce the weight. The relief hole is an effective way of reducing weight because due to the triangular geometry and two-edge tension loading method gussets undergo, there is very little stress flow through the center thus making the material there is inconsequential.

Figure 9: Roll Cage Gussets

Figure 9 clearly depicts the addition of gussets to the roll cage. The primary purpose of these gussets was to increase the roll cage safety factor and provide better protection for the driver in a roll over scenario. They also help to increase the overall frame stiffness which will benefit vehicle control and feel during normal or bumpy driving conditions.

Stressed Body Panels

Monocoque chassis are popular in aeronautics and F1 race cars because of their light weight in comparison to other frame types. In a monocoque chassis the support structure and skin are incorporated into one unit. Because of the often complicated geometry and high strength requirements associated with monocoque chassis, CFCs (carbon fiber composites) in conjunction with sheet metals are the most commonly chosen construction materials.

The design of an entirely monocoque chassis for use in SAE Baja would be innovative and advantageous, but unfortunately it would not be permitted to enter competition. This is because the rule book mandates, via section 31.2.1, the use of steel for all of the approximately twenty required frame members. Therefore, the most radical frame design that would be allowed to compete is a space frame/monocoque hybrid chassis in which the body panels double as stressed members.

The use of stressed body panels was discussed as a chassis design feature that would increase torsional stiffness, better distribute the imposed loads, and primarily reduce the overall weight. The weight reduction is achieved by replacing certain steel bracing members in the frame, that are not required by the rules, with body panels that have both structural and cosmetic value. However, there are as many benefits as there are drawbacks with stressed body panels in this application. While a significant weight reduction could be achieved the structural body material would be costly to purchase, manufacturing the panels would be time consuming and complex, and attaching the panels in a secure yet easy-to-fix method that is lightweight would be very difficult. The team decided that the weight savings would prevail over the pitfalls and thus proceeded to research the implementation of stressed body panels.

Great consideration was given to the material choice for the stressed body panels. Bracing members are most effective when added in such a way that they diagonally bisect a gap between major frame members by tying two opposite nodes together and are orientated to experience tensional loading. Thus, the material had to possess an extremely high tensile strength to weight ratio. This pared the material choice down to sheet aluminum and CFC, both of which also have an extremely attractive appearance. While the aluminum sheet was a much less expensive option, the CFC was chosen because of its superior performance characteristics. The larger expense for CFC panels was further justified because they can be purchased with a clear coat and no additional money would have to be spent on finishing products.

After the material was chosen, the second step in evaluating the stressed body panels was to run a mathematical analysis and determine the most effective bracing method. Three test configurations were developed and are shown in Figure 10.

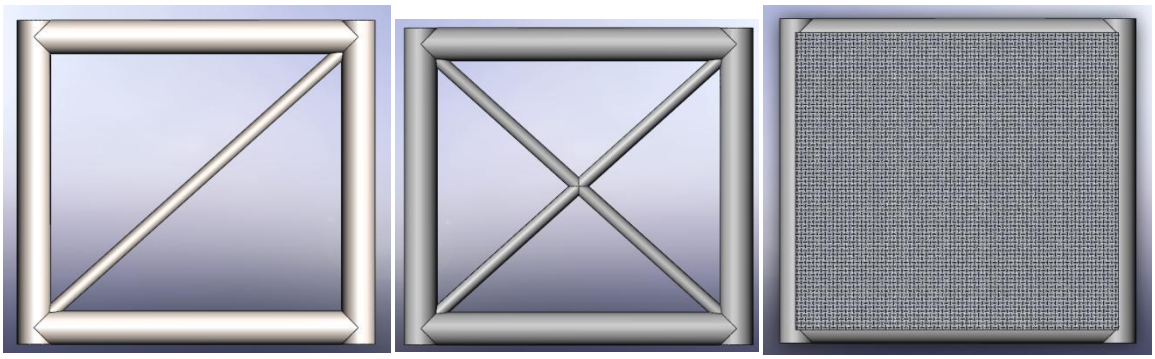

Single Brace X-Brace CFC Panel

Figure 10: Test Frames

Each frame measured 12in by 12in from tube centers and was 1.25in OD x .065in wall AISI 4130. The single and X brace tube members were AISI 4130 with an outer diameter of .50in and diagonally intersected the frame on center. The CFC panel was a 0-90 weave (material specifications in appendix) that measured 12i inches by 12 inches. Six analysis' were performed using a shell mesh in ABAQUS by varying the section assignment of the bracing tubes from .035 inches to .120 inches and the CFC panel thickness from 1 ply (.0185 inches) to 5 ply (.0925 inches). The frames were fixtured on the inner face of the left tube and a vertical load of 2000 pounds was applied to the bottom face of the right tube. For the CFC panel simulation, a tie constraint was used to couple the panel and frame together; a constraint method which assumes an ideal bond. The fixturing method and load case is illustrated in Figure 4. Results pictured are just for reference and were produced using COSMOS.

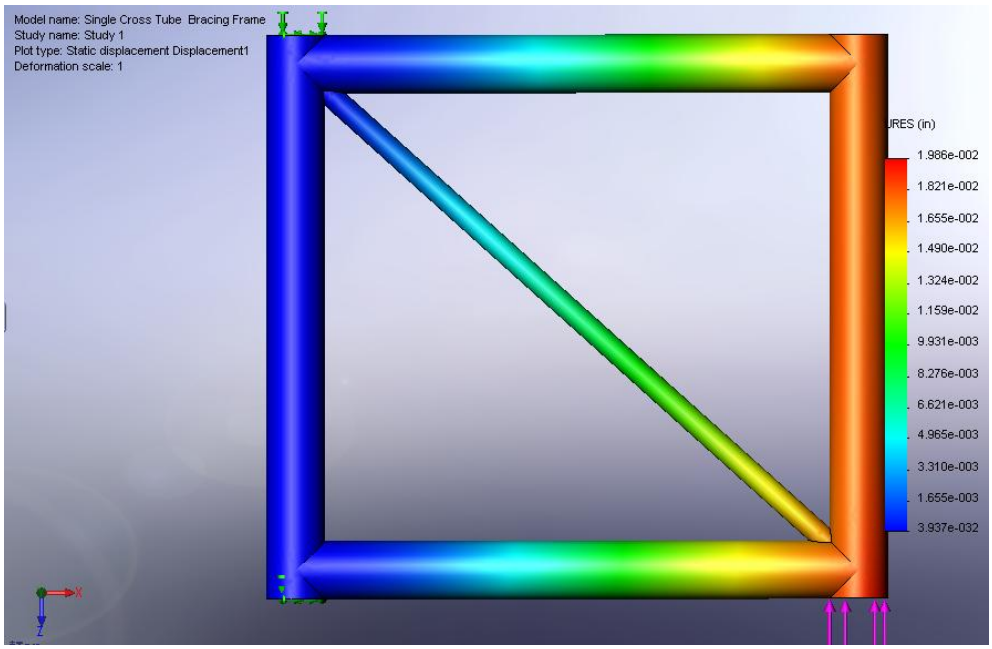

Figure 11: Test Frame Analysis

The next step was to determine which bracing method was the most effective. In order to do this, a stiffness coefficient with factors of weight (lb), displacement (in), and load (lb) was developed. The stiffness coefficient was calculated via the equation:

$$C = \frac{Load}{(Displacement * Weight)}$$

This equation was developed such that decreasing values for weight and displacement would incur a relatively large increase in the overall stiffness coefficient by taking a larger coefficient to indicate better performance. Thus, the equation has a high degree of sensitivity for changes in displacement because of the 10^{-2} order of magnitude; this was useful because it simplified the comparison through a large variance in the test frame stiffness coefficients. The final stiffness coefficients can be seen in Table 8.

Brace Type	Brace Spec	Coeff (in^-1)	Norm Coeff
Bare Frame		2944	
CF-Brace	1 Ply (.0185in)	7545	3
	2 Ply	10281	3
	3 Ply	11282	4
	4 Ply	13160	4
	5 Ply	13538	5
X-Brace	.5x.035	23023	8
	.5x.049	27811	9
	.5x.058	30288	10
	.5x.065	32229	11
	.5x.095	36870	13
	.5x.120	23566	8
1-Brace	.5x.035	31937	11
	.5x.049	53241	18
	.5x.058	19547	7
	.5x.065	20719	7
	.5x.095	24569	8
	.5x.120	26881	9

Table 8: Friction Coefficients

Finally, all of the test frame stiffness coefficients were normalized and compared graphically. The coefficients were normalized against the stiffness coefficient calculated for an un-braced frame, which was 2944 in^{-1}. When the normalized coefficients are plotted vs. sample number, some interesting trends develop and are illustrated in Figure 12.

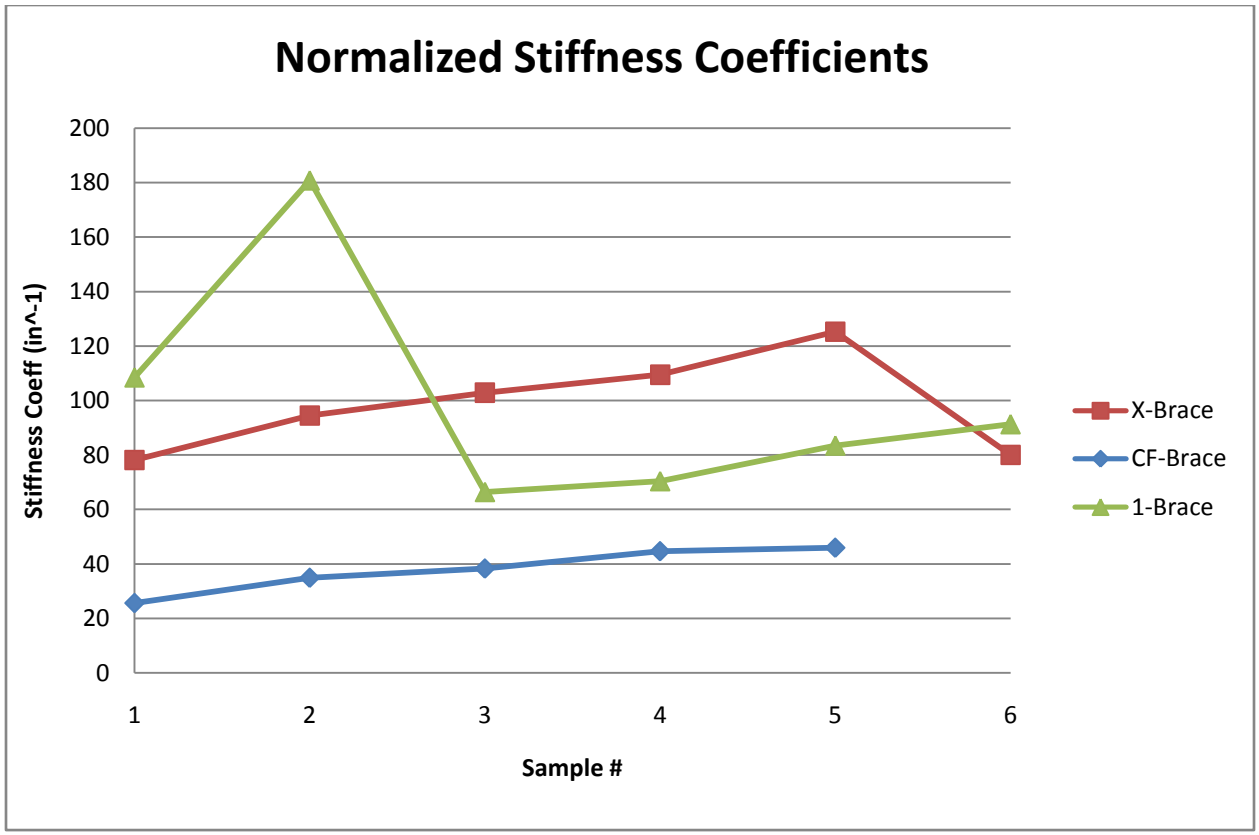

Figure 12: Normalized Stiffness Coefficients Vs. Sample #

The CFC panel exhibits an expected increase in the stiffness coefficient with an increase in the number of ply. It is important to note that it scored the lowest in terms of overall coefficient performance for all samples. Both of the steel bracing members display maxima at some point along the trend line rather than at the end; this is especially true for the single brace that peaks and drops off sharply after the second sample. This behavior is very odd because one would expect to see a trend line of increasing performance that levels off at the end, similar to what the CFC panel exhibited. A peak in the trend line can be explained through a stress concentration in the frame which resulted in localized buckling. Localized buckling would cause the stiffness coefficient to decrease rapidly because of the larger and inconsistent displacements in the compromised portion of the frame. Hence, this indicates that there is an optimal bracing tube thickness which is dependent on the brace geometry. Furthermore, if the optimal thickness is exceeded then it will cause the super structure to fail due to a lack of compliance in the brace. Based upon Figure 5, the best bracing geometry to use is a single diagonal with .049in wall thickness. However, the single diagonal brace with .035in wall thickness performed third best in

terms of coefficient rating, but at 3.643 lbs it is the lightest tube structure and would still provide an ample increase in stiffness, thus making it the optimal choice.

Based upon the data acquired from this simulation, the team decided that the use of stressed CFC body panels was not the most beneficial method for increasing chassis performance. Rather, it was discovered that .5 inch OD by .035 inch wall tubular steel members were the optimal choice with because of the superior stiffness they provide while still maintaining a comparatively light weight.

Body Panel Selection

After it was decided to not use the carbon fiber body panels, we had to choose what the body panels would be made of. It was understood that the body panels had to be light, moldable, and have a high Impact resistance. Table 9 shows four different polymers that were compared to choose what would be used. The data used to form these ratings was from CES EduPack 2008 Level 3: Polymers. One of the main goals for this car was to keep weight to a minimum so obviously density was a large concern. ABS, Polyurethane and Polycarbonate had lower densities with ABS having the lowest density.

	ABS Plastic	Polyurethane	Polycarbonate	PVC
Density (lb/ft^3)	5	4	4	2
Impact Resistance	5	5	5	5
Moldability (scale of 1-5)	5	5	5	5
Price USD/lb	4	3	3	5
Total	19	17	17	17

Table 9: Body Panel Design Matrix

The SAE Baja rules state that the body panels need to be able to stop rocks and other object from entering the car so Impact resistance was also a large concern. All of the plastics that were look at in the CES software had similar strengths under impact.

Figure 13 is a graph of impact strength to density of different thermoplastics. (There are a lot of materials on the graph that are different forms of the same materials, the graph looks cluttered because of this.) You can see that the four plastics chose to be compared were selected. Limiting the graph to moldable plastics under 2 dollars, you can see that ABS has the best impact resistance to density ratio with PVC performing the worst.

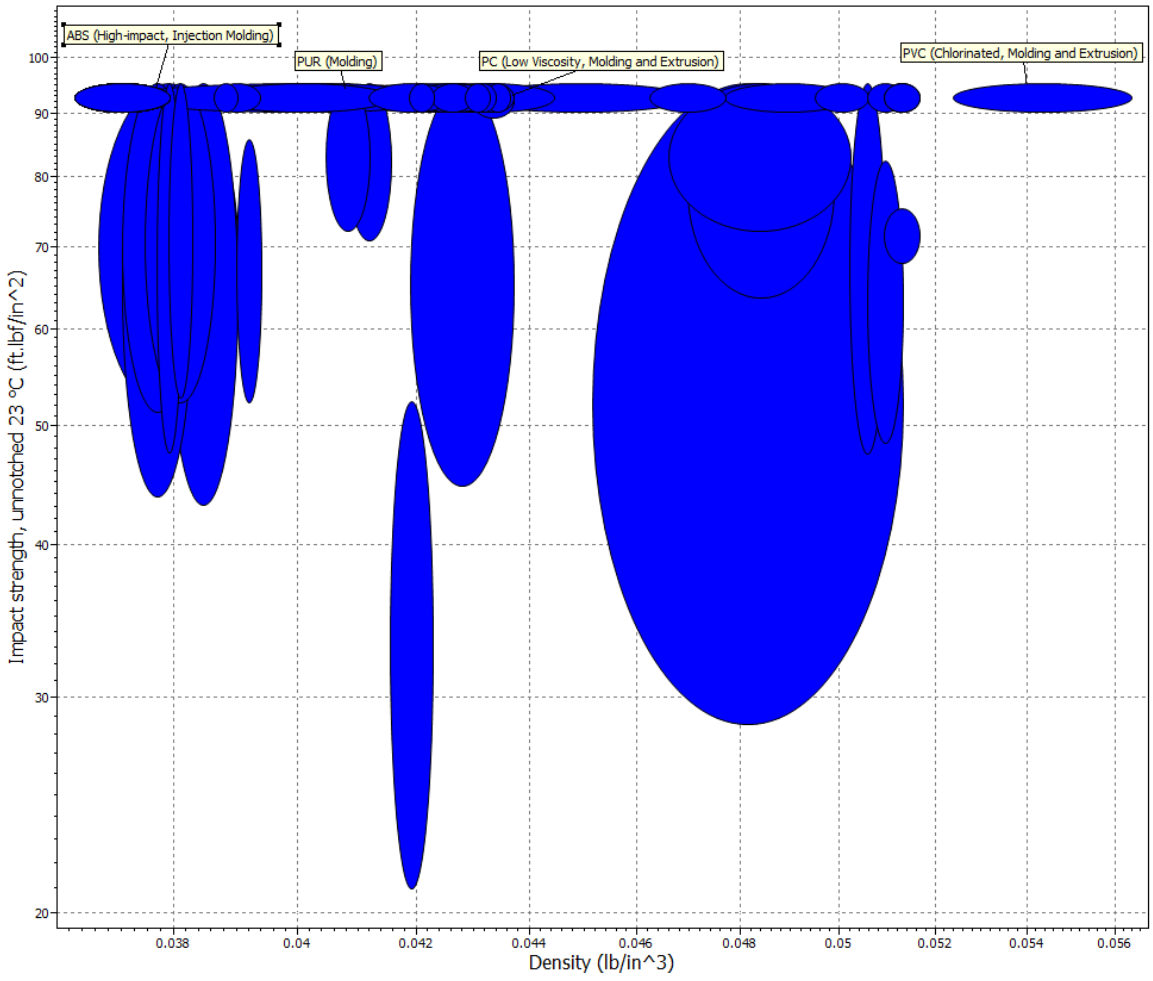

Figure 13: CES Graph of Impact Strength vs. Density

Fabrication

One of the criteria that had to be taken into consideration by the team throughout the design process was the manufacturability of each design feature incorporated into the vehicle. This was because the team felt that it was necessary to fabricate as much of the vehicle in house by utilizing the WPI manufacturing facilities in order to best fulfill the MQP degree requirement. The total range of abilities required to fabricate the car were fixturing, cutting, bending, notching, fitting, welding, and machining. All of these skills were represented by different team members which made collaboration and team work vital for the successfully completion of the car.

Chassis Fabrication

The chassis fabrication process enlisted all of the different skills possessed by each individual team member. The team worked diligently to setup the frame table and necessary fixturing in order to ensure that the chassis geometry would be accurate to the 3D model after completion. Tube notching, fitment, and cleanliness were a top priority and guaranteed good weld penetration as well as maximum joint strength. Quality was always a top priority for the team throughout the entire chassis build and because of this it was sometimes necessary to alter the design during construction in order to meet certain time constraints.

Frame Table and Coordinate system

The first step to assembling the chassis was to acquire a frame table. The table that was used in fabrication of the chassis was the same table used by the 2007 team and therefore making it ideal for this years' build. The table was prepped by grinding the surface smooth and re-tapping the positioning holes that were already in the table. After the surface grinding was complete, a coordinate system was drawn on the table top in order to properly orient the fixtures and jigs as well as accurately position frame members on the table. The coordinate system was drawn with the base plane at the bottom of the roll hoop as well as the central axis of the car. which was used for both the chassis manufacturing as well as accurately locating jigs such as the one for suspension mounts.

Bending

To construct the space frame chassis it was necessary to bend the tubes very precisely in order to achieve the proper geometries. This was accomplished by using the manual bender available in the shop. Because of the minimal wall thickness of some frame members, localized tube buckling occurred when bending them to angles typically above 15 degrees. In order to achieve high angle bends in these tubes, it was necessary to use a bending alloy which provided additional support and helped to prevent buckling. The bending alloy is based on a bismuth metal and has a low melting point. The metal was first melted and then poured into the tubes. It was then shock cooled by running cold water over the tube for a short period of time. After the fixturing alloy had solidified it was then possible to bend the tubes to any desired angle. Another tactic that was used to ensure that the tubes were bent to the proper angle was printing out full scale drawings of the bent tube geometry. In some frame members containing compound bends it was necessary to ensure that the tube remained level in the bender throughout the entire bending process and thus an angle finder was magnetically attached in order to measure and correct any rotational deviations.

Notching

Another major portion of chassis fabrication was the notching and fitment of the tubular frame members. Tube notching was performed by hand using a motorized tube notcher, pedestal grinder, and smaller handheld grinder. To make notching the tubes easier and increase the notch geometry accuracy, templates were printed and wrapped around the members. To make these templates it was necessary to use the new sheet metal features in the 2008 version of SolidWorks. This template is then printed out and wrapped around the tube at the proper spacing in order to grind down the desired shape. After notching, the tubes were then placed in their respective locations in the chassis and ground further to ensure a proper fitment and make the welding process easier.

Welding

All of the chassis components were bonded through GTAW (Gas Tungsten Inert Gas Welding) performed by team members using a Millermatic Syncrowave 185 welder. Due to the fact that there are a large number of intricate parts coupled with the thin wall material that the

chassis was made from, TIG was the preferred method because of the intrinsicly high amount of control. The Millermatic TIG welder uses a water cooled torch with 2% thoriated tungsten of varying diameters as well as cup sizes varying from #4 to #8. The diameter and cup size for the torch was chosen based up the type of joint that was to be welded as well as the thickness of the material involved. After the tubes were properly notched, the ends were either sandblast or hand sanded to remove the mill scale. Then the ends were cleaned with acetone and were ready to be welded. These manufacturing and cleaning processes ensured complete weld penetration and thus allowed for high strength joints. As stated in the Chassis Design section, it was necessary to use AISI 4130 filler rod in all of the chassis welds due to the fact that the entire structure was heat treated after fabrication.

Suspension

Front Suspension

Preliminary Design Parameters

By defining the objective of the vehicle's suspension, it is possible to start the design process. Through analyzing different suspension systems, it was decided that a fully independent system would best suit the terrain of the Baja competition. The design must provide adequate vertical wheel movement, which allows for bump absorption through the wheels during the changes in ground conditions. Change in toe during the wheel movement must also be minimized in an effort to isolate the steering input to the driver's actions. Effective positive castor is integrated into the suspension design to aid in straight-line stability and steering wheel return-to-center. Additionally, there should not be any compliance within the suspension system or its attachment to the vehicle (the sprung mass). Both the suspension link and their attachment points should rigid such that the shocks and the tire are the only members changing dimension during suspension travel. Also, by minimizing unsprung mass, the response time of the suspension to changes in the track surface is minimized. This allows the tire to maintain constant contact with the surface as much as possible.

A list of suspension envelope specifications was defined at the beginning of the design process, which included the general vehicle dimension parameters. An attempt was also made to define reasonable goals for specific dynamic performance requirements. Table 10 details the design envelope of the front suspension dictated by the overall vehicle goals as discussed in the design parameter section.

Vehicle Dimensions at Ride Height	
Track Width	
Front	60-64 inches
Rear	56-60 inches
Wheelbase (center of wheel to center of wheel)	
	60-64 inches
Inclination Angle (rake) in front suspension plane	
	20 Degrees
Ground Clearance	
	11.5 inches
Wheel Size	
Both Front and Rear	17 inches
Tire Size	
Both Front and Rear	25 inches

Table 10: Preliminary Design Envelope

The 2009 Baja SAE Competition Rules states that the course is designed around a vehicle "with the maximum dimensions of 64 inches width by 108 inches length". Considering this overall width and the size of the tire and wheel combination, the suspension must be designed around a maximum width tire edge surfaces of 64 inches at ride height. The rear track width is designed to be smaller than the front to aid in maneuverability. Furthermore, through our mock chassis, driver dimensions, drive-train considerations, and performance requirements a wheelbase between 60 to the maximum 64 inches was chosen prior to further design. To maximize obstacle avoidance and account for varying terrain, a ground clearance of 11 inches from the ground to the lowermost member on the chassis was chosen.

Researching previous vehicles provided the possibility of inclining the suspension place past vertical. Thus, if an axis were drawn through the rotation points of the control arms at the chassis, it would not be parallel to the ground. This rake angle improves the suspension's ability to absorb impact under landing. The nature of the vehicle results nose-diving condition when landing, causing resultant forces that are not perpendicular to the overall plane of the chassis. The value of 20 degrees of chassis rake at the suspension mounts was chosen based on previous vehicle designs, and the examination of landing conditions as well as driver comfort.

Because of the variety of suspension designs available and the inability to perfectly control the path of the tire for a link type suspension in every situation, compromises are made in the kinematic behavior, and certain features are prioritized over others. Prior to modeling the

suspension attainable values for the kinematic behavior were quantified. Through examination of possible situations that the vehicle will encounter in competition, and the vehicle's physical reaction, we created a list of basic suspension behavior goals for the front and rear of the vehicle.

Kinematic Suspension Performance Goals (Front)	
Wheel Travel	
Up	7 inches
Down	5 inches
Toe	
	Minimize change during travel
	Adjustment via tie rods
Camber	
Ride Height	0 degrees
Compression	Maximum Negative
Droop	Minimum Positive
Adjustment	Adjustment via heim joints
Track Width	
	Minimize change

Table 11: Front Kinematic Performance Goals

The parameters listed above were the basic design goals for the front suspension prior to choosing a link configuration or performing either mathematical modeling or utilizing computer aided design methods. With our ground clearance, available joints, and possible link lengths due to the track width and foot box area, 7 inches of up travel and 5 inches of droop from ride height were deemed acceptable. As stated earlier, change in toe angle of the tire during suspension travel is undesirable.

Keeping the distance between contact patches constant throughout suspension travel is important. Tire scrub across the track surface through compression or droop in either cornering or bump travel can cause a loss in traction. With this in mind, track width and the distance between contact patches are important considerations in the design.

Other factors, such as wheel travel, are constraints in the design of the front suspension. The wheel travel is ultimately limited by the available angle change of the chosen suspension joint. It is important to monitor the steering angles and bump steer through travel to create an envelope for the steering rack. Furthermore, some level of adjustment must be available to

change camber at ride height, differences in castor angle due to manufacturing, and toe at ride height.

Component Design

Figure 14 illustrates the final front suspension assembly including control arms, tie rod, knuckle, hub, spindle, and wheel.

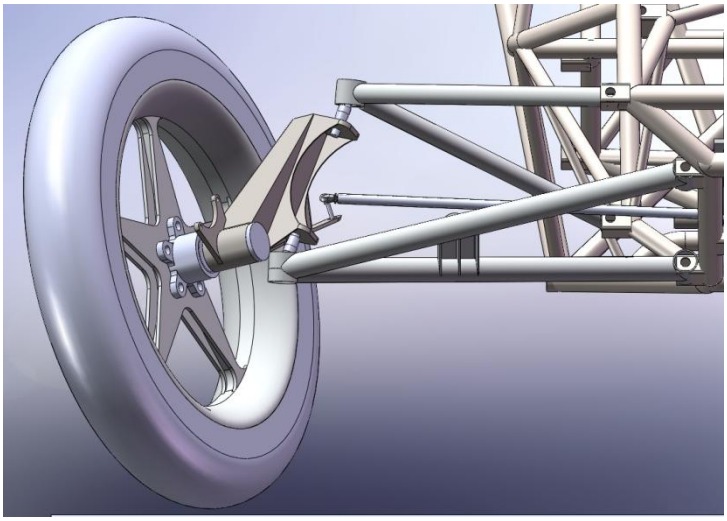

Figure 14: Front Suspension Model

Figure 15 shows an exploded view of the front hub assembly including spindle, knuckle, taper bearings, seals, hub, and wheel.

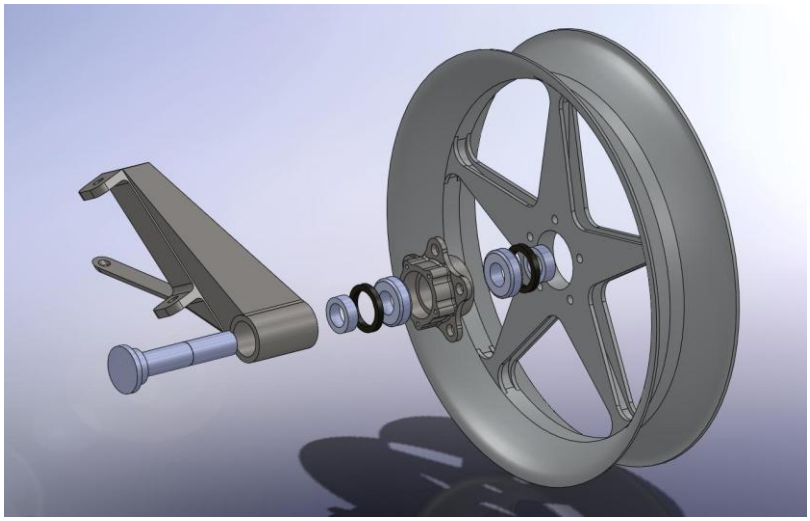

Figure 15: Exploded Hub Assembly

This section will detail the design, analysis and fabrication of the suspension components.

Knuckle

Design

The suspension upright, or steering knuckle, in a front A-arm configuration, connects the upper control arm to the lower control arm and provides a mounting location for the wheel. In addition, it rotates about the axis between the upper and lower joints of the suspension arms, hereafter referred to as the steering axis. A tie rod is attached to the knuckle by a steering arm that controls the knuckle rotation and vehicle steering. Functionally, the knuckle must hold the spindle, mount the brake caliper, serve as a steering linkage, and orient the steering axis as desired. The knuckle must also be strong enough to support the loading scenarios encountered through driving.

In order to produce negative camber through steering, the steering axis, defined as the axis through the spherical joints of the knuckle, must be inclined. The orientation of the steering axis is defined by the angles of castor and kingpin inclination, as illustrated in Figure 16.

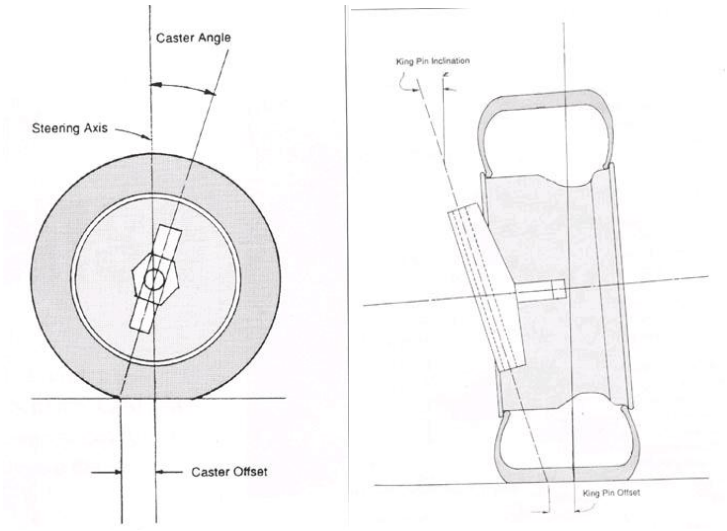

Figure 16: Castor (left) and Kingpin Inclination

Image from www.minimania.com

As castor is increased, the wheel effectively "lays over" as it is steered. At a set castor angle there is an optimal kingpin inclination which will produce the most camber within a range

of steering angles. The relationship between kingpin inclination to input steering angle is given by the following equations (Reimpell & Stoll):

Outside of bend: $\tan \sigma_{out} = \tan \sigma_0 \cos \delta_{out}$

Inside of bend: $\tan \sigma_{in} = \tan \sigma_0 \cos \delta_{in}$

Where,

σ_{out} or σ_{in} = KPI during cornering

σ_0 = KPI under initial design conditions

δ_{out} or δ_{in} = Steering angles

When accounting for castor, auxiliary angles are calculated as:

Outside of bend: $\tan(\sigma_{out}) = \tan(\sigma`)\cos(\delta`-\delta_{out})$

Inside of bend: $\tan(\sigma_{in}) = \tan(\sigma`)\cos(\delta`-\delta_{in})$

Auxiliary angles

$\tan(\delta`) = \tan(\tau_0)/\tan(\sigma_0)$

$\tan(\sigma`) = \tan(\tau_0)/\sin(\delta`)$

τ_0 = Initial Castor Angle

The camber of the tire relative to the camber at ride height for a given steering angle is then calculated as:

$\varepsilon_{W,out} = (\sigma_0 + \varepsilon_{W,0}) - \sigma_{out}$ or $\varepsilon_{W,in} = (\sigma_0 + \varepsilon_{W,0}) - \sigma_{in}$

$\varepsilon_{W,0}$ = Camber at ride height (0 steering angle)

Use these equations, the Matlab program in Appendix was written, allowing a static castor and kingpin inclination to be entered, and looping through the expected range of steering angles. As such the camber through steering could be plotted. It was apparent that as castor increased, the camber induced also increased. However, as the castor and kingpin inclination

angles of the steering axis increase, the intersection of the steering axis and the ground moves away from the contact patch of the tire.

The lateral offset of this intersection with the center of the tire is known as “scrub radius” as illustrated in Figure 17.

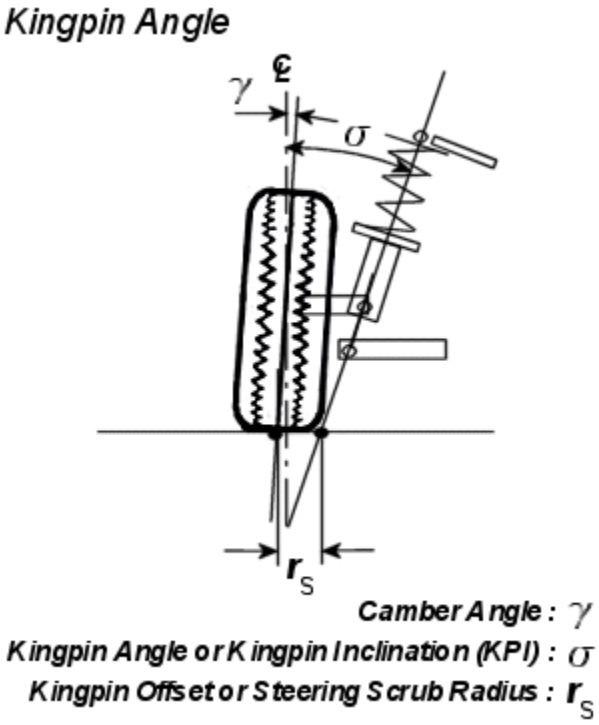

Figure 17: Scrub Radius Diagram

Image from www.lancerevoclub.org

In order to keep the tire in pure rolling when steered, this scrub radius must be kept at a minimum. Otherwise, tire friction with the ground will resist the effort of the driver when steering. Thus, when increasing kingpin inclination, the wheel must be offset away from the vehicle by the knuckle. This incurs greater moments on the body of the knuckle, and is more structurally demanding.

The distance from the center of the contact patch to the steering axis at the ground is known as castor trail, as illustrated in Figure 18.

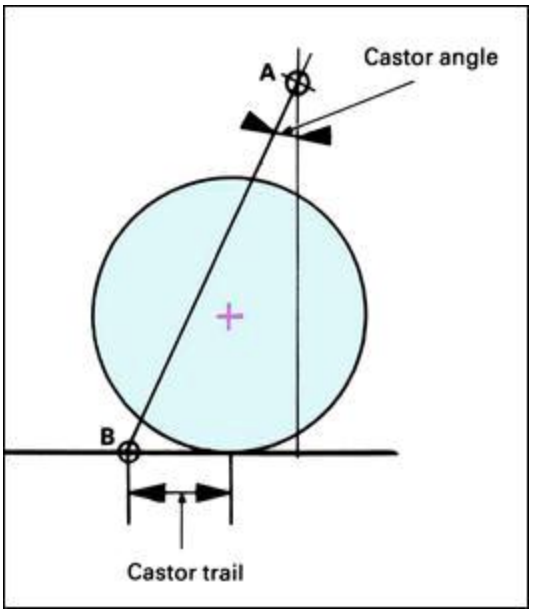

Figure 18: Castor Trail Diagram

Image from www.webpublications.com

Castor trail also has the effect of resisting driver effort, but as the friction force incurred by the tire is always directed opposite of the vehicle motion, a "return to center" moment is produced. A certain amount of castor trail is thus desirable to stabilize steering. However, at large castor angles, the castor trail will be greater that necessary and hinder driver performance. As such, the wheel must be offset forward by the knuckle. This will again incur greater moments on the knuckle and increase needed strength.

It was decided that a 4 inch longitudinal offset could be reasonably designed for, which would in turn allow a maximum castor angle of 25 degrees given the intended tire diameter and desired castor trail. Using the Matlab model, the optimal kingpin inclination at this castor was 20 degrees. This kingpin inclination would require a 3.5 inch lateral offset. The knuckle then had to be designed to orient the steering axis to these angles, and position the tire with the necessary offsets, while still resisting expected loads and remaining lightweight.

Due to the complex geometries and compound angles, the knuckle could not be a purchased part because none exist on the market today with our intended specifications. The design process for the knuckle went through multiple iterations with the focus of the proposed designs started with geometric constraints, then focused on structure, and finally were iterated for improved manufacturability.

The first few iterations of the knuckle design were intended to be machined or cast out of 6061 T6 aluminum. Iterations of the machined aluminum design can be seen in Figure 19.

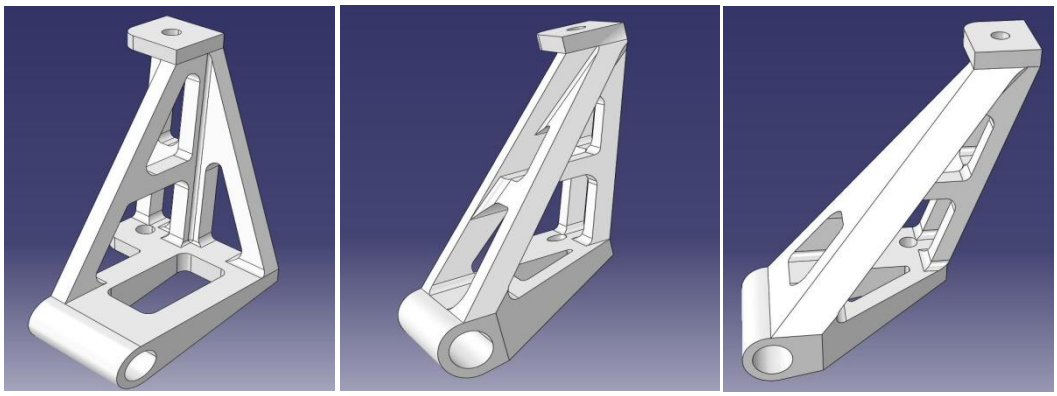

Figure 19: Aluminum Designs

Heading into the manufacturing phase it was decided that the final aluminum design would not be suitable for our purposes. This decision was made due to difficulties that would be encountered during machining. Due the complex nature of the knuckle's structure, machining the aluminum knuckle would required multiple refixtures and day's worth of machining time. In light of the machining difficulties, the chosen material for the knuckle was also reevaluated, and because aluminum has a finite fatigue life, it was decided that the knuckle should be made out of AISI 4130 sheet steel. In the past, aluminum knuckles have been problematic, breaking under extreme and repetitive loading during driving, so switching to a more durable material like steel should prove beneficial.

The final knuckle was a "torque box" structure utilizing .065 inch bent sheet steel. The design used the same geometrical constraints as the aluminum design, so no dimensional parameters had to be changed when changing materials. The sheet metal design is illustrated in Figure 20.

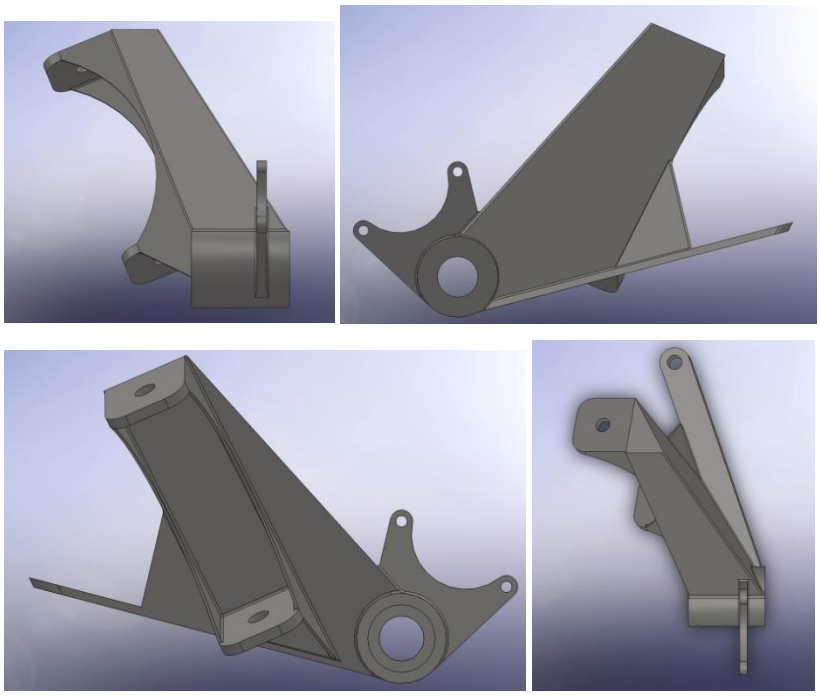

Figure 20: Sheet Metal Final Design

Because steel is a much heavier material than aluminum, it was an important consideration to maintain the same strength to weight ratio as the aluminum design. The final design had a final weight of approximately 3.5 pounds which was comparable to the weight of the aluminum design.

Finite Element Analysis

The knuckle was evaluated using the ABAQUS finite element program. From previous research done by the 2007 Baja team, it was determined that the most extreme loading condition the car would encounter would be a 3G loading of approximately 1500 pounds. It is important to note that this 3G load represents double the deceleration expected to be encountered, and a corresponding safety factor of 2. Based on basic material properties and general change after heat treatment, the knuckle has a yield strength of approximately 140 Ksi. In the suspension system, all the interaction between the knuckle and the wheels occurs in the spindle, therefore it was determined that all loading scenarios should be loaded through the spindle. The knuckle was tested under 6 specific loading cases to account for loading scenarios the knuckle would likely see under normal use conditions. The knuckle was loaded in the X, Y, and Z direction directly through the spindle. These loads simulated basic impact loads through the spindle,

whereas the most extreme cases actually occur as moment at the outermost radius of the tires. In these scenarios, the knuckle was loaded with 1500 pounds at a 12.5 inch moment arm. All 6 of these cases were used to pinpoint high stress areas and optimize the knuckle accordingly. The following results are analysis of the final production knuckle after iterative testing.

DIRECTIONAL CASES

X-Direction

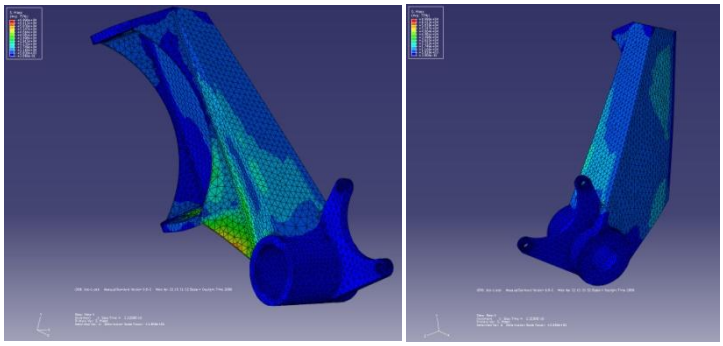

Figure 21: X Direction Loading Case

In the X-direction, the knuckle was loaded directly through the center of the spindle. This simulates a side impact directly into the knuckle. The peak stress in this scenario was approximately 64 Ksi, which is well below the yield strength.

Y-Direction

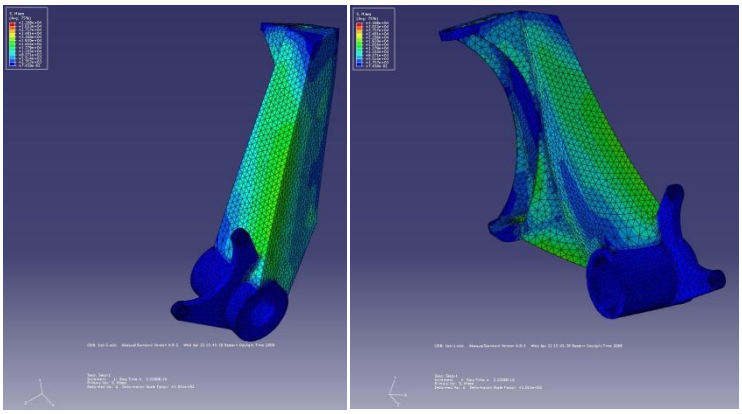

Figure 22: Y Direction Loading Case

The Y-direction was loaded vertically through the spindle, which essentially simulates the forces encountered through the cyclic motion of the suspension up and down. In this scenario, the highest stress seen is approximately 20 Ksi.

Z-Direction

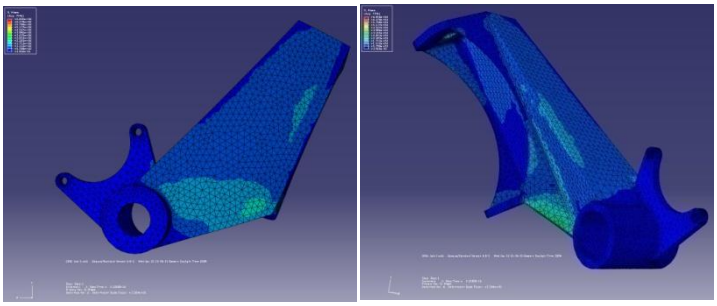

Figure 23: Z Direction Loading Case

The Z-direction is loaded from front to back through the spindle to simulate frontal impact at the spindle. The peak stress in this scenario is approximately 26 ksi.

The overall conclusion from the directional cases is that the knuckle can easily handle any of the forces encountered directly through the spindle. These results lend themselves to analyze the knuckle for areas of low stress where material could be removed and weight could be lessened, however, not until after all the moment cases are tested as well.

MOMENT CASES

It was determined that the most extreme loads encountered in the knuckle would be a moment about the tire radius. This is a 3G loading scenario located about a 12.5 inch moment. The Y- and Z-directions essentially simulate a side or frontal impact with a rock or log at the tires edge, whereas the X-moment is representative of the braking force. The knuckle was constrained at the ball joint mounts, and the force was applied to a reference point constrained 12.5 inches away from the spindle housing of the knuckle.

X-Moment

The moment about the X axis is an exception to the standard loading case because it is representative of the braking force. The moment incurred in this case is equivalent to the friction force at the contact patch multiplied by the tire radius. Given a friction coefficent of 0.65 and a 100% weight transfer to the front tires during breaking, the force at the contact patch was calculated to be 175lbs. The stresses produced in this case are significantly less than the 1500 lb impact cases detailed below.

Y-Moment

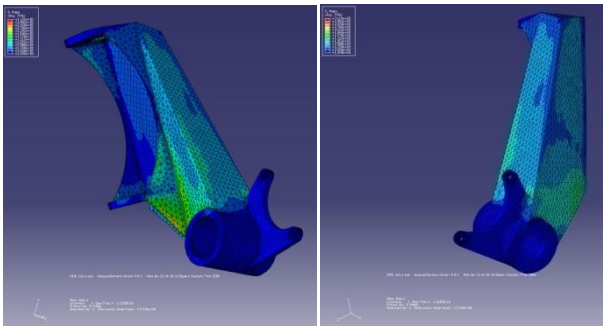

Figure 24: Moment About Y Axis

The moment about the Y axis was loaded laterally towards the interior of the car at a reference point constrained 12.5 inches away from the spindle mount. This loading scenario simulates a side impact into an object at a 3G load. In this situation, the maximum stress observed is 135 Ksi, which is the largest stress of any loading scenario. Prior to analysis this was

assumed to be the most vulnerable loading situation because of the way the kingpin is attached to the rest of the knuckle.

Z-Moment

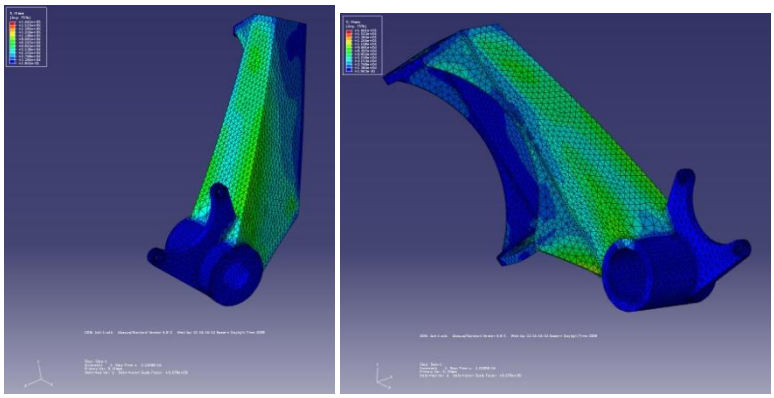

Figure 25: Moment About Z Axis

The moment about the Z axis loading case loaded the knuckle with 1500 pounds at a 12.5 inch moment arm. This loading situation represented an impact located at the front-most point of the wheel directed inward. The highest stress observed in this case was 124 Ksi.

Fabrication

The sheet metal body of the knuckle was modeled using the SolidWorks sheet metal feature. This resulted in a three-flange model as illustrated on the left-hand image of Figure 26 which could be unfolded to give the 2-dimensional profile seen in the right-hand image.

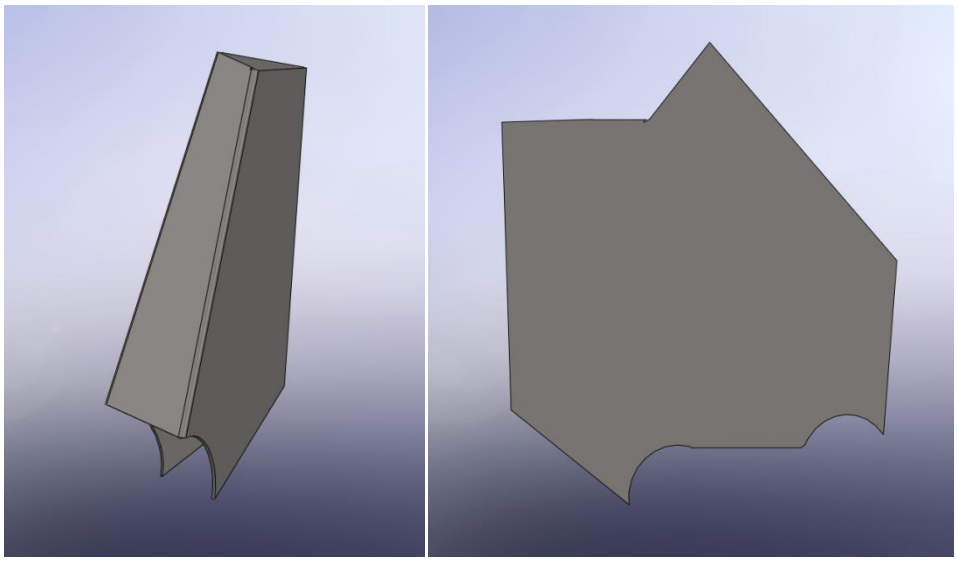

Figure 26: Sheet Model Bent and Unfolded

This profile was then CNC machined out of .065 inches sheet stock. Using a manual sheet metal bender, the inboard face of the knuckle was bent to the final angle measured from the model. In order to fully close the second bend, a custom jig was built to hold one panel down while allowing the other bend to fully close.

The additional sheet metal components including the 0.25 inches ball joint mounts, caliper mount, and steering arm, and .065 inches mount supports and steering arm gusset were CNC machined. The spindle housing was made from 2 inches cylinder stock and bored using a CNC lathe to the internal diameters as modeled.

Jigs were made to maintain the correct steering axis orientation during welding. The spindle housing was first clamped to the table. Next, a 20 degrees wedge was sheared from sheet stock, and clamped to the weld table running parallel to the spindle housing to maintain the desired kingpin inclination. A length of sheet was then bent to 25 degrees and clamped perpendicular to the spindle housing in order to maintain the desired castor angle. As such, the angles of the inboard face and back edge of the knuckle - corresponding to the kingpin inclination and castor angles - could be held absolute relative to the spindle housing. The features of the knuckle were then seam welded sequentially.

Control Arms

Design

The control arms serve as two of the four links in the A arm suspension, the other two being the knuckle and chassis (ground). With the geometry of the knuckle chosen, the track width defined, and the width of the bottom of the foot box defined, the only remaining design variable was the length of the upper control arm and in turn its point of attachment to the chassis. Using SolidWorks' sketch feature, the existing dimensions of the linkage were drawn, and the effect of differing the upper control arm's length observed. As the connection point of the upper arm corresponds to existing nodes of the chassis, the upper arm length was constrained to a limited range of values. Figures 28, 29, and 30 show the selected planar geometry at ride height, full compression, and full droop.

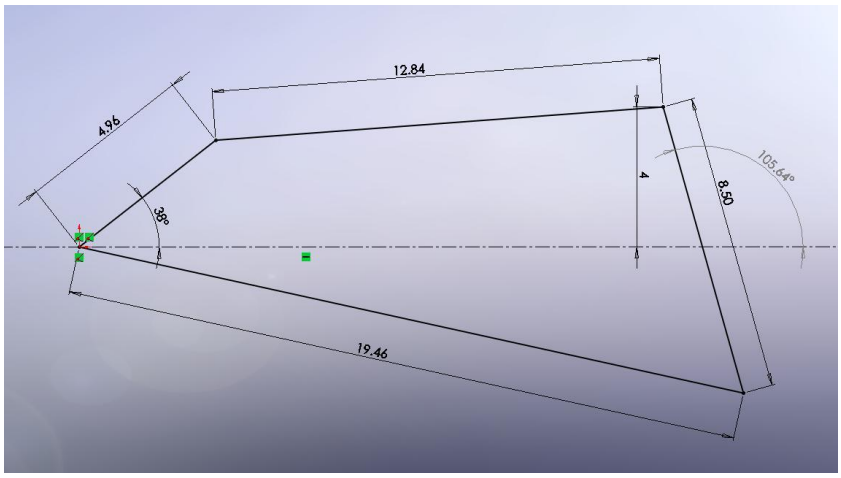

Figure 27: Front Suspension at Ride Height

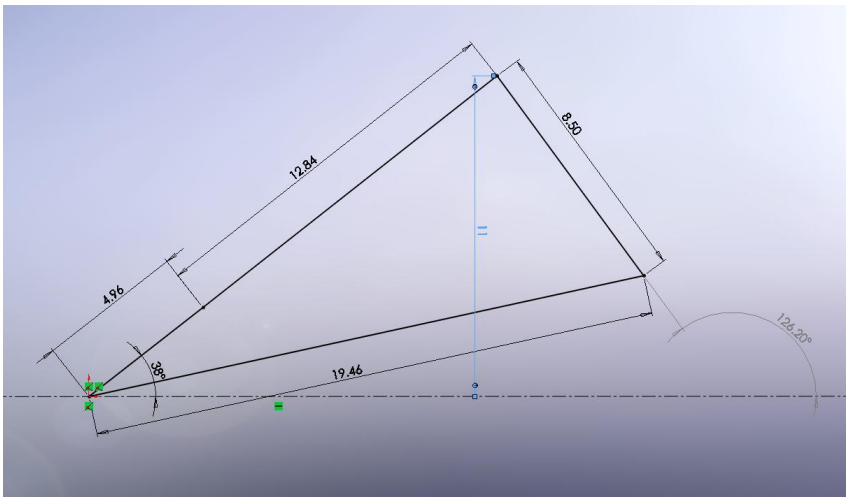

Figure 28: Front Suspension at Full Compression

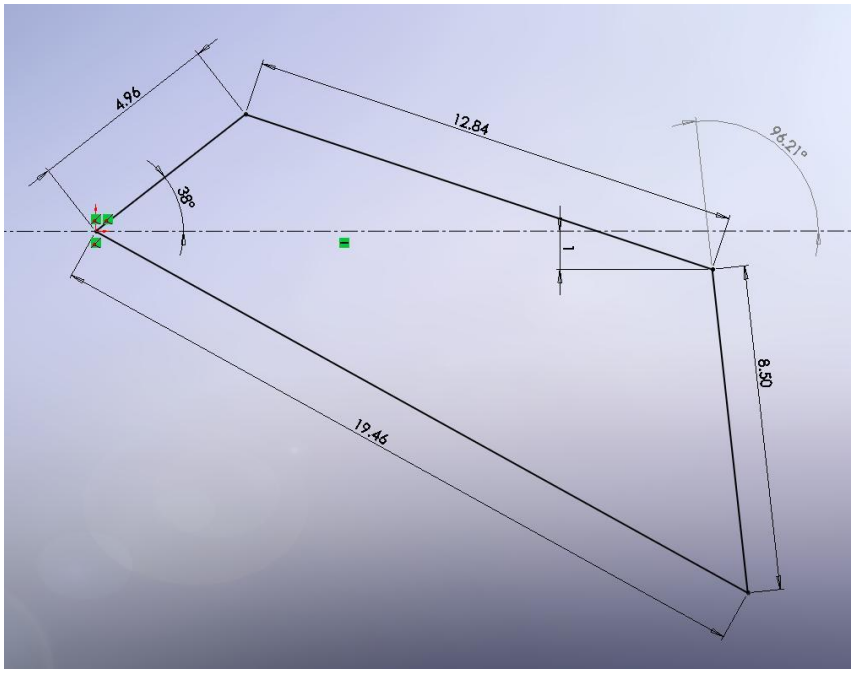

Figure 29: Front Suspension at Full Droop

This geometry results in approximately 20 degrees of negative camber in compression, and 7 degrees of positive camber in droop. The high kingpin inclination allows for a significantly shorter upper arm than lower, which provides high negative camber through kinematic motion, as was originally desired.

The arms were designed using 1.25 inches diameter 4130 tube stock. As was demonstrated by the 2007 team, stress distribution around the ball joint housing improves with

larger diameter tubing. Also, by increasing material spacing from the neutral axis, the material is used most efficiently to resist bending.

The upper arm would utilize a heim joint at each of its two mounts to the chassis, allowing static camber adjustment by threading the joint in or out. The lower arm mounts house delrin bushings acting as a pin joint. Once solid models were made given the necessary kinematic geometry, finite element testing was performed to determine the minimum necessary wall thickness of both the upper and lower arms.

Finite Element Analysis

The optimization of the front control arms was done through finite element analysis using ABAQUS finite element software. The solid models of the control arms were imported into the program, and a load of 1500 pounds, as with the knuckle, was applied as the extreme case. The analysis results would allow us to verify the minimal wall thickness under expected loading.

Frontal loads transferred through the spindle are distributed to the upper and lower arm in a ratio equal to the ratio of the distances from each ball joint to the spindle. As the knuckle is designed to place the lower ball joint at the same height as the spindle, nearly all frontal impact force is reacted through the lower arm. As such, the lower arm was loaded with a full 1500 lbs in this case. Side impact cases put the arms in compression, and were negligible in comparison to the frontal impact bending scenario. As with previous years, the minimum wall thickness allowable for the lower arms was found to be 0.065 inches at a 1.25 inch diameter.

The upper arms are mainly used for positioning, and a worst case scenario is incurred in tensile and compressive loading where the bottom of the tire is impacted and the lower ball joint serves as a lever for force transfer. In this case the load is equal to 1500 lb times the ratio of the tire diameter to the knuckle height, resulting in an upper arm load of 1125 lbs laterally. In this case, 0.035 inch wall tube sufficiently handles the incurred loads.

Fabrication

The ball joint housings were made from 2 inch cylinder stock turned down to a 1.5 inch OD. The inside press fit surface was bored to 0.22 inches (the OD of the ball joints) minus 5 ten-thousandths. A spring clip groove was bored .125 inches above the press fit surface, placing the clip at the top of the ball joint when pressed in.

The tube features of the control arm solid models were unwrapped and printed, and these templates wrapped around the appropriate tube stock. The tubes were then notched using a bench grinder conforming to the templates.

The bushing housings of the lower control arms and the rod-end holders of the upper arms were spaced using threaded rod and washers. A template was drawn on the weld table orienting the tube members and ball joint housing relative to the bushings (the rotation axis of the arm). A lockable protractor with a clamped piece of sheet stock was used to angle the ball joint housing relative to the plane of the weld table. Once all components of each arm were in place they were tacked and seam welded.

Front Hub

Design

The hub pictured in Figure 30 was designed to mount the wheel and brake rotor, and houses two taper bearings.

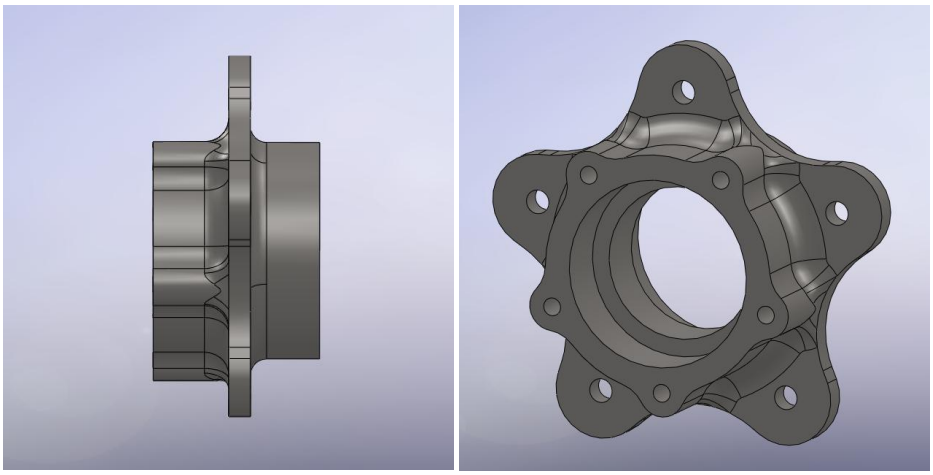

Figure 30: Hub Model

It was desired that the wheels be interchangeable front and rear, and so a 5-hole bolt pattern with 1.75 inch radius was to be used on both the front and rear hubs. The outer diameter of the hub corresponds to a clearance fit with the inner diameter of the wheel at 2.25 inches. The inner diameter corresponds to a press fit with the outer race of the selected bearing, a 1 31/32 inch Timken taper bearing with 1600 lb thrust load capacity. This gave a ~ 1/8 inch wall thickness surrounding the bearings. The wheel-side flange face was spaced from the rotor

mounting face such that the brake caliper would have sufficient clearance. The width of the hub (length along the spindle axis) was dimensioned such that the wheel flanges are centered, loading each bearing equally. This resulted in a width of 1.975 inches. The bearings are spaced by an internal lip which is loaded by the outer bearing race.

Finite Element Analysis

Once the solid model was created, FEA was performed using ABAQUS to optimize material thicknesses where possible. The intended material was AISI 4140, given its availability in the stock size needed, machinability, and high yield strength through heat treatment. By heat treating the hubs, the expected yield strength was ~ 140 Ksi. The hub was given boundary conditions limiting translation and rotation at the flange holes, and loads were applied to the bearing contact surfaces. The extreme loading case was a 1500 lb. impact at the outside edge of the tire (12.5 inch moment arm), where a single flange is in line with the impact point. This load case is illustrated in Figure 31.

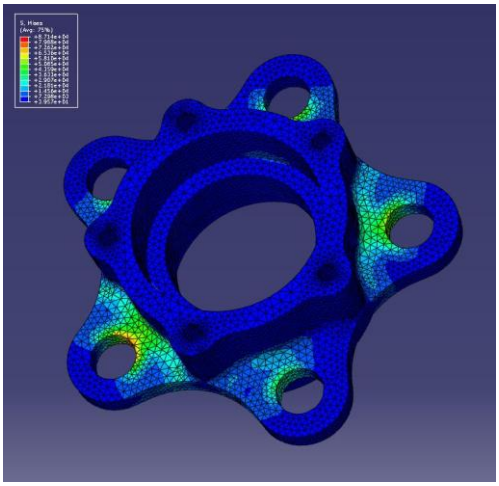

Figure 31: FE Model of Hub

Given the initial stresses seen, the original flange thickness of 3/8 inch was reduced to ¼ inch. With these final dimensions the hub was predicted to weigh 1.79 lbs.

Fabrication

The billet for the hubs was 5 inch diameter by 2 inch long round stock 4140. The parts were CNC machined, using a surfacer for most of the volume removal, an end mill for contouring, and a ball end mill for the radii at the flange bases. The internal bore was also done on a CNC mill. A micrometer was used to measure the bearing race diameter exactly, and the ID of the hub was left ~ 5 ten thousandths under this dimension resulting in an interference fit. The holes for mounting the wheel and rotor were hand tapped 3/8 inch – 16 and ¼ inch – 20 thread respectively.

Rear Suspension Design and Analysis

The rear suspension we decided to use on this car is not a customarily used design in the Baja SAE competition. It has been used before by a couple teams including Western Washington who won the suspension design award for it. The rear suspension used on this car was decided upon through numerous decision matrices gone through with the team. Included in the decision making process was; weight, complexity, manufacturing time, cost, durability, kinematics of motion and numerous other parameters. After a lengthy decision process the team decided to go with a setup that utilized a single upper control arm that is double pin jointed to the knuckle and a longitudinally stressed axle that will double as the lower control member and torque transmitting axle. This setup if done correctly can be done typically lighter than most other set ups. It is lighter than a conventional double wishbone geometry which uses an upper and lower with an axle strictly for transmitting torque. The independence of the system allows the cars wheel to move without affecting the geometry of the opposing wheel. This allows the car to traverse more harsh terrain with less movement of the chassis.

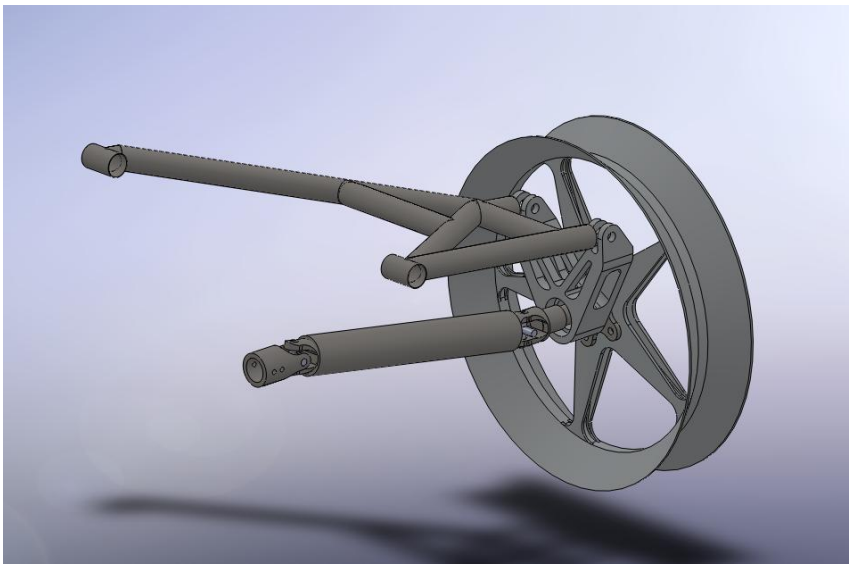

Figure 32: Rear Suspension Assembly

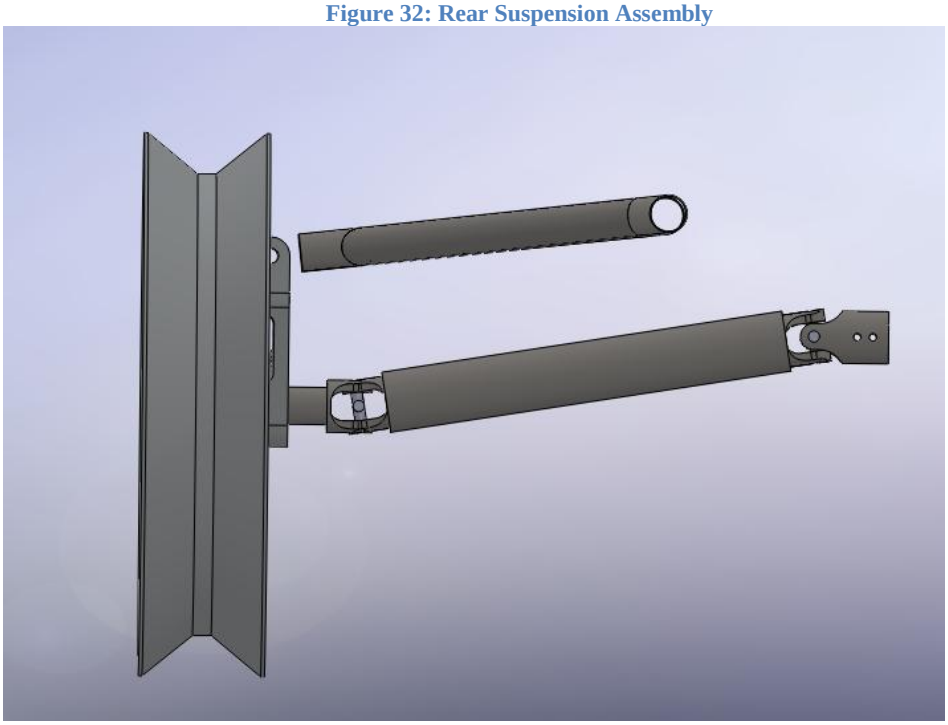

Figure 33: Rear Suspension Front View

Although you remove a member from the typical geometry of a double A-arm system, you make the system more complex. The axle needs to be designed such that it does not change length so it can be used as a control member. The axle also must be robust to handle the torque produced from the motor as well as the compressive and tensile forces of the wheel impacts. For these and other reasons a carbon fiber axle was used in our rear suspension. Carbon fiber has

many advantages over a typical aluminum and steel drive axle. It is lighter and more ductile. It will bend more will still remaining intact. It can be epoxied with great strength to many materials.

U-joints were chosen for the driveline. They allow the axle to vary its angle in all directions while not allowing a change in length. This allows them to act as ball joints in the lower suspension system like a standard A-arm. They can be purchased rather cheaply and modified to fit many scenarios.

Once the U-joints and axle were chosen the angular displacement of the lower member could be determined. The more in line the axle is with the wheel spindle the more efficiently it can transmit load into the chassis. In order to minimize the angle between the axle and spindle the length of the axle must be maximized. The limiting factor on the axle length track width in the rear. The axles can only be so long to allow for the gearing/motoring system as well as knuckle/wheel configuration. The maximum length that could be attained was 15.42 inches. The rear suspension also needed to droop to gain 2.5 inches at ride height to attain the desired 11.5 inches. of ride height.

To reduce the side loading the wheels must endure the rear suspension geometry was to be designed to camber the wheels a significant amount in max compression and full droop. The maximum camber that could be maintained while keeping the roll center and upper control member mounts in a manageable location was 9.56 degrees. The maximum camber change in max droop is 2 degrees. When the suspension is in maximum compression the axle is at an angle of 17.28 degrees and in full droop an angle of 29.14. These values are well within the efficient transfer of torque and loads of the U-joints.

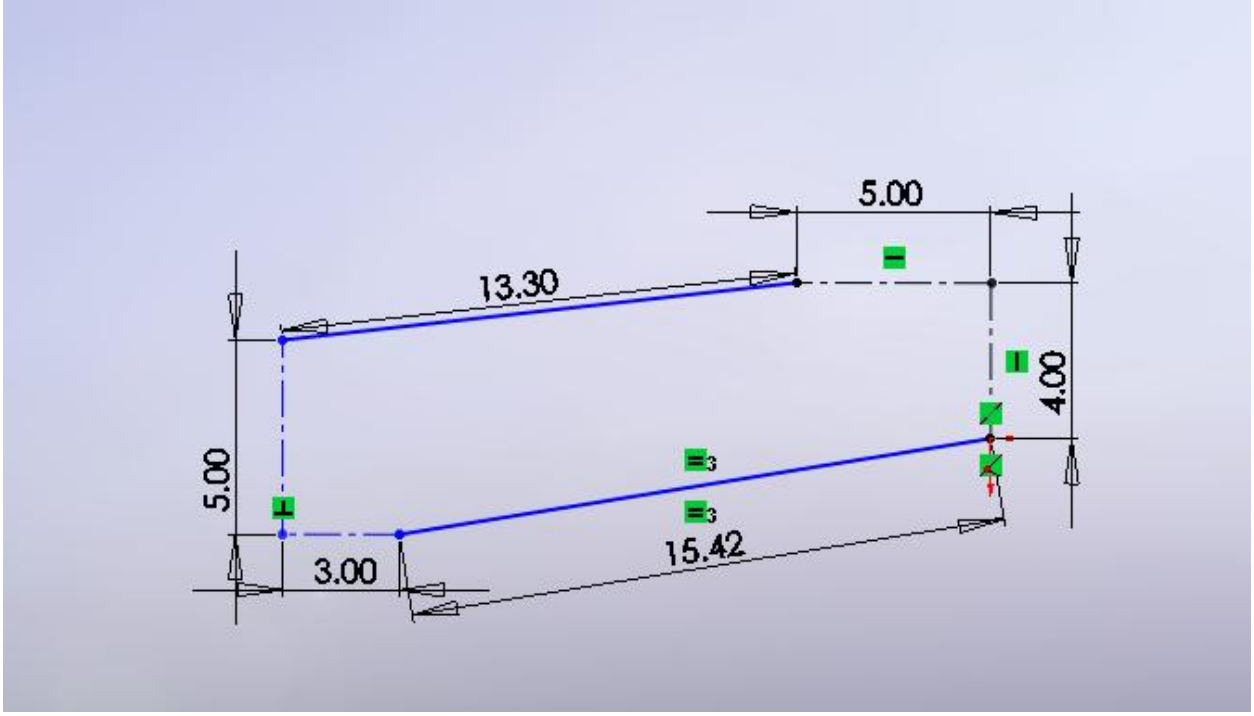

Figure 34: Planar Geometry

To model the kinematic motion of the rear suspension a Matlab file was made. It became complex and hard to use. Since the motion of the rear suspension does not vary with steering the model could be made in a 2-D system. A drawing was made in SolidWorks and parameters were guess and checked in an iterative fashion until favorable parameters were met. In the future a better method could be used to determine the rear suspension geometry. This method worked well and was near fool proof. No lengthy calculations were necessary and kept mistakes to a minimum.

All components of the rear suspension were drawn in SolidWorks. This allowed them to be created in an assembly to test the functioning of the rear suspension. Since CosmosWorks is an extension of the SolidWorks family finite element analysis was utilized on all rear suspension components to determine the proper sizing.

The upper rear arm was designed and iterated through SolidWorks and CosmosWorks. The chock placement on the upper arm is not ideal but because of the geometry and limited room in the aft of the vehicle there were not many places for it. Ideally the upper arm would not have a member between the forward facing arm and the triangulating member. It puts both members in a bending scenario which lowers their strength.

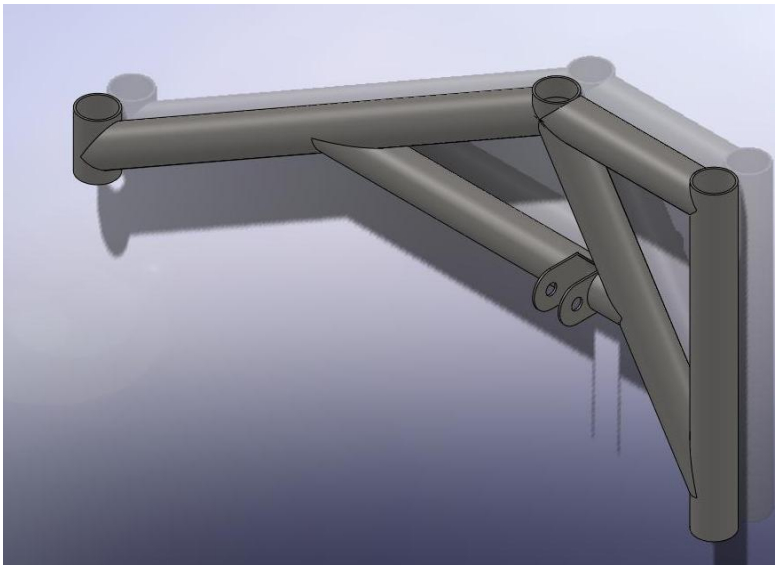

Figure 35: Rear Upper Control Arm

The wall thickness was determined through FEA run on the component. The upper arm will use heim joints on both inner and outer mating. This will help to reduce the binding of the connections and reduce energy losses in the system. It also allows for more adjustment to be done to the system. Since there is no lower arm to also modify length more adjustment in the upper arm is beneficial. The FEA was done with a 1000 lb load towards the rear of the car as well as 1500 lbs up with a 1500 lb shock load. The shock load was calculated from the engineering data given through the shock company and the rest of the data was gathered from previous year's values to prevent from breaking components.

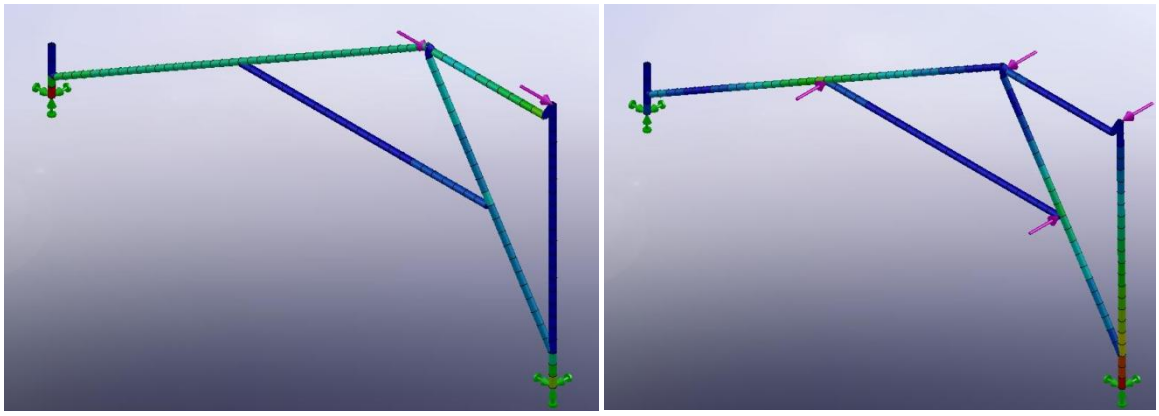

Figure 36: Rear Upper Arm FEA

The axle was made from 2 kinds of purchased parts which were then modified to be used in our particular application. The axle is made from a carbon fiber tube laid in a filament wound configuration that was purchased from CST Composites in Australia. The U-Joints were purchased from Curtis Universal and are rated to handle 1000 Ft-lbs of torque and 2500 lbs of compression or tension. To attach the two 3m donated an Aerospace utilized epoxy, Ec-2216. The area of mating between the U-joints and axle is 9.2 sq. in. and the epoxy can withstand 1400 psi of shear stress. This allows the axle to handle well over the 1500 lbs of tension or compression as well as over 500 ft-lbs of torque. CosmosWorks was used as an FEA solver to iterate the design. The axle was loaded in a longitudinal direction with 1500 lbs and axially torque with 500 ft-lbs.

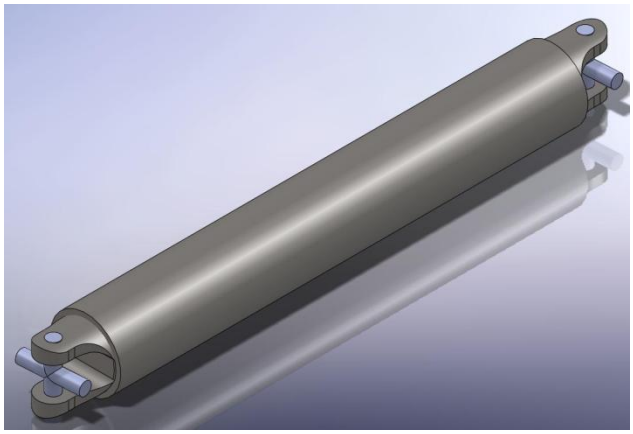

Figure 37: Stressed Axle Model

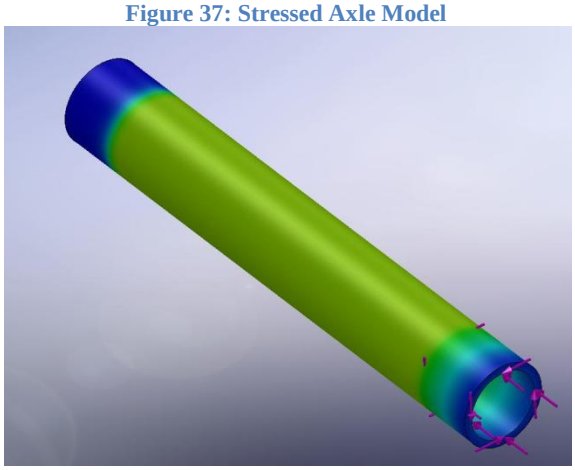

Figure 38: Carbon Fiber Axle FEA

The rear knuckle was designed to fit inside the wheel while holding the upper control member and lower control member/axle in the correct geometric places to allow the suspension

to move properly. The knuckle was designed to offset the lower u-joint 3 inches from the upper control member mount and also to displace them vertically 5 inches. This gives rather long moment arms to the design that must be overcome to produce a structurally worthy arm. Since the wheel has a 25 inch outside diameter when the forces applied to it are transmitted to the knuckle the stress gets rather large. To reduce the amount of stress seen in the knuckle the width of the knuckle needed to be maximized while allowing room for axle length. Aluminum can be easily purchased in 2 inch thick pieces which was a factor in designing the knuckle. The knuckle was designed to be easily and cheaply machined while being relatively light and robust. The knuckle also unlike the front needed to allow the axle to pass through it while allowing it to spin and transmit torque to the ground. This meant bearings needed to be part of the design. To handle the lateral loads taper bearings were used.

The knuckle was designed like the other rear suspension components through much iteration in CosmosWorks and SolidWorks.

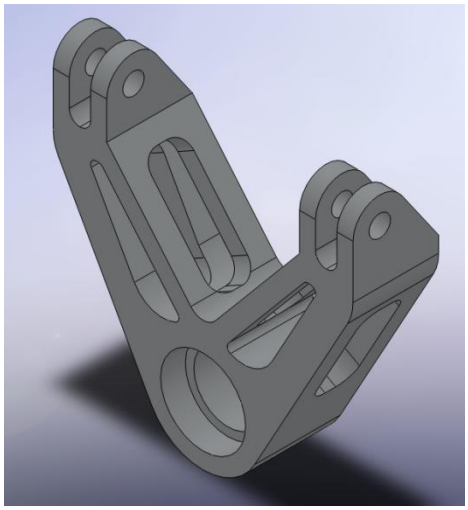

Figure 39: Rear Knuckle Model

To transmit the torque between the axle and wheel a spindle was used. It is made from a 1 inch outside diameter piece of AISI 4130 and is threaded on one end and welded to a U-join end on the other. It sandwiches the hub in the middle and holds the bearings to the correct tolerance. The 1 inch shaft is slightly larger than necessary and could be hollowed but because of the keyway cut in the shaft to hold the hub in place it will lose much of its capabilities. The design and analysis was done in SolidWorks and the FEA was done through CosmosWorks.

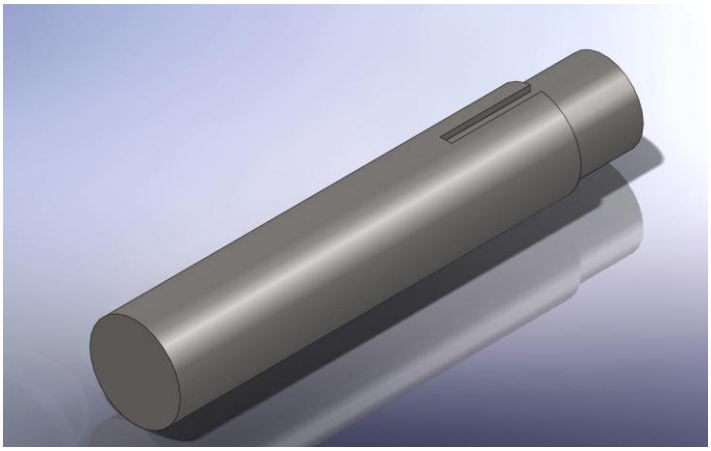

Figure 40: Rear Spindle Model

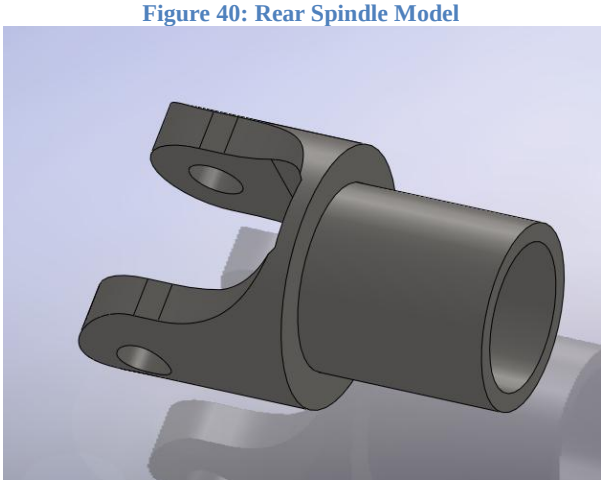

Figure 41: Universal Joint Model

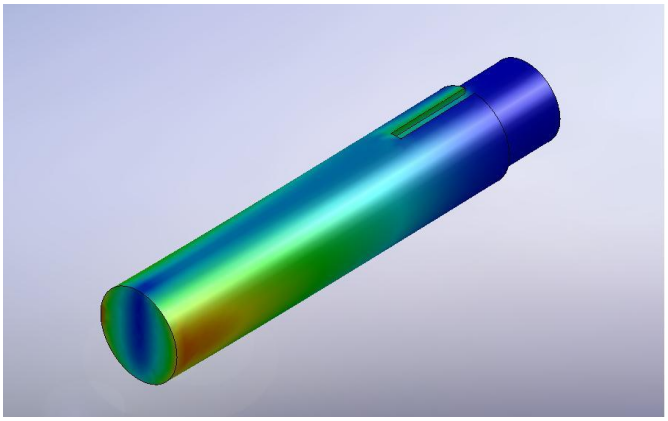

Figure 42: Rear Spindle FEA

The hub for the rear suspension is designed to transmit the torque from the spindle to the wheel. It sees much stress as the link between the wheel and the rest of the suspension. The track

width was mostly taken up by the axle and knuckle geometry so there was limited room for the hub. For this reason the hub was made from AISI 4130 steel and was heat treated to handle the stress it was going to see. This allowed the hub to be relatively lightweight and still robust. The ears of the hub are .25 inch thick and can still handle the 1500 lbs of side load the wheel was designed to see. The hub was drawn and designed through SolidWorks and CosmosWorks. It was designed in an iterative fashion. It was loaded in a 1500 lb side load configuration as well as a 500 ft-lb of torque seen in the axle.

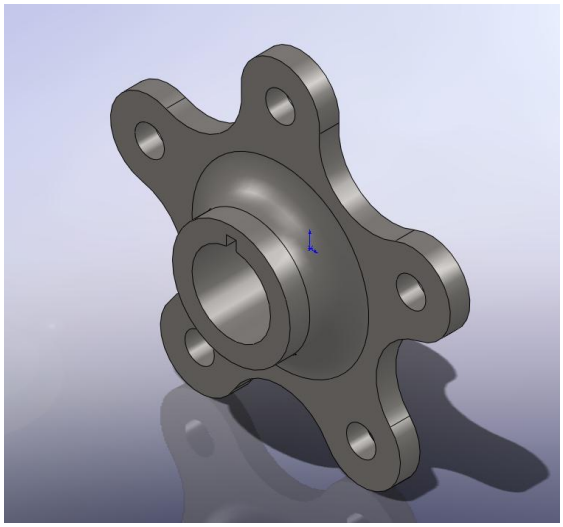

Figure 43: Rear Hub Model

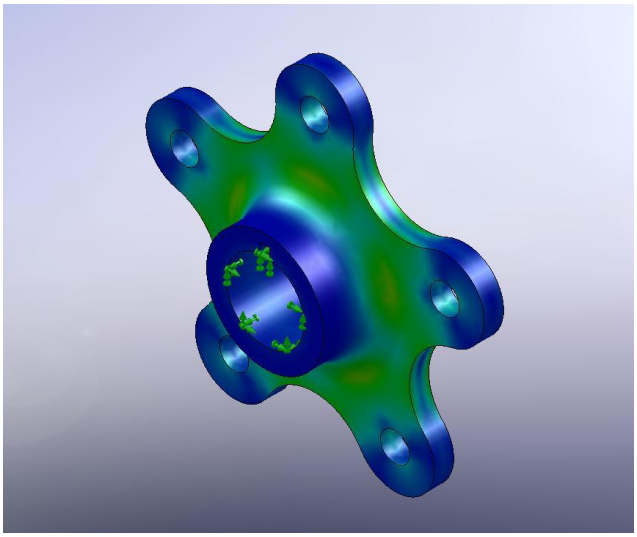

Figure 44: Rear Hub FEA

Rear Suspension Manufacturing

The rear suspension was manufactured over C-term 2009. The knuckle was machined from a 2 inch thick piece of 6061-T6 aluminum. It was machined in a Haas VF-4 vertical milling center in WPI's Washburn shops. It had to be refixtured 5 times to fully complete the part. It took 5 hours to machine and cost $45. The main concern with machining of the knuckle was the 2 inch depth. It needed small tooling to contour the pockets. Small tools that are long vibrate in the part and produce a poor surface finish. This meant that special tooling needed to be purchased to machine the parts. The tooling used was a ¼ inch 3-flute flat carbide end mill and a ¾ in 3-flute flat carbide end mill.

The upper arm was constructed from hand notched and bent .065 inch wall tubing. It was welded in WPI's weld shop. The plugs needed for the ends of the tubes to thread in the heim joints were turned on a Haas TL-1 lathe in the Washburn shops. The plugs were welded and then tapped to the right specifications. After all welding was done the upper arm was fixture to maintain its dimensions and sent out for heat treating. This allowed the part to be stronger than it was previous to welding allowing it to be lighter and stronger.

The hubs were machined for a 5 inch round piece of AISI 4130 steel. They were machined on a Haas VF-4 in WPI's Washburn shops. The machining time took 4 hours. The tools used were; 15/32 4-flute flat carbide end mill, 3 inch 4-flute carbide insert face mill; 5/16 4-flute ball nose carbide end mill; and a 3/8 2-flute high speed steel drill bit. The part was sent out for heat treating after completion to increase the stress the part could handle before failure. This allowed it to be more lightweight without reducing strength.

The axle was made from a tubular piece of carbon fiber with a 3.5mm wall thickness. It was mated to the U-joints with 3m EC-2216 epoxy. The U-joints were machined from their original dimensions to reduce weight. The interior of the U-joint was relieved of material on a Haas SL-10 Lathe. The parts were then cleaned with an acetone cleaner, sand blasted, re-acetoned and then epoxied. The epoxy was designed to cure at 200 degrees Fahrenheit for 30 minutes. The part was left for 45 minutes to assure the temperature penetrated through the carbon tube into the joint.

The spindle was made from a 1.25 inch OD piece of AISI 4130. It was turned down on a Haas TL-1 lathe to the proper dimensions to interface with the bearings/hub. The key was then machined in a Haas MiniMill vertical milling center.

Wheel Design and Analysis

Moment of Inertia

To determine the Moment of Inertia (MOI) of the previous MQP's wheel/tire choices an experiment was undergone in the Washburn shops. If the MOI of an object can be determined about any axis parallel to an axis of interest the MOI of the axis of interest can be determined through the parallel axis theorem. The MOI of an axis can be determined by allowing an object to oscillate about the axis and timing the period of oscillation. If the weight of the object and distance from the axis of interest is known then the MOI about the axis of interest can easily be determined through the formula:

$$I_{zz}=Wr(\tau/2\pi)^2-\frac{W}{g}r^2$$

Where,

I_{zz}= Moment of inertia, W= Weight of the object, r= distance between axis and central axis, g=acceleration due to gravity.

Figure 45 - MOI Testing

The original thought was that the MOI of the motorcycle wheels/tires would be less than that of the ATV wheels/tires. So far, the analysis doesn't agree with that hypothesis. There are numerous reasons for this and it may be too early to decide. It should be stated that thus far in the testing the parameters for testing have not been set. To accurately design an experiment only one parameter should be changed. It is a biased test to try to decide which will have a higher MOI if you do not take into account the tire sizes and there subsequent affects. The design for this year's car is for 25" outside diameter tires. In order to decide if the ATV or motorcycle tire has a higher MOI the test would need both a 25" ATV and motorcycle tire. This test used a motorcycle tire in excess of 27" and ATV tires less than 23". This is going to create dramatic changes in MOI. The most contributing effect to MOI is the radius of the tire.

Oscillations	5	10	20
Time 1	8.1	15.5	31.7
Time 2	8.1	15.6	31.4
Time 3	7.9	15.7	31.7
Time 4	7.9	15.7	31.7
Time 5	7.5	15.8	31.8
Average	7.9	15.66	31.625
Oscillation time	1.58	1.566	1.58125
Radius	8.9375		
Weight	13		
Izz	7.358694		
Transport	32.24925		
Icg	39.60794		

Table 12: Dunlop D756 110/100-18

Oscillations	5	10	20
Time 1	7.5	15.1	30.2
Time 2	7.7	15.2	30.3
Time 3	7.8	15.3	30.1
Time 4	7.6	15.3	30.2
Time 5	7.6	15.2	30.3
Average	7.64	15.22	30.2
Oscillation time	1.528	1.522	1.51
Radius	3.59375		
Weight	23		
Izz	4.773862		
Transport	9.225028		
Icg	13.99889		

Table 13 - Carlisle Badlands

Oscillations	5	10	20
Time 1	6.8	13.6	27.1
Time 2	6.9	13.4	27
Time 3	6.7	13.5	26.9
Time 4	6.8	13.4	27.1
Time 5	6.8	13.6	
Average	6.8	13.5	27.025
Oscillation time	1.36	1.35	1.35125
Radius	4.6875		
Weight	20		
Izz	4.335937		
Transport	13.64761		
Icg	17.98355		

Table 14 - Carlisle at489 at23x7-10

Wheel Acceleration

The wheels and tires used in the previous years of the SAE Baja projects here at WPI and throughout the competition have been an ATV style. This year the team is incorporating an off-road motorcycle style wheel and tire. One of the reasons to use a motorcycle style tire was to reduce the moment of inertia of the wheel and tire combination. This will increase the acceleration of the wheel under a given torque. The tire and wheel follow a linear pattern of acceleration under a given applied torque.

$$T = I_{zz}\alpha$$

Where,

T= Applied Torque, I_{zz}= Moment of inertia of the wheel about its central axis, and α = wheel acceleration.

Torque	At489			Badlands			D756
100	5.560637			7.143367			2.524742
125	6.950797			8.929209			3.155928
150	8.340956			10.71505			3.787114
175	9.731115			12.50089			4.418299
200	11.12127			14.28673			5.049485
225	12.51143			16.07258			5.680671
250	13.90159			17.85842			6.311856
275	15.29175			19.64426			6.943042
300	16.68191			21.4301			7.574227
325	18.07207			23.21594			8.205413
350	19.46223			25.00179			8.836599
375	20.85239			26.78763			9.467784
400	22.24255			28.57347			10.09897
425	23.63271			30.35931			10.73016
450	25.02287			32.14515			11.36134
475	26.41303			33.931			11.99253
500	27.80319			35.71684			12.62371
525	29.19335			37.50268			13.2549
550	30.58351			39.28852			13.88608
575	31.97366			41.07436			14.51727
600	33.36382			42.8602			15.14845
625	34.75398			44.64605			15.77964
650	36.14414			46.43189			16.41083
675	37.5343			48.21773			17.04201
700	38.92446			50.00357			17.6732

Table 15 Acceleration vs. Torque

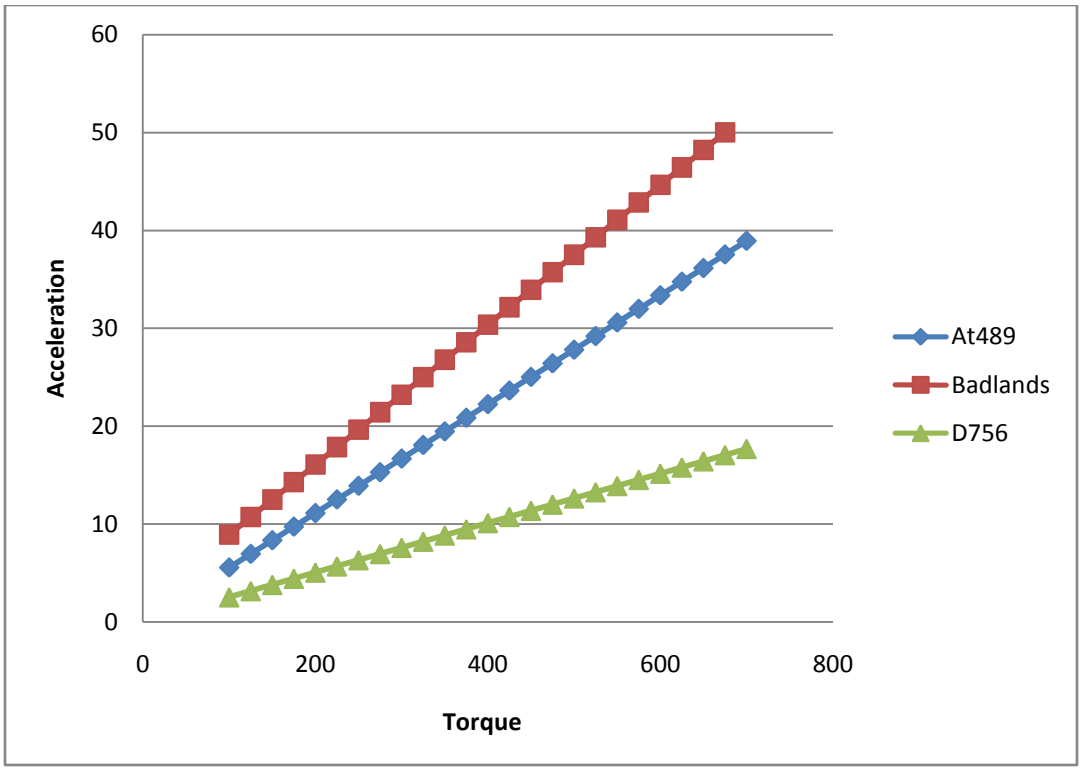

Figure 46 - Wheel Acceleration vs. Applied Torque

In the design of the Baja car for this year, an idea that was incorporated was motorcycle style tires. In order for this to be accomplished, the rest of the car needed to be designed with this in mind. We have encountered numerous obstacles this year while trying to use wheels in this style and dimension.

The major problem with using a motorcycle style tire on this or any car is wheel design. On a motorcycle, the wheel is designed such that most loads are transmitted radially into the hub/axle. This is accomplished by cambering the wheel to turn the vehicle. This is explained in greater detail in the front suspension section. A by-product of cambering the wheel to induce turning is the force transmitted to the wheel is ideally planar with the wheel. On most cars, the wheels do not camber much if at all. Since the wheels do not camber the force is not transmitted efficiently into the hub/axle. Instead any lateral force is used to create a large moment on the wheel mounts. It causes a lot of stress in the wheel and wheel mounting apparatus.

To use the motorcycle tires on the car we needed to design our own wheel to incorporate the tire size with the strength of a car wheel. A typical motorcycle tire is not sized to fit on a car

or ATV rim so mounting the tire on a wheel designed for this loading was not an option. Also, mounting the motorcycle style tire on a motorcycle wheel was not an option because the wheel is not designed for the side loads. For these reasons, the wheel needed to be custom designed and fabricated.

The wheel size chosen for this car was seventeen inches. This size was chosen based on availability, weight, price, and the correct outside diameter. Due to the generosity of All-American Wheel Co., ten aluminum wheel blanks were donated to the team. These blanks had the dimensions of a standard motorcycle tire; 17 inches in diameter and 3.5 inches wide. This allowed the team to create the wheels necessary. A size of twenty five inches was chosen as a tire outside diameter parameter. This was a good size for ground clearance, rolling resistance, moment of inertia and others. Once the wheel size was chosen tires were determined for the car and material to manufacture the wheel out of was found.

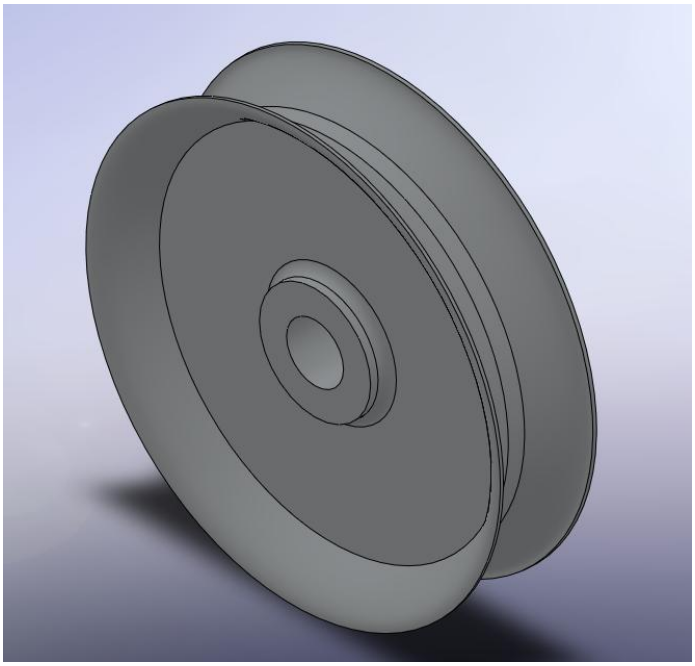

Figure 47: Wheel Blank Model

The wheel blank started as a 24 lb slug of 6061-T6 aluminum. Wheel design began by determining what parameters of the wheel were most important. The team wanted to be able to use the same wheel/tire on the front or rear of the car. To do this, the wheel needed to be designed with a bolt pattern that would work with both the front and rear suspension and knuckle

set ups. A bolt pattern of 5 x 1.75 inches was chosen. This allowed ample room for the front hub which was the major concern with the packaging of the wheel.

With the bolt pattern chosen, the design process began by looking at previous vehicle wheel designs. It was seen that a standard design for motorcycle and car wheels is a spoke design that uses a varying numbers of spokes. A typical number of spokes is between 3 and 12. Differing amounts of spokes are stronger in different scenarios as well as weight configurations.

The wheel blank was modeled and used in CosmosWorks to start to design where material could be removed while still maintaining a strong wheel. The finite element method was used to break the part down and determine where stress concentrations were in the wheel. After numerous attempts with varying amounts of spokes it was determined that a 5 spoke design would be best suited for our configuration. Using 5 spokes allows the stress to adequately transmit into the hub. If more spokes were used, the odds of an impact on the wheel directly loading a single spoke increases. If less spokes are used, a force between the spokes is used to twist the spoke rather than bend a spoke. An ideal force would be directly in between two spokes and would cause the spokes to be in bending and not torsion.

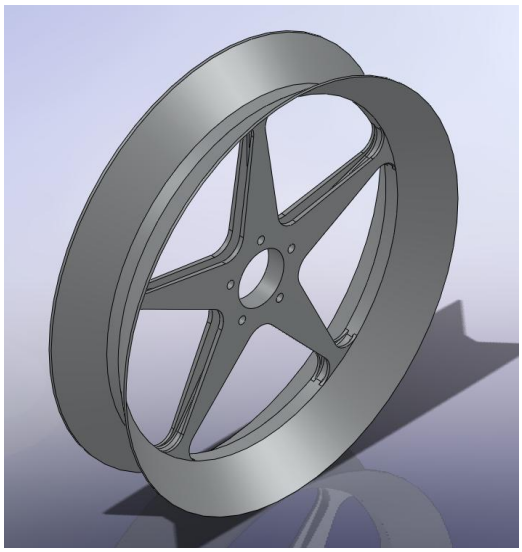

Figure 48: Final Wheel Design

After much iteration and with the help of FEA, a wheel design was chosen. After machining, the weight of the wheel is 6.5 lbs and can handle side loading of up to 1500 lbs. The wheel was also designed to handle in excess of 1500 lbs of torque axially and be able to handle a radial force of

2000 lbs. These numbers were chosen from what has been successful in previous years of WPI's Baja MQPs.

To increase the side loading stiffness and decrease the weight of the wheel, an I-beam configuration was used on the spokes. This removes material from where it is least efficient and keeps material where it the most useful to the structure. The wheel was also designed so that it could be machined here at WPI's machining facilities to reduce manufacturing costs. Some original design concepts incorporated welding in additional material to improve stiffness, but because of the added time and cost of manufacturing these concepts where not used.

The wheel was extensively tested and iterated with the use of FEA within CosmosWorks and ABAQUS. CosmosWorks uses a much larger element size and is therefore not as precise as ABAQUS. CosmosWorks was used as a preliminary design check because of its timely completion of analysis. ABAQUS was used to make sure the information output from CosmosWorks was accurate. Many times in the design process, it was seen that CosmosWorks could be off as much as 80%. For this reason, it was only used as a preliminary FEA solver.

The three loading scenarios checked in the FEA solvers are side loading, torque loading, and a landing scenario.

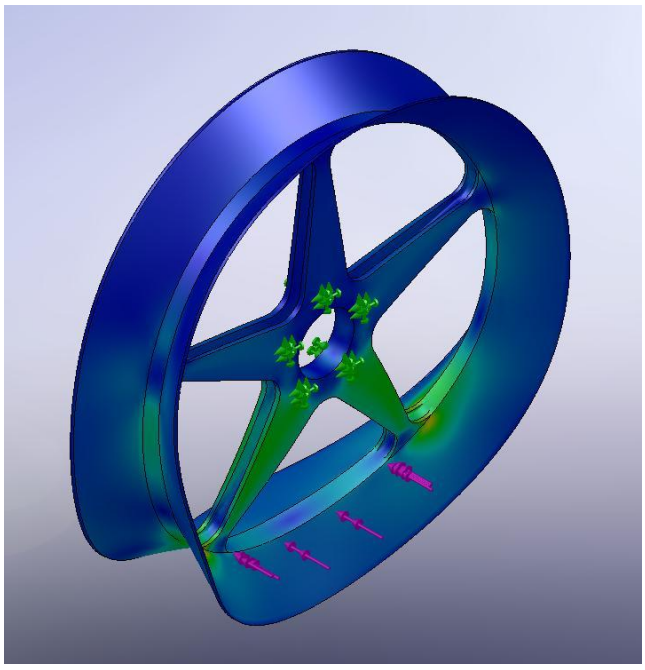

Figure 49: Side loading

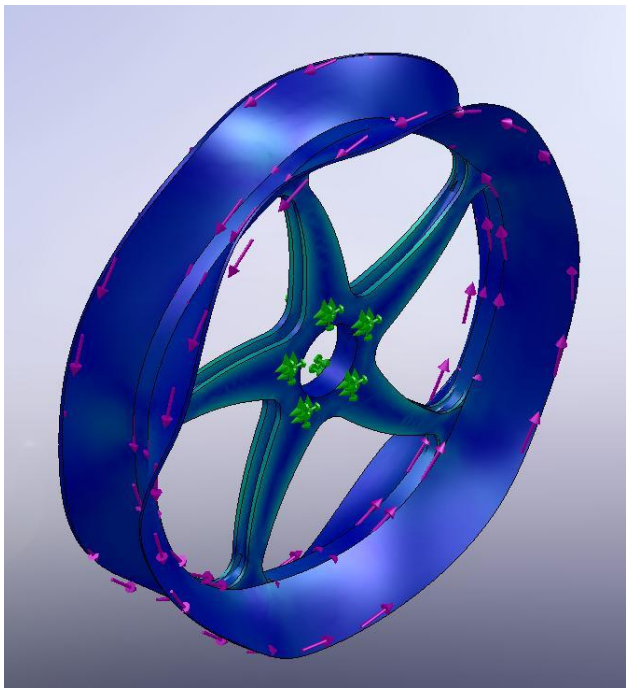

Figure 50: Torque Loading

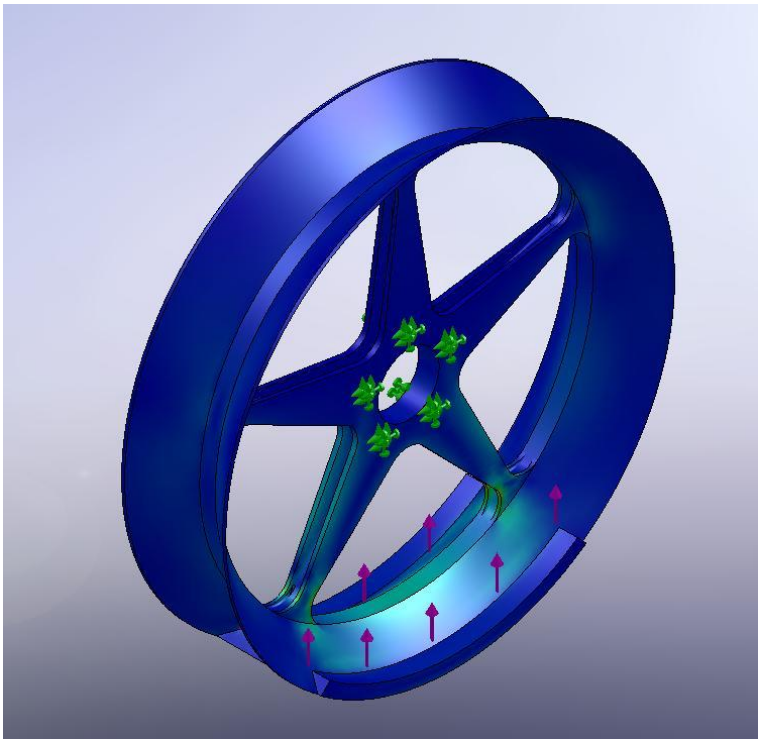

Figure 51: Landing

The tire was decided upon from numerous parameters. Included in the parameters were; weight, price, availability, size, traction/lug design, and durability. A Bridgestone Trailing TW-18 was eventually chosen, as shown in Figure 52. It is a fairly lightweight tire that will handle the terrain we intend to traverse. The price is fairly inexpensive compared to other options at about $87. The tires are of a tubeless design which should also help to reduce moment of inertia (MOI).

Figure 52: Selected Motocross Tires

Image from www.bridgestone.com

Wheel Fabrication

The wheel design was also done with the manufacturing process in mind. Designing a wheel that could not be manufactured from the wheel blanks that were donated was not an option. It was also necessary to make sure that it could be machined at the WPI facilities due to the fact that this was the only shop at our disposal.

GibbsCAM was used to create the machining code. The machining code will be left from the report due to its extreme length but can be seen upon request. The wheel manufacturing was done on a Haas VF-4 vertical milling machine. It has 3-axii and enough travel in the x, y, and z directions to machine the 17 inch wheel. Numerous tools were used on the wheel including; 6

inch long by ¾ inch wide 3-flute flat carbide end mill; 3 inch long by 15/32 inch wide 4-flute flat carbide end mill; 3.75 inch long by 3 inch wide 4-flute carbide insert face mill; 3 inch long by 1.625 wide high speed steel t-slot cutter.

Figure 53: Machine Tools Used

The major pockets of the wheel were cut out using the ¾ inch end mill. This end mill was used near the exterior of the wheel because the machine tool needed to clear the lip of the wheel. Using a tool this long is not ideal because it creates a vibration and can leave a poor surface finish. The interior pockets were done with the shorter 15/32 end mill. This reduced the vibration and made the surface finish better. The holes for the bolt pattern were done by first center drilling and then following through with a 3/8 2-flute high speed steel drill bit.

Figure 54: Wheel Machining

The machining design was to plunge into a pre-drilled hole to reduce vibration and reduce wear on the cutting tools. A 1/8 deep depth of cut was used over most of the wheel. Once the pockets were removed from the wheel the T-slot cutter was used to remove the material on the sides of the spokes. This created the channel in the spoke making them an I-beam structure. This tool was not ideally designed for this use but it worked fairly well. Much vibration was seen during the machining and a poor surface finish was the outcome. It should not affect performance of the wheel.

The total time for each wheel was 4.5 hours. Four wheels were completed for testing and the remaining blanks will be used if testing shows a more rugged design is needed.

Driver Controls

It is important to keep in mind that the controls be designed around the comfort of the driver as well as complete each task affectively. The controls must be designed to complete their full range of motion without being compromised and also operate each system to its full capability even under extreme conditions.

Rack

For the application of Baja, selecting the type of steering mechanism is based on many of the characteristics chosen for the chassis and suspension as well as the rules set forth. One of the major design goals for the project was to complete the endurance race in good standings. To accomplish this, driver comfort was one of the first design criteria examined which made many of our decisions quite easy. The first criterion that was determined was to limit the amount of steering wheel rotation to roughly 180 degrees in each direction to achieve full translation of the mechanism. If this angle is exceeded, then the driver would need to readjust their hands which would be impossible because wrist straps must be used during the competition; attaching the driver's hands to the steering wheel. Therefore the mechanism must be able to travel from steering stop to steering stop with less than 360 degrees of steering wheel rotation, while having a maximum steering angle of 30 degrees. Also, limiting the amount of rotation necessary to travel from steering stop to steering stop it will increase response time allowing the driver to use counter steer to correct for over steer.

Another important design criterion that must be used in selection of a steering mechanism is size. The specific layout of the track and the size and shape of the chassis (most specifically the foot box), set a number of design parameters for the system. Due to the fact that this is an off-road vehicle, the tie rods will experience a great deal of vertical motion, through suspension travel, as well as lateral travel through the action of the suspension and steering while navigating the course. If the steering mechanism is not wide enough, clearance issues between the tie rods and chassis may arise, rendering the system ineffective. The mechanism must also have a relatively low profile so that it will not occupy a great deal of space within the chassis making it uncomfortable or making it difficult for the driver to exit the car within the required time of 5 seconds. Along with the sizing characterizations mentioned, the design must also be lightweight to comply with the overall design characteristics of the car.

Through an examination all the design criteria, it was shown that there were many designs that would meet our specifications. These designs were then compared in regards to their design time, adaptability, manufacturability, weight, and cost. After this analysis, it was determined that a rack and pinion system would be the best choice for our application. The option of a linkage system was considered but the possibility of binding in the joints during rapid corrections deemed the system less effective. Even though it would have been possible to design and fabricate a custom rack and pinion system, the complexity of many of the components, as well as material costs, made purchasing a prefabricated system much more beneficial to the project. It was determined that an 11 inch rack with a 12:1 ratio and weighing in at roughly 2 pounds would be sufficient for the design.

After determining the type and size of the steering system, the next step was to place the rack in the optimum position within the chassis. After investigating a number of ways to properly orient the rack, one method that has been proven to be very effective was that of the 2007 WPI MQP group. In this method, the front suspension is set to ride height and axes were drawn from the ball joints through and normal to the axis of their respective mounting locations, which determined the instant center of our chassis. A line was then drawn from the instant center to the tie rod attachment point on the knuckle. A plane was then drawn through and parallel to both axes through the upper and lower mounting points of the suspension. The center of the tie rod point is then determined based on the point where the previously drawn axis intersects the plane. The point is then mirrored to the other side of the chassis, determining the other tie rod attachment point. Once the tie rod location was known it was then possible to determine how the steering column would facilitate the transfer of forces from driver input to the rack and pinion.

Steering Column

The steering column of the car is what is responsible for transferring driver input from the steering wheel to the rack and pinion system. As with all of the other driver control systems, the steering column must first and foremost be easily accessible by the driver as well as handling any forces that it may see. In order to properly determine the location of the steering wheel in relation to the driver, many team members were seated within the chassis and dimensions were taken to where they felt the steering wheel was most comfortable for them. After comparing the data gathered here, the location of the steering wheel was determined to be 19.5 inches forward

of the rear roll hoop and 20 inches above the lower frame members. Using this information and the location of the rack and pinion, the column was able to be designed. Because of the extreme angle that is present between the location of the rack and location of the steering wheel, it was necessary to incorporate a double universal joint (u-joint) system for the column linkage. The first u-joint will be attached to the rack at one end and to a .75 inch shaft that will run to the second u-joint. After the second joint, the shaft will run through a detachable support in order to reduce the amount of unsupported shaft. This support is made up of two delrin bushings which are press fit into a piece of 1.25 inch OD tubing, one close to the second u-joint and the other close to the steering wheel quick-release. Before press fitting the bushings, the tube is welded to a bent piece of 0.040 inch 4130 sheet. To secure this to the chassis, an additional gusseted plate of 0.040 inch sheet was cut, shaped, and welded to existing chassis members.

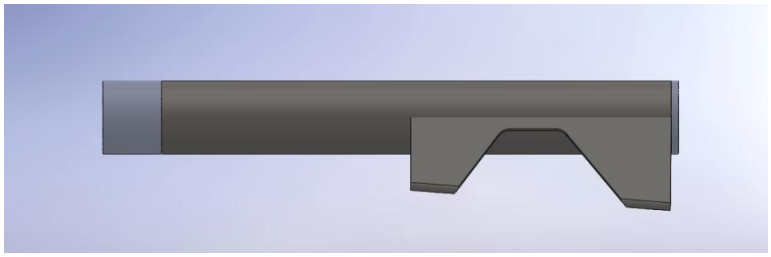

Figure 55 - Steering Rack Attachment

The final portion of the steering column was attaching the steering wheel to the upper shaft. To increase the speed of driver exit, it was deemed necessary to attach the steering wheel with a quick-release hub so that the steering wheel may be removed during the exit test at competition. In previous cars, a hex head release with a button release, shown below in Figure 56 had been used. However, this system was proven to be too slow because the driver would often miss the pin or have to take the time to locate it and then exit the vehicle. The current design employs a spline shaft with a circular disconnect switch, as shown in Figure 56. This design eliminates the need for the driver to search for a button, they must only reach through the wheel and pull the ring and the wheel disconnects making for a much quicker exit time. The design of this quick-release hub also answered many questions as to the type and design of the steering wheel that would be used in the vehicle.

Figure 56 – Connecters

Image from www.jegs.com

Steering Wheel

For the purposes of the Baja competition, the types of steering wheels that are used are various and in most cases custom made. Before design of the steering wheel can begin, many dimensions are needed such as the diameter and hole pattern on the quick-release hub that the wheel will be attached to, the amount of space available within the chassis, and the height of the average driver to ensure that the driver's view will not be interrupted. These factors will allow us to accurately choose or design a wheel that will be comfortable as well as functional within the chassis. Many different designs were considered such as a butterfly, handle bar, and traditional steering wheel. After examining the options, it was found that a traditional d-shaped steering wheel with an outer diameter of 11.75 inches, which is 1.75 inches larger than the previous year's design because it gave the driver a greater mechanical advantage. Due to the short time table to complete the project, coupled with the ability to easily find this type of steering wheel commercially, the steering wheel was purchased.

Pedals

When the pedals were designed compact foot box limits the amount of space creating a challenge. The pedals must also be designed to fit all drivers comfortably to ensure the efficiency of the system in which it controls. The parameters were determined that they be light weight but complete each task without error.

The brake pedal was designed with the help from the WPI Formula SAE team, to withstand a high amount of force created by the driver and transfer that input force to the master

cylinders through the brake circuits. The brake pedal must withstand a high amount of force created during panic scenario without fatigue. Deflection in the pedal would lead to an un-safe drop in the drivers control of the vehicle. The pedal is a push mechanism pinned at its pivot point to the base plate using a shoulder bolt to decrease wear on the material as well as prevent the loosening of the fixture. It also contains a spherical inside along with locking spacers using the pedal to prevent any unwanted lateral motion. The spherical is directly connected to the bias bar and master cylinder mounts completing the attachment. Both the spherical placement and base plate pin are attached at the distances for an efficient braking ratio used in the braking force calculations in Appendix . The pedal is also designed to fit comfortably in the foot box and against the sole of the driver's foot. A foot plate is attached along with grip tape to increase the surface area and decrease any slip of the driver's foot during use.

The gas pedal design is based off the brake pedal design with changes to allow for it to be lighter in weight but also appear to match for aesthetics. The pedal is pined also with a shoulder bolt to the same base plate in the bottom of the foot box with the throttle cable attached to a tab containing three different mounting holes allowing for throttle adjustment extended from the side of the pedal under the driver's foot. The gas pedal is also equipped with footplate and grip tape.

To increase the driver's comfort during extended driving the mounting of a dead peddle was determine from previous research of past driver's experience of muscle fatigue. The driver can rest their left foot on the dead peddle while accelerating as well as providing the driver with a brace to press against in case of impact from a landing.

Brakes

The design of the brake system was created to comply with all SAE regulations to prevent any problems during the competition's tech inspections preventing the team from competing. SAE regulation 34.1 states "All vehicles must incorporate a foot-operated braking system capable of locking the front the front and rear statically and dynamically on pavement and unpaved surface". Rule 34.2 states "Independent brake circuits, systems must have two separate reservoirs" to prevent incident should one system fail, two wheels will still be operational. Finally illustrated in regulation 34.4, "The brakes on the driven axle must operate through the final drive axle. Braking through differentials is not permitted". In our case the

bakes must not be mounted to any or the secondary shafts contained in the double reduction other than the final output shafts.

With the rules setting our parameters the design two master cylinders; one operating two front calipers and the other operating a single rear caliper. All braking components were purchased from Polaris used on ATVs except for the rotors which were manufactured using CNC machines to the exact specifications calculated in Appendix D. The front calipers are a single sided single 1.14 inch diameter piston outboard design with rotors attached to the wheel hubs and calipers connected to a steel strut on the upper front knuckles. The rear caliper is a single sided one inch diameter dual piston caliper connected directly to the chassis. To account for more rolling inertia the dual caliper was deemed necessary to lock the rear tires with a single caliper. The single rear brake design also decreases weight and simplifies the system allowing the caliper to apply equal force to both rear tires from the rotor connected to the center of the final output shaft complying with all regulations.

The braking forces calculated in Appendix D were determined using a number of parameters such as: input force from the driver, pedal ratio, weight of vehicle with driver, weight distribution, master cylinder bias, as well as tire and brake pad coefficients of friction (COF). The tire to ground COF can range between 0.5 and 1 depending on type of asphalt and tire used. Since the Baja is equipped with off road motocross tires the COF used for calculations was 0.8. Research of materials used for the rotors and brake pads the COF was determined to be 0.6. Research done the SAE Baja team of 2007 tested and recorded a range breaking forces to use in their calculations and derived table 5 below.

Light Braking Force	Average Braking Force	Panic Braking Force
10 lbs	30 lbs	60 lbs

Table 16: Braking Force

Other statistics have shown that panic forces can reach three times that shown in the table but they have been recorded in real life scenarios. These parameters along with other constraints such as wheel diameter, caliper and master cylinder selection the final calculations were determined.

Brake Plate design

The design of the throttle and break system was conducted with three main goals; that the system be light in weight, compact, and simple adjust. The decision to have a pin jointed push mechanism allowed the system to fit in the small area of the foot box and allow the pedals, master cylinders, and bias bar to be contained on one mount plate modeled below with the use of SolidWorks in Figure 57. All pieces are fixed except the threaded bias bar allowing minimal error allowed during adjustments.

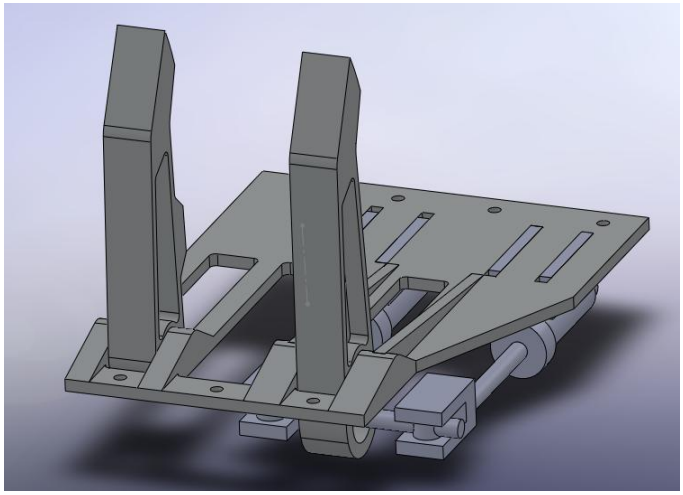

Figure 57: Brake Assembly

The base plate was designed to withstand the loads forced upon it by the brake and master cylinders. The system's bias bar is added to allow the driver some adjustability in the braking force to the front and rear calipers.

The bias bar contains a spherical connected to a threaded rod. That rod is then spun to relocate the spherical within the one inch bore of the brake pedal changing the contact point of the pedal and moments on the master cylinders. The closer the spherical is to the master cylinder the more force is applied to that braking circuit be rear or front calipers. Shown below in Figure 58 is the bias illustrated in two different positions; 50:50 and 60:40 ratios front/rear or rear/front.

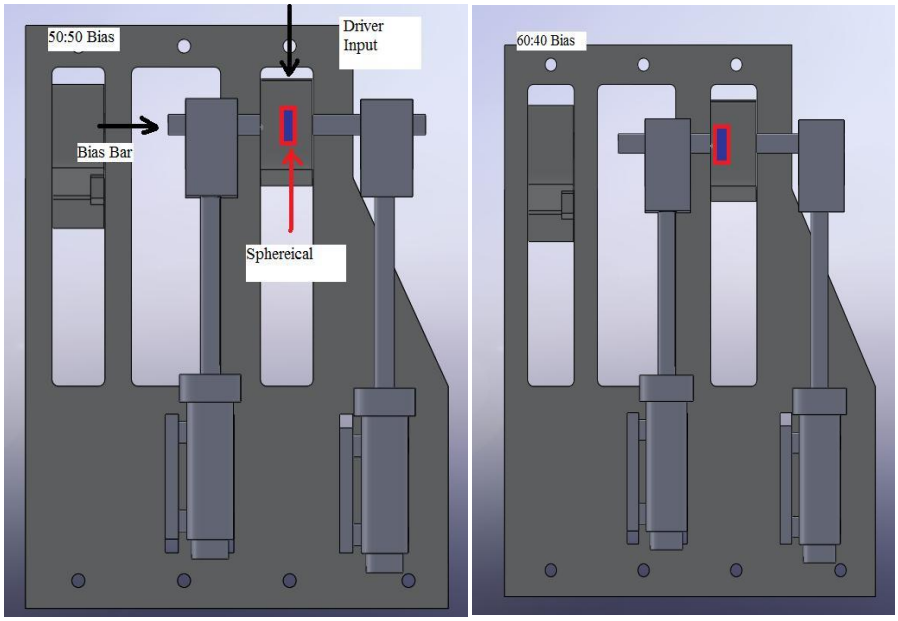

Figure 58: Brake Plate

The spherical is adjusted to the desired position based on driver feedback then locked in place by lock nuts and spacers to prevent any lateral movement. The design of the plate also allows the system to be manufactured easily to since it would only need to be mounted three times in a vice and be completed in under two hours.

Thermal Analysis of the Rear Disc

The rear brake disc was analyzed to obtain a better understanding of the heat transfer of a brake disc in a Baja vehicle; the heat created in the disc under braking conditions, the heat transfer rate of the disc to the air, and the conduction of the brake disc to the hub were all analyzed. The velocity of the car was used to compute the angular velocity of the brake disc before braking. The air velocity was assumed to be full of the rotor velocity due to the rotation of the disc giving a positive and negative tangential air velocity.

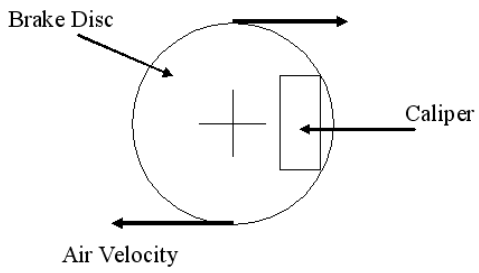

Figure 59 - Diagram of Heating Analysis

The following assumptions were made for the braking analysis

1. Steady State.
2. Lumped Mass
3. Heated volume was equal to three times the contacted section of the disc. Due to the area in the center of the disc being empty.
4. Convection is uniform across surface.
5. Air velocity is assumed to be half the speed of the car.
6. Air flow is turbulent (see Reynolds number calculations).

Force (lbf)	Car Speed MPH	Air Temp (F)	Air Speed MPH	Break Disc Density (lb/in^3)	Brake Heating mass (lb)	Area (in^2)
1200	40	70	20	0.284	4.359	0.25

Cp Disc (BTU/lb-F)	Heat Volume (in^3)	kf
0.12	15.3	120

Table 17 – Critical Parameters for Equations

Energy Balance

$$E_{in} = Q_{conv} + Q_{Cond} \quad (1)$$

Where E_{in} the braking heat is generated by the caliper, Q_{conv} is the about of heat transferred through convection to the air, and Q_{cond} is the about of heat transferred through conduction to the hub. This can be stated due to the steady state assumption. It is noted that a

transient analysis would serve a better approximation of this problem with a relationship of the disc temperature over time.

Braking Analysis

$$E_{in} = \mu_k \int F_n(x)dx \ (2)$$

$$E_{in} = \frac{\mu_k F_n (V_s - V_f)}{2t} \ (3)$$

F_n is the force on the brake disc, μ_k is the coefficient of kinetic friction, x is the position equation, V_s is the starting angular velocity, V_f is the final angular velocity, t is time. Equation 3 is used to calculate the total heat produced in the disc from normal braking. The force calculations can be seen above in the braking selection section. Once total heat was discovered, a convection analysis of the disc to the surrounding air was done.

Convection Analysis

$$Q = h\,A\,(T_{disc} - T_{\infty}) \ (4)$$

T_s is the temperature of the surface, T_{∞} is the temperature of the fluid (air) at infinity, A is the area (assumed to be twice the area of a face of the disc), q is the heat transfer rate from the disc to the air.

$$Re = \frac{\rho v L}{\nu} \ (5) \quad \Pr = 0.713$$

$$Nu = 0.023\, Re^{0.8} Pr^{0.4} \ (6) \qquad Nu = \frac{hL}{k_f} \ (7)$$

V is the average speed of the car, L is the approximated length of the air flow over a cylinder, k_f is the conductive coefficient, Nu is the Nusselt number, Pr is the Prandtl number, Re is the Reynolds number, and h is the coefficient of convection. Equation 6 and 7 were used to determine the convection coefficient; 0.023 and 0.8 are for steady state turbulent flow, which is

proved with solving equation 5 for the Reynolds number (Re >> Re_{cr}) , and 0.4 is for heating of a fluid as opposed to 0.3 for cooling a fluid. The Nusselt number was found to be 121.3, the Prandtl number was 0.713, the coefficient of convection was equal to 14327, and the Reynolds number was found to be 53202.15. Once h was found the heat transfer rate and total heat transferred could be found using equation 4. The total heat transferred from the disc to the surrounds also includes a conduction analysis from the disc to the hub. Equation 8 was used to determine the total heat transferred down one spoke of the four spoke hub.

Conduction Analysis

$$Q = \frac{Ak_f \Delta T}{\Delta x} \quad (8)$$

X is the distance from the outer disc to the hub, A is the cross sectional area, ΔT is the difference in temperature from hub to the disc. The cross sectional area was of one spoke of the hub (about 0.25 $inches^2$).

Results

$$\frac{\mu_k F_n (V_s - V_f)}{2t} = h\,A\,(T_{disc} - T_\infty) + \frac{Ak_f \Delta T}{\Delta x} \quad (9)$$

The results are as follows; solving for T_{disc} a temperature of increase 114 °F was found on the surface of the disc with a start speed of 40 mph, a stopping speed of zero and a braking time of 15 seconds. This is a close approximation that can be used to allow further analysis of the use of other types of materials for brake disc in a Baja vehicle such as aluminum.

Drive Train

Engine

The source of power to the drive train begins at the engine which is a stock four cycle, air cooled, Briggs & Stratton OHV Intek Model donated by Briggs and Stratton who are the official sponsors of SAE Baja. The Model 20, weighs 52 pounds with 305 cubic centimeter engine produces a mere 10 horsepower at 3800 rpm and 13.5 pound feet of torque at 2400 rpm. This engine serves as a common governing agent between all teams competing.

Maximum Power

The following is a graph of the Briggs and Stratton motor's horse power at different rpm's. It was determined that the governor was a progressive system which limits the power the closer it gets to the maximum rpm's. For this reason the optimum rpm's for the motor is in the 3100 to 3300 range, the chart in Figure 60 taken from the 2008 WPI Baja team.

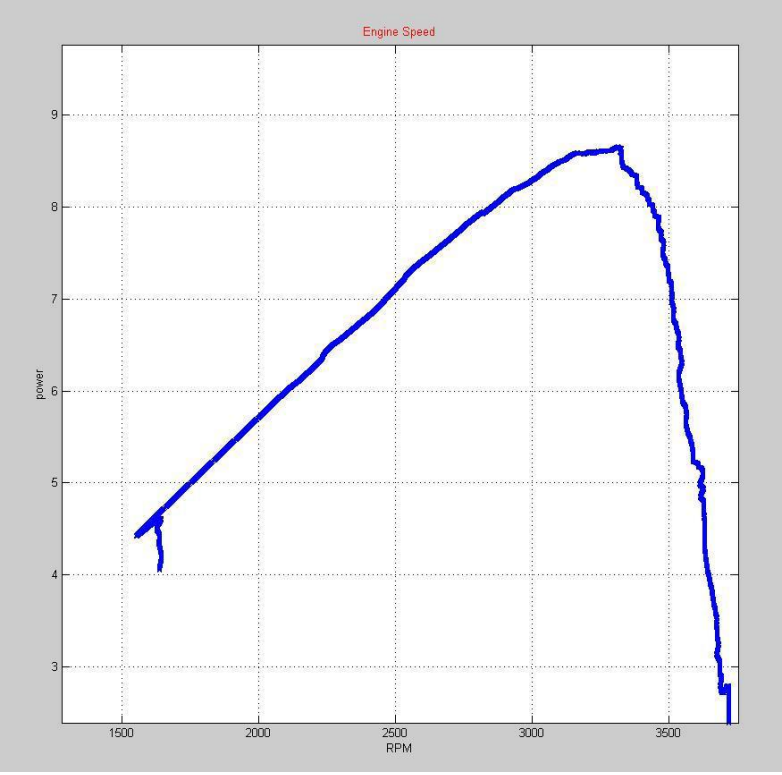

Figure 60: Power vs. RPM

Drive Train Selection

Previous research of past competitions and projects determined that the average speed of a Baja during the endurance race was between 30 and 40 miles per hour due to the fact that there is not enough room to accelerate to top speeds greater than that. The majority of the time is spent accelerating and decelerating to account for a multitude of obstacles such as rocks and other vehicles. It was also discovered that the average top speed's for the Baja vehicles are around 40 to 45 miles per hour. For this reason the drive train will need to provide the most power to the wheels at the greatest efficiency within that range.

The first step in the design process is to determine the type of reduction needed to complete the power transfer within specified design parameters set by the team. The most important design constraints that drove the team's decisions are: the drive train must be light in weight and compact due to the small size of the vehicle, it must transfer the calculated amount of power to the drive shaft allowing it to complete both high and low gear applications that will be necessary to complete all aspects of the endurance portion of competition without failure, lastly complete the previous tasks around a single supplied engine and a tire size of 25 inches. With these in mind the calculated ratio of 1:9 was determined the best design. The maximum efficiency for the CVT is at a one to one ratio and the maximum horse power for the engine occurs at 3250 rpm. Refer to calculations in which obtained the average and top speed for the Baja vehicle.

Thrust and Accelerations Calculations

The following table is a list of parameters based upon the current proposed average CVT selection gearing and efficiencies, top speed and rpm limits, tire diameter, and overall weight.

Tire Diameter	25	inches
Circumference	80.11	inches
Reduction Engine Internal	1	
Reduction Gear Box	1	
Reduction (Max CVT)	0.75	
Reduction (Chain)	9	
Top Speed	43	MPH
Rev Limit	3750	RPM
Total Reduction (2,3)	6.62	
Total Mass	400	lbs

Table 18: Drive Train Parameters

Table 19 shows the calculated thrust based on the parameters above and a given velocity of the Baja. The table starts at 5 mph due to the inability to account for slip in the CVT at low speeds.

RPM	Reduction	Speed (mph)	Efficiency	Power (hp)	Thrust (lbf)	Accel (m/s^2)	Time (s)
2300	4.05	5.03	0.76	6.48	366.67	7.00	0.16
2350	4.05	5.14	0.76	6.59	365.49	6.98	0.17
2400	4.05	5.25	0.76	6.71	364.36	6.96	0.18
2450	4.05	5.36	0.76	6.83	363.28	6.94	0.19
2500	4.05	5.47	0.76	6.95	362.24	6.92	0.19
2550	4.05	5.58	0.76	7.07	361.24	6.90	0.20
2600	4.05	5.69	0.76	7.19	360.28	6.88	0.21
2650	4.05	5.80	0.76	7.31	359.35	6.86	0.21
2700	4.05	5.91	0.76	7.43	358.46	6.84	0.22
2750	4.05	6.02	0.76	7.55	357.61	6.83	0.23
2800	4.05	6.13	0.76	7.67	356.78	6.81	0.23
2850	4.05	6.24	0.76	7.79	355.98	6.80	0.24
2900	4.05	6.35	0.76	7.91	355.21	6.78	0.25
2950	4.05	6.46	0.76	8.03	354.47	6.77	0.26
3000	4.05	6.56	0.76	8.15	353.75	6.75	0.26
3050	4.05	6.67	0.76	8.27	353.05	6.74	0.27
3100	4.05	6.78	0.76	8.39	352.38	6.73	0.28
3150	4.05	6.89	0.76	8.51	351.72	6.71	0.29

3200	4.05	7.00	0.76	8.63	351.09	6.70	0.29
3250	3.91	7.37	0.76	8.75	338.24	6.46	0.32
3250	3.76	7.65	0.76	8.75	327.54	6.25	0.34
3250	3.62	7.96	0.77	8.75	316.72	6.05	0.36
3250	3.48	8.28	0.77	8.75	305.76	5.84	0.38
3250	3.33	8.64	0.78	8.75	294.68	5.63	0.41
3250	3.19	9.03	0.78	8.75	283.46	5.41	0.44
3250	3.05	9.45	0.78	8.75	272.11	5.19	0.48
3250	2.90	9.92	0.79	8.75	260.63	4.98	0.52
3250	2.76	10.44	0.79	8.75	249.02	4.75	0.57
3250	2.62	11.01	0.80	8.75	237.28	4.53	0.62
3250	2.47	11.65	0.80	8.75	225.41	4.30	0.69
3250	2.33	12.36	0.80	8.75	213.41	4.07	0.76
3250	2.19	13.17	0.81	8.75	201.28	3.84	0.86
3250	2.04	14.10	0.81	8.75	189.02	3.61	0.97
3250	1.90	15.16	0.82	8.75	176.62	3.37	1.10
3250	1.76	16.40	0.82	8.75	164.10	3.13	1.27
3250	1.61	17.85	0.82	8.75	151.44	2.89	1.49
3250	1.47	19.59	0.83	8.75	138.66	2.65	1.77
3250	1.33	21.71	0.83	8.75	125.74	2.40	2.14
3250	1.18	24.34	0.84	8.75	112.70	2.15	2.66
3250	1.04	27.70	0.84	8.75	99.52	1.90	3.40
3250	0.90	32.12	0.80	8.75	81.72	1.56	4.55
3250	0.75	38.23	0.76	8.75	65.22	1.25	6.49
3300	0.75	38.99	0.76	8.65	63.22	1.21	6.77
3350	0.75	39.59	0.76	8.60	61.92	1.18	6.99
3400	0.75	40.18	0.76	8.40	59.59	1.14	7.22
3450	0.75	40.77	0.76	8.10	56.63	1.08	7.46
3500	0.75	41.36	0.76	6.95	47.89	0.91	7.72
3550	0.75	41.95	0.76	5.79	39.36	0.75	8.04
3600	0.75	42.54	0.76	4.64	31.06	0.59	8.43
3650	0.75	43.13	0.76	3.48	22.99	0.44	8.94
3700	0.75	43.72	0.76	2.32	15.14	0.29	9.67
RPM	Reduction	Speed (mph)	Efficiency	Power (hp)	Thrust (lbf)	Accel (m/s^2)	Time (s)

Table 19: Thrust Data

The cells in green represent the maximum efficiency of the CVT and the maximum amount of horse power being produced from the engine at about the average speed of 28 mph.

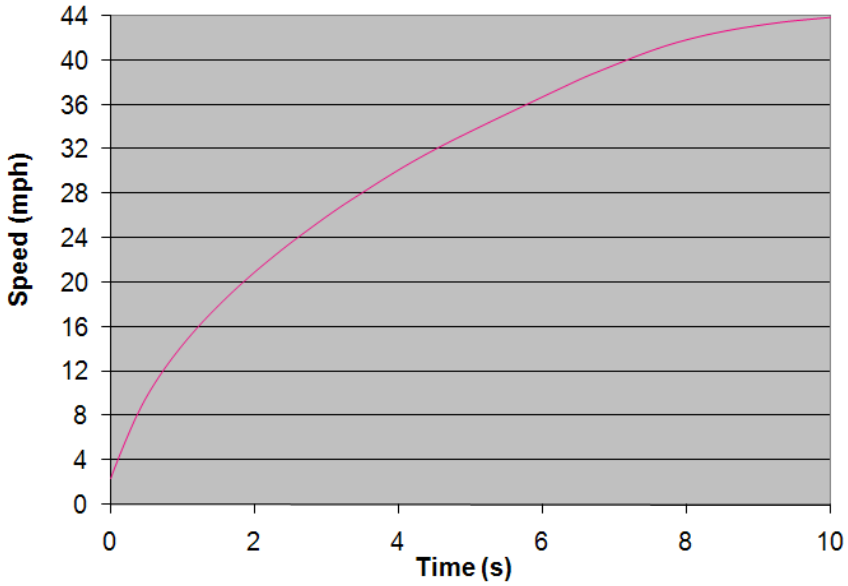

Figure 61: Time vs. Speed

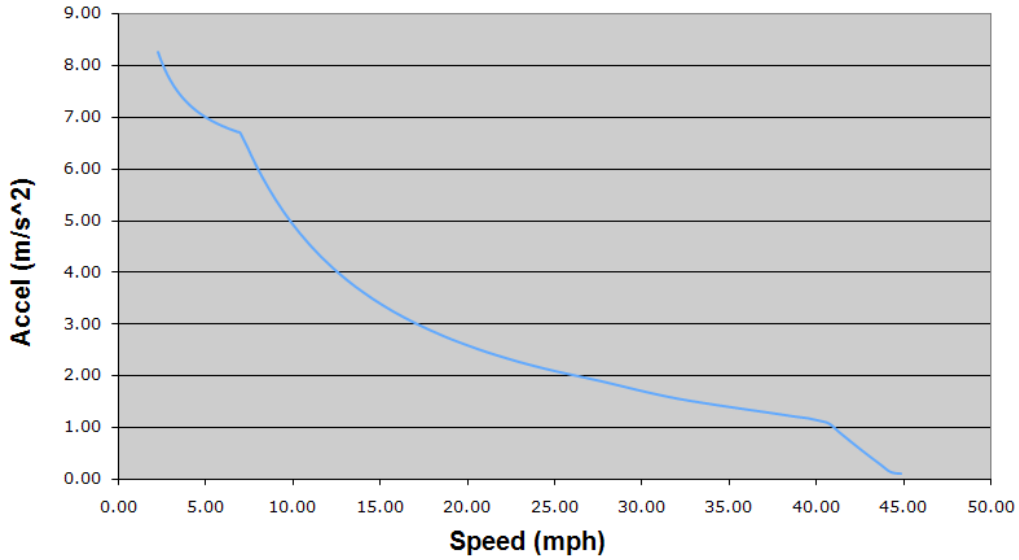

Figure 62: Acceleration vs. Speed

Rolling Resistance Test

The current Baja Car was towed at increasing speeds at 5 mph intervals to measure the rolling resistance of the vehicle. Once the car was at a constant speed it was released from the towing vehicle and the distance that it took to slow to a stop was measured.

Figure 63: Overall Test Setup

Figure 64: Shackle Release Setup

This information coupled with the equations below can provide a reasonable approximation of the vehicles overall rolling resistance. Where m is the mass, V_o is the initial velocity and K_r is the drag force per mph.

$$m * \dot{a} = K_r * V \qquad x(t) = \frac{-V_o m}{K_r}\left[e^{\left(\frac{-K_r}{m}t\right)}\right] + \frac{V_o m}{K_r}$$

$$v(t) = V_o\left[e^{\left(\frac{-K_r}{m}t\right)}\right] \qquad a(t) = \frac{-K_r}{m}V_o\left[e^{\left(\frac{-K_r}{m}t\right)}\right]$$

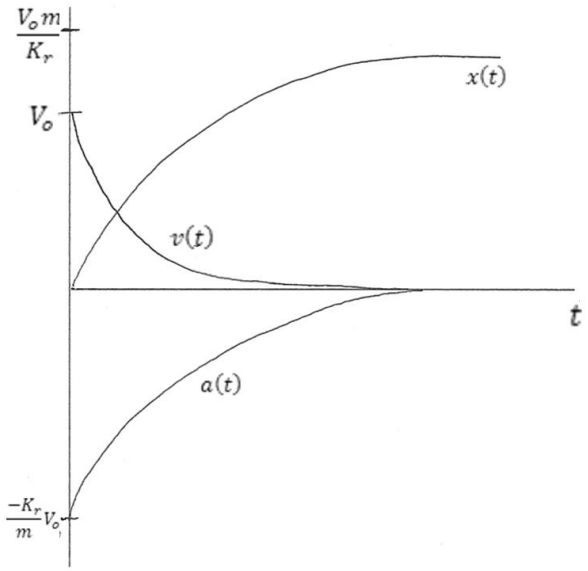

Figure 65: Position vs. Acceleration vs. Velocity

Speed (mph)	Speed (feet/sec)		Dist (feet)		Mass (lbm)	Drag Force lbs/mph
5	7.33		19.08		18.03	6.9266
5	7.33		22.92		18.03	5.7661
10	14.67		38.08		18.03	6.9459
10	14.67		35.25		18.03	7.5035
15	22		55.00		18.03	7.2120
15	22		52.75		18.03	7.5196
20	29.33		129.25		18.03	4.0914
20	29.33		133.25		18.03	3.9686

Table 20: Rolling Resistance Test Results

Table 20 shows the results from the test performed. A top speed of 20 mph was the highest velocity that could be performed due to the shackle used (see Figure 66). Over 20 mph the load on the pin in the shackle was too large and it could not release.

Figure 66: Release Mechanism

As shown the force of the rolling resistance decreases as the velocity increases. This can be contributed to the temperature of the drive train and of the tires. With a higher velocity and running time the grease and bearings will heat up causing a higher efficiency allowing for a lower rolling resistance.

Air Resistance

Drag Force = $.5*\rho*v^2*A*C_d$

$\rho = .0767$ lb/ft^3 v = 0…45 MPH A = 9.554 ft^2 $C_d = 0.6, 0.7, 0.8$

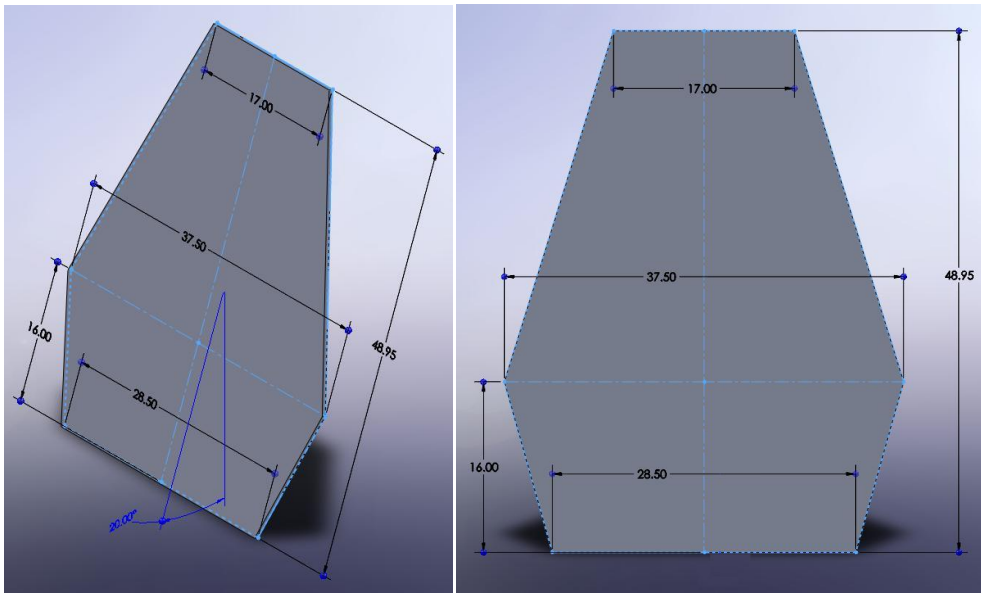

Figure 67: Rear Fire Wall Dimensions

The biggest cross sectional area on the Baja vehicle is the firewall. The area of the firewall is 10.167 ft^2 but taking into account the angle of attack of the flow of the air, 20 degrees, the front area of the vehicle is 9.554 ft^2.

The density given is the density of the fluid, in this case this is air. The average temperature for Milwaukee, Wisconsin for the past four years is 15.5^0 C looking at the densities of air compared to the temperatures and linearly interpolating the data, you get an air density of .0767 lb/ft^3.

The velocities that are graphed are velocities that the vehicle could possibly reach in intervals of 5 miles per hour. The graph also shows the data point for 28 miles per hour which is our optimum velocity for maximum power and efficiency of our transmission.

The coefficient of drag (C_d) was hinted at by the Bosch Automotive Handbook for box-like autos at 0.8 and the Mechanical Engineers Handbook states that a high drag vehicle the coefficient of drag is 0.55. The graph has three plot lines for 0.6, 0.7, 0.8 coefficients of drag trying to estimate a close number.

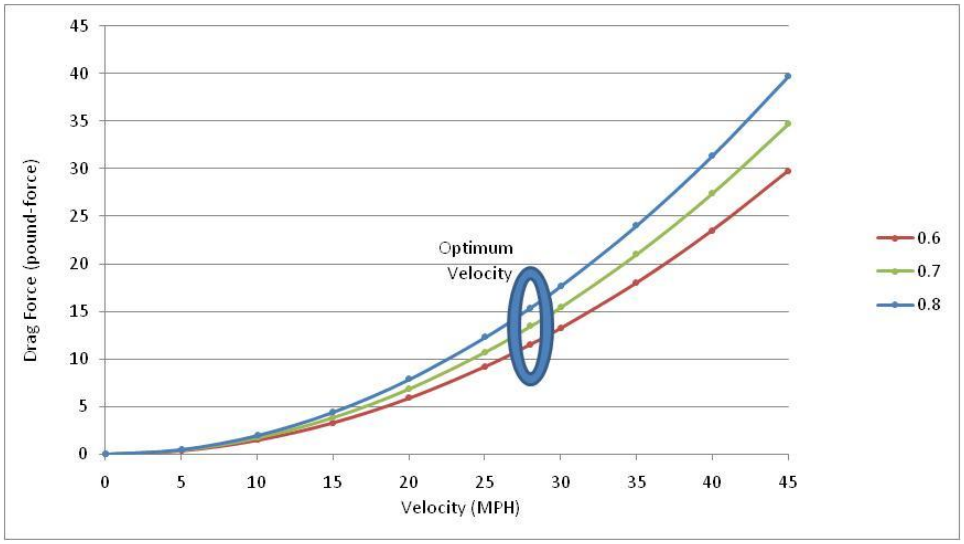

Figure 68: Drag Force vs. Velocity

Velocity (mph)	Drag Force (lb_f)		
	@C_d=0.6	@ C_d=0.7	@C_d=0.8
0	0	0	0
5	0.367451	0.428692	0.489934
10	1.469803	1.71477	1.959737
15	3.307056	3.858232	4.409408
20	5.87921	6.859078	7.838947
25	9.186266	10.71731	12.24835
28	11.52325	13.44379	15.36434
30	13.22822	15.43293	17.63763
35	18.00508	21.00593	24.00677
40	23.51684	27.43631	31.35579
45	29.7635	34.72408	39.68467

Table 21 - Velocity vs. Drag Force

The graph and chart above shows the drag resistance in pound-force of the vehicle at different velocities. The graph plots a point at the optimum velocity showing a resistance between 11.5 and 15.5 pounds of force.

Below is the graph and charts for the power it takes to overcome the drag forces are below. The power equation is: $P=f_d*v$, where f_d is the drag force and v is the velocity. Therefore the function for power to overcome drag is: $P = .5*\rho*v^3*A*C_d$.

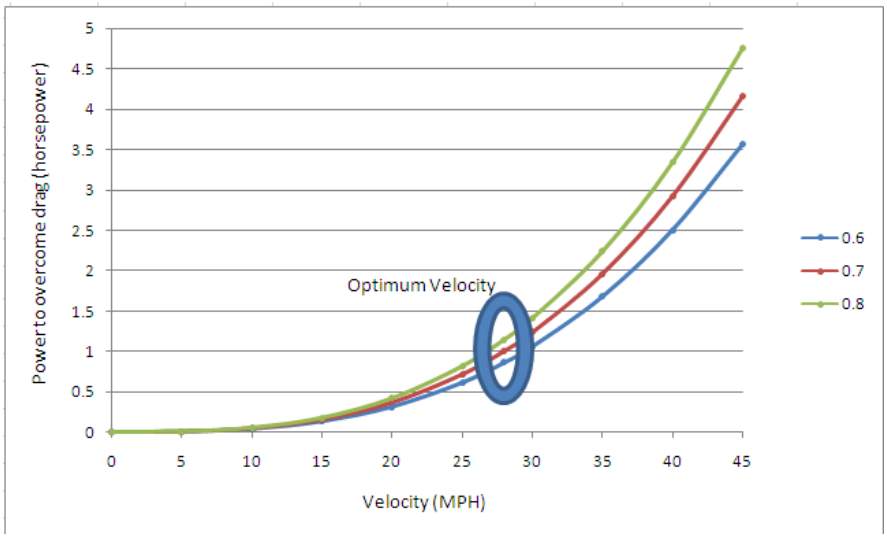

Figure 69 - Horsepower vs. Velocity

Velocity (mph)	Power required at the wheels (HP)		
	@C_d=0.6	@ C_d=0.7	@C_d=0.8
0	0	0	0
5	0.004899	0.005716	0.006532
10	0.039195	0.045727	0.05226
15	0.132282	0.154329	0.176376
20	0.313558	0.365818	0.418077
25	0.612418	0.714487	0.816557
28	0.860403	1.003803	1.147204
30	1.058258	1.234635	1.411011
35	1.680475	1.960554	2.240632
40	2.508464	2.92654	3.344618
45	3.571621	4.166891	4.762161

Table 22: Velocity vs. Horsepower

On the graph and table above you can see that the horsepower required at the wheels to overcome the drag forces at the speed where the CVT is at maximum efficiency, in the worst case scenario is 1.14 HP.

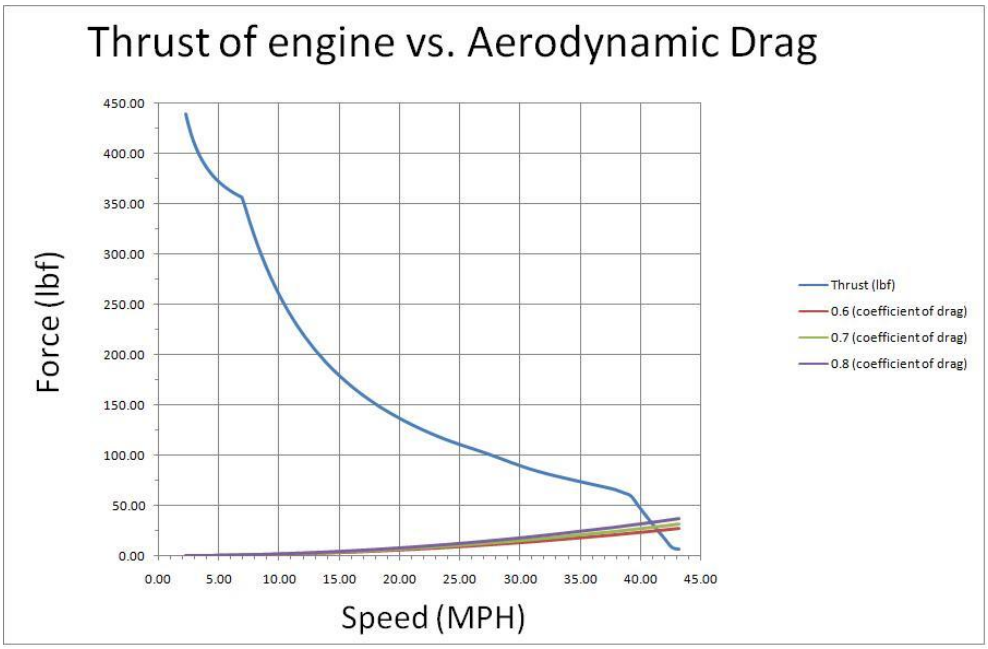

Figure 70: Thrust of Engine vs. Aerodynamic Drag

RPM	Speed (mph)	Thrust (lbf)	0.6 (coefficient of drag)	0.7 (coefficient of drag)	0.8 (coefficient of drag)
3250	8.51	299.08	1.06531158	1.242863511	1.420415441
3250	8.90	287.72	1.162989008	1.35682051	1.550652011
3250	9.31	276.23	1.274743128	1.487200316	1.699657504
3250	9.77	264.61	1.403414698	1.637317148	1.871219597
3250	10.28	252.85	1.552598978	1.811365474	2.07013197
3250	10.84	240.96	1.726899623	2.014716227	2.302532831
3250	11.47	228.94	1.932288156	2.254336182	2.576384208
3250	12.17	216.79	2.17662232	2.539392707	2.902163093
3250	12.96	204.50	2.470408966	2.882143793	3.293878621
3250	13.87	192.08	2.82795277	3.299278232	3.770603693
3250	14.91	179.53	3.26913104	3.813986214	4.358841387
3250	16.13	166.85	3.822217282	4.459253495	5.096289709
3250	17.55	154.03	4.528526552	5.283280977	6.038035403
3250	19.26	141.09	5.450361119	6.358754639	7.267148159
3250	21.33	128.01	6.685235715	7.799441668	8.91364762
3250	23.90	114.79	8.392767848	9.791562489	11.19035713
3250	27.17	101.45	10.84897312	12.65713531	14.46529749
3250	31.48	83.39	14.56523948	16.99277939	19.42031931
3250	37.42	66.65	20.57775174	24.00737703	27.43700232

Table 23: Thrust of Engine vs. Aerodynamic Drag

The graph of the Thrust of engine vs. Aerodynamic Drag shows the top speed of the Baja along with the losses of force from the engine and CVT. During the moment of maximum efficiency of the CVT, the table below shows that there is a difference of forces from 90.6 lbs_f in the worst case and 106.4 lbs_f in the best case of aero drag at the optimum speed. The rolling resistance data will be added and graphed when the final tow test is done.

Speed	Thrust	Power (lbf)		
(mph)	(lbf)			
8.51	299.08	298.02	297.84	297.66
8.90	287.72	286.56	286.37	286.17
9.31	276.23	274.96	274.74	274.53
9.77	264.61	263.20	262.97	262.74
10.28	252.85	251.30	251.04	250.78
10.84	240.96	239.23	238.95	238.66
11.47	228.94	227.01	226.69	226.36
12.17	216.79	214.61	214.25	213.88
12.96	204.50	202.03	201.62	201.21
13.87	192.08	189.25	188.78	188.31
14.91	179.53	176.26	175.72	175.17
16.13	166.85	163.03	162.39	161.75
17.55	154.03	149.51	148.75	148.00
19.26	141.09	135.64	134.73	133.82
21.33	128.01	121.32	120.21	119.09
23.90	114.79	106.40	105.00	103.60
27.17	101.45	90.60	88.79	86.99
31.48	83.39	68.82	66.39	63.97
37.42	66.65	46.07	42.64	39.21

Table 24: Difference in Forces at the Maximum Efficiency of the CVT

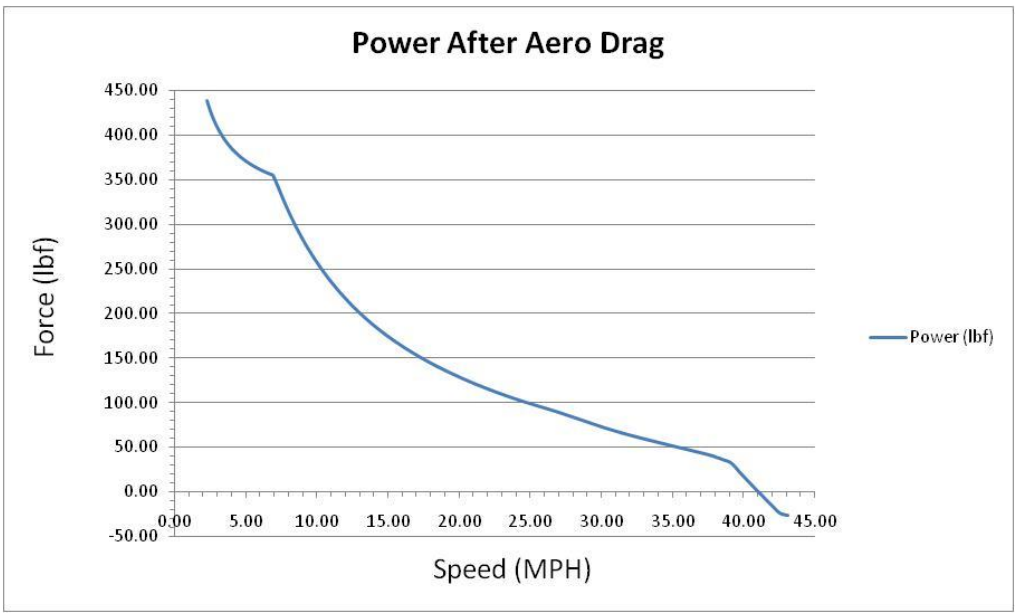

Figure 71: Power at the Wheels After Aero Drag

This graph represents the power at the wheels after the aerodynamic drag calculated. Taking in to account only aerodynamic drag and not rolling resistance, you see the top speed of the Baja would be around 41 MPH because the output of the engine will not produce enough force go any faster.

Drive Train Design

The first step of the drive train selection was determining chain pitch and type that would prove capable of all forces determined by the worst case scenario. To complete this objective the sprocket dimensions and reduction train would need to be determined. Due to the compact space and large reduction a two stage reduction is the best decision. By sprocket specifications no tooth pattern shall contain less than 12 teeth per sprocket which would lead to binding in chain due to lack of degree of chain wrap on the sprocket. Another specification considered is the larger the sprocket the less chain tension allowing room for a smaller chain with less rows and weight. With all considered the final reduction is to be completed as two 3:1 ratios consisting of two different sprocket dimensions to add simplicity to the design with two of the same reduction.

The first reduction consists of a 15 tooth to a 45 tooth sprocket connected by a single row RS35 roller chain. The sprocket dimensions were defined to be the maximum diameter allowed

on the secondary jackshaft complimenting the gear frame dimensions. The RS35 chain proved substantial since the first reduction would only face a maximum torque from the CVT of 14 ft*lbs divided by radius of the 15 tooth sprocket creates a max force of 186 lbs. A single row RS35 chain has tensile strength 2,530 lbs much higher than the force acting on it.

The second reduction consists of a 16 to 48 tooth sprocket train connected by an RS35 double row roller chain. The "worst scenario parameter" was set to be a 2G torque to the rear wheels demonstrating a jump landing and all forces translated through driveshaft and wheel to calculate the tension created in the chain. With more room in the gear frame the largest sprocket capable of fitting would be used to decrease as much chain tension as possible. The chain tension was calculated in Appendix E to 3600 pounds leading to the need of a stronger chain. Keeping the same chain pitch for simplicity the increase from a single to a double row 35 pitch chain is capable of handling the forces presented with a tensile strength of 5,060 pounds.

Sprocket Design

Following the main design parameters of lightweight and compact some of the sprockets were designed and manufactured on campus. This design also proves to be cost effective since there is excess aluminum already purchased. The tooth design was created for an RS35 chain and is illustrated in Figure 72 below.

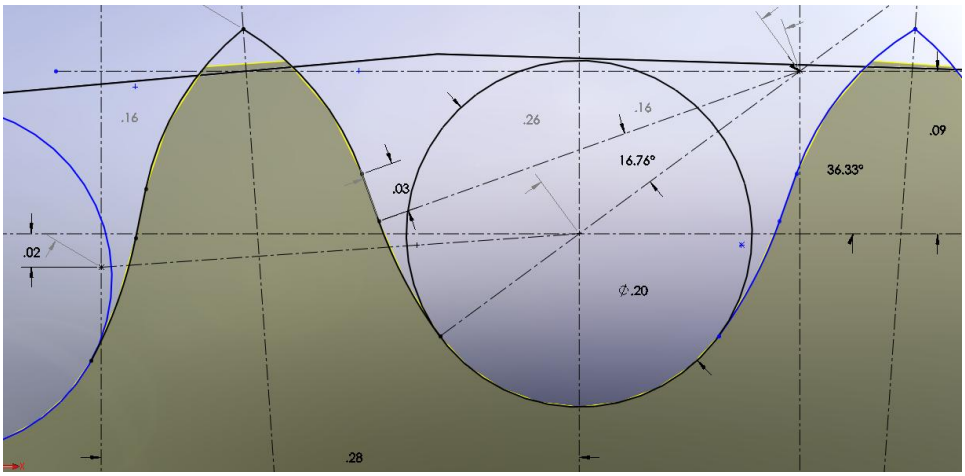

Figure 72: Sprocket Dimensions

Only the larger sprockets of the two chain drives would be manufactured out of lighter material aluminum and the smaller sprockets were purchased and made of 4130 steel since they encounter more stress and wear than that of the larger ones.

The 45 tooth sprocket on the secondary jack shaft is designed as a single row roller chain sprocket that is connected to the shaft using a 0.125 inch steel flange. The sprocket uses the same five tapered spoke design as the wheels mentioned earlier since it has proven to be much stronger in transferring the torque of the chain to the shaft.

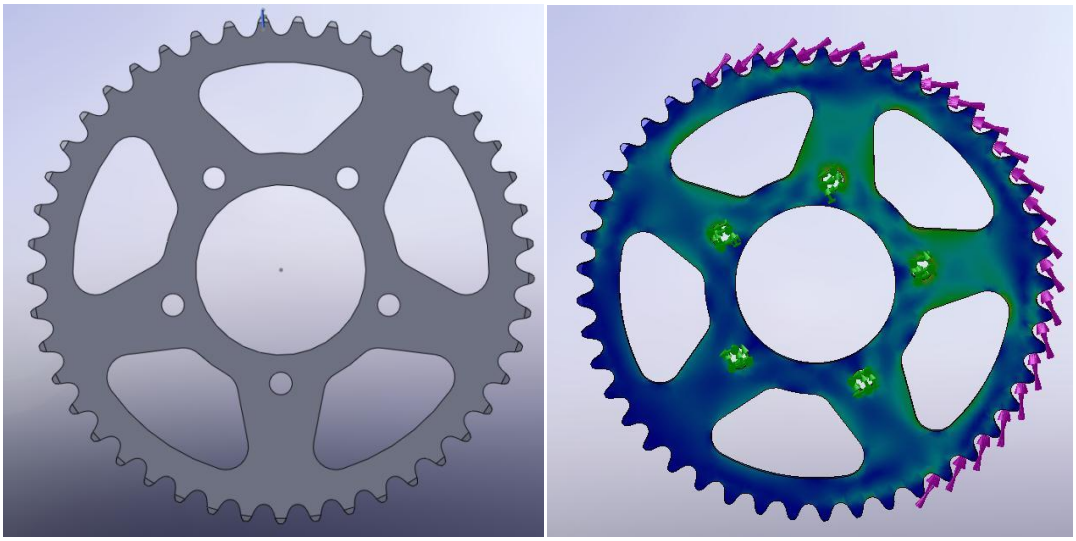

Figure 73: Secondary Sprocket FEA

The 48 tooth sprocket was designed under different parameters due to the lack of room allowed in the gear frame. The tooth patter was developed using the same drawing techniques but was implemented to a more solid outer radius increasing the sustainability of the large tension loads presented in calculations.

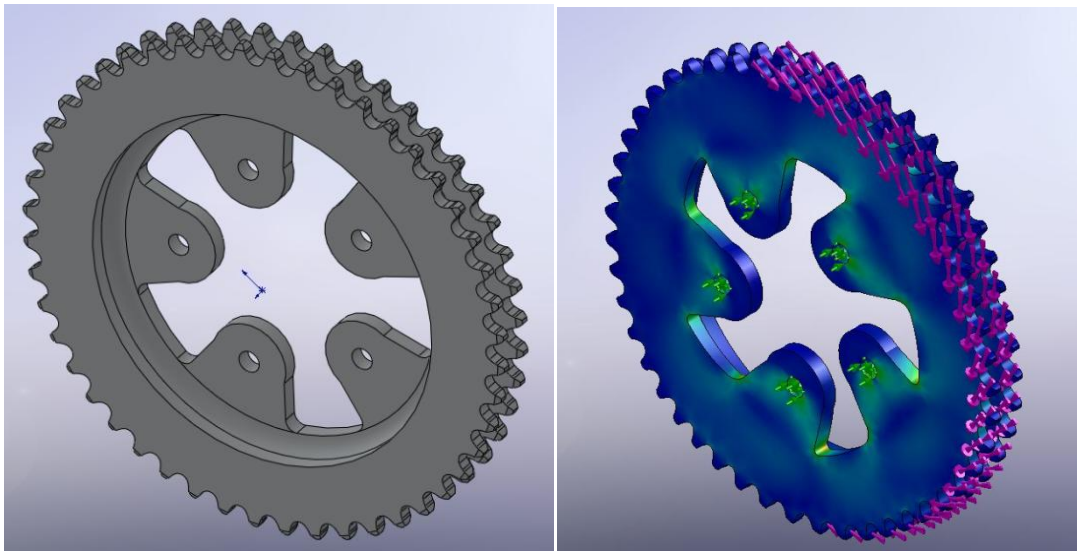

Figure 74: Final Sprocket FEA

The sprocket will be mounted similarly to a flange shared by the rotor on the final output shaft. The tabs were chosen to allow the assembly of the driveshaft where the sprocket will be slid around the flange which is a negative of the sprockets inner mounting design.

When testing the forces acting on the sprockets, the chain tensions were calculated then divided by the number of teeth engaged during impact. For the final drive sprocket the parameter set to calculate for was determined by calculating a 2G force on the rear wheels created during a landing or extreme breaking. The force was calculated to create a max torque 875 ft*lbs. With about 180 degrees of chain wrap, this means that 24 teeth are engaged at all times. Dividing the amount of force of the chain by the number of teeth engaged the force per tooth was determined to be 153 pounds per tooth. This force was then recreated doing finite element analysis to show the effect of the chain on the sprocket and flange. This test was run for both sprockets leading to the final designs shown in the figures above.

Manufacturing

When fabricating both sprockets a custom mount created that would allow the stock to be mounted to larger scrap piece completing the entire piece and only mount it three times. The same jig was used to create both sprockets keeping the process simple. The 6061 aluminum stock would already be surfaced to the correct thickness and mounted first on top of a level

surface of aluminum. Five 0.25 inch holes were drilled in the same pattern as both flanges on the secondary and final drive shafts.

45 Tooth Sprocket

The 0.160 inch piece is then mounted to the jig where the machine would pocket out the spokes as well as the 2.0 inch diameter center with a 15/32 4-flute carbide end mill to remove as much material as possible. Then the 5.588 inch diameter outside before using a 0.1875 inch flat end mill to machine the tooth profile. The next step was to create the chamfer on one side then re-fixture it to complete the operation on the other side.

48 Tooth Sprocket

The 48 tooth sprocket was manufactured using many of the same tools but with a larger piece of stock. Since this was a double sprocket fabricated from a single piece of aluminum a different order of operations needed to take place. Just as the previous sprocket the mounting holes were drilled to mount the 0.561 inch thick blank to the jig. With a 15/32 4-flute carbide end mill the 4.25 inch diameter center and 5.946 inch diameter outside were fabricated. The inner edge was filleted with a .25 inch ball mill before using a 3/16 carbide end mill to fabricate the tooth profile. The spacing created between the two rows of teeth was fabricated using a precision 1 inch diameter by 3/16 thick slitter saw in small step passes as to not disrupt the teeth. Finally like the previous sprocket the last chamfering operations were completed. All manufacturing took place using the VM-3 3 axis vertical CNC milling machine with coding completed with GibbsCAM and CAD models completed using SolidWorks.

Intermediate Shafts

The drive train of the Baja vehicle is a double reduction chain and sprocket as stated previously. Because of the double reduction, intermediate jackshafts are needed to transfer the power from the motor to the final driveshaft. The first driveshaft holds the CVT and the first reduction gear. The shaft is 9 inches in length and was designed to be 4140 steel rod, cold drawn. The Endurance limit of 4140 steel is ~ 70 Ksi. This is under the fatigue stresses the shaft will see during extreme cases. Deflection of the shaft was also looked at because of the loading scenarios. Finite Element Analysis was done along with excel calculations to determine the correct diameter of the shafts as illustrated in Figure 75.

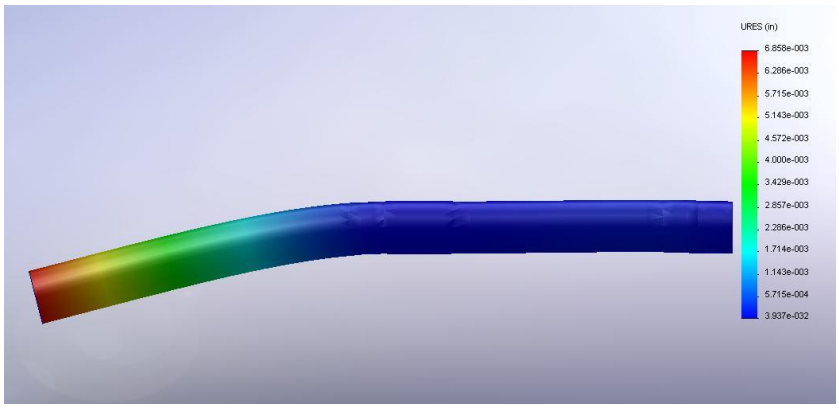

Figure 75: FEA of CVT Jackshaft

For this shaft, at 3/4 inch in diameter, the maximum deflection occurred at the end where the CVT was and it deflected $6*10^3$ inches or 6 thousands of an inch. The angle of twist was also calculated and was found to be .008 degrees.

The second shaft holds the large diameter sprocket from the first reduction and the smaller diameter sprocket of the final reduction. This shaft is 5 inches in length and was designed to be 4140 steel rod, cold drawn. Because the small sprocket is seeing the forces from the tires during extreme loading and the other sprocket is seeing the force applied in the opposite direction from the CVT, the shaft has to be a larger 1 inch diameter shaft. Analysis was also done on this shaft for fatigue stress, deflection, and angle of twist as you can see in Figure 76

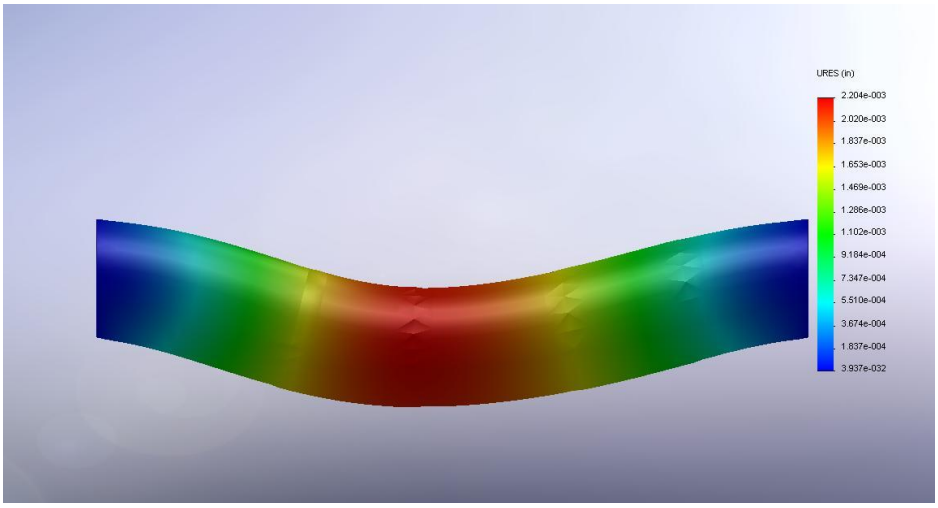

Figure 76: FEA of Secondary Jackshaft

For this shaft, at 1 inch in diameter, the maximum deflection occurred in the middle where the two sprockets would be applying a force to the shaft and it was $2*10^3$ in or 6 thousands of an inch. The angle of twist was also calculated and was found to be 0.07 degrees.

Final Shaft

The final reduction shaft was designed to carry both the final sprocket as well as the brake disc for the rear wheels. The parameters given from the rear suspension were as follows, able to translate 1500 lbf laterality into the chassis and must be less than 12.5 inches wide. From the drive train parameters, it must be at least 7/8 inch diameter to handle the output torque. With these in mind the shaft was designed to have dual taper bearings with a simple washer a nut to both preload the bearings as well as handle the side load force. The taper bearings are rated to handle an axial load of 1640 lbf, and have an outer diameter of about 2 inches. The shaft has a flange welded to it to attach both the sprocket and the rear disc to it. This flange was designed 'in car' to ensure that everything was a proper fit.

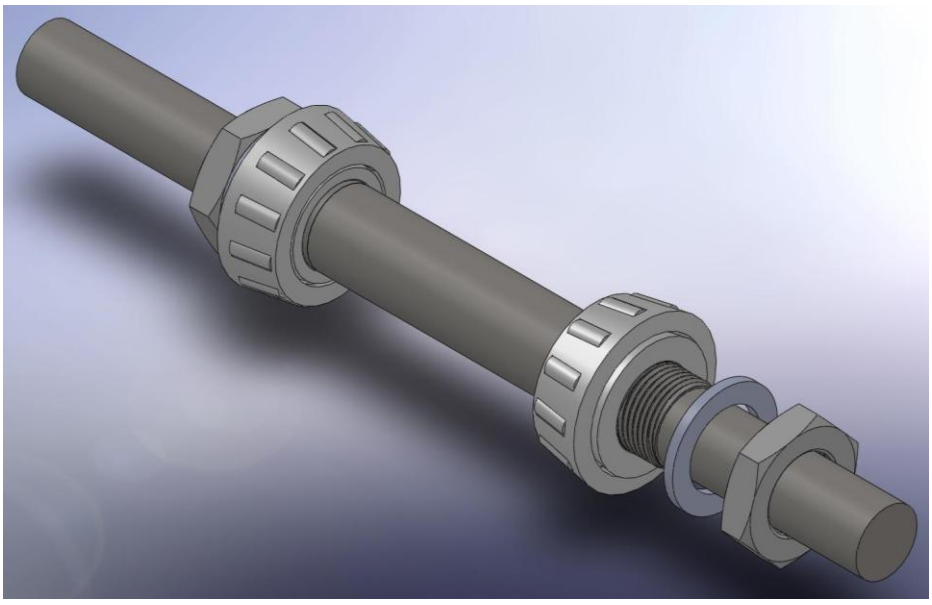

Figure 77: Final Drive Shaft

Gear Frame Parameters

The main design parameters of the gear frame are as follows; be able to house a double chain reduction, light as possible, able to support 2000 lbf from second jackshaft, small as possible, able to support the engine, and have the ability to be removed entirely from the chassis. In addition to these primary parameters other requirements were required for the gear frame; machinability, ease of assembly, and built out of cheap and readily available materials. With this in mind the frame was designed to be built out of 6061-T6 aluminum simple machined parts that could be welded together. The frame around the second jackshaft after FEA needed to be at least 0.75 inches thick to support the tension of each chain pulling on the frame. The remainder of the frame is only ¼ inch thick which allows the frame to be extremely light. This frame profile was created using a simple sketch of the distances of the CVT center to center (200mm) and the smallest distance the chains jackshafts can be to ensure at least a 180-degree wrap on the sprocket.

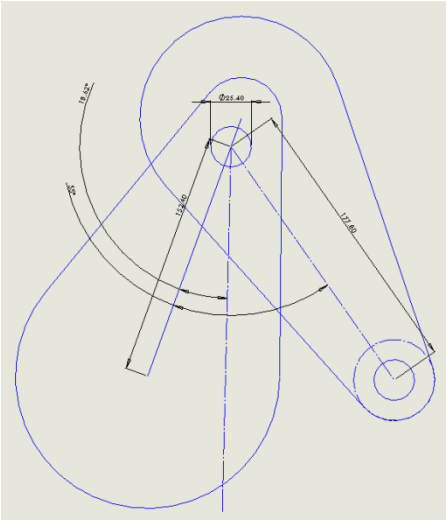

Figure 78: Chain Path Diagram

With the distances determined a frame was drawn including enough material to support the approximate load but also being small enough to fit into the rear of the chassis. The first iteration of the frame is below. This first iteration included two sliding tesnioners any many attachment points to connect to the chassis.

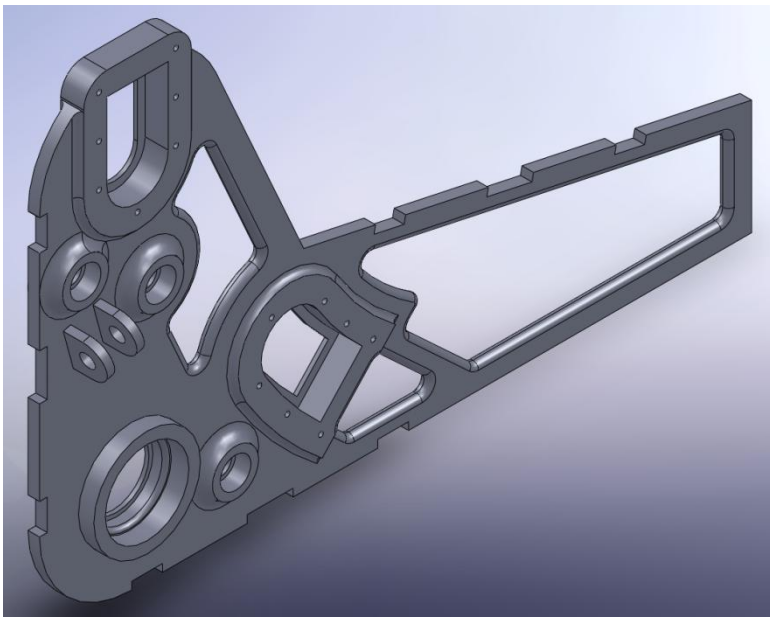

Figure 79: First Design Iterations

This design was not the best method for a total integration of the gear frame into the chassis. A hoop design was then created after much design iteration and brainstorming; this not only allowed a much simpler attachment method but also allowed the chassis to handle the 1500 lbf side force seen by the drive axle (see Bearing Housing section). The second iteration when subjected to several load cases in FEA was found to fail around the engine mount and the area below the tensioner.

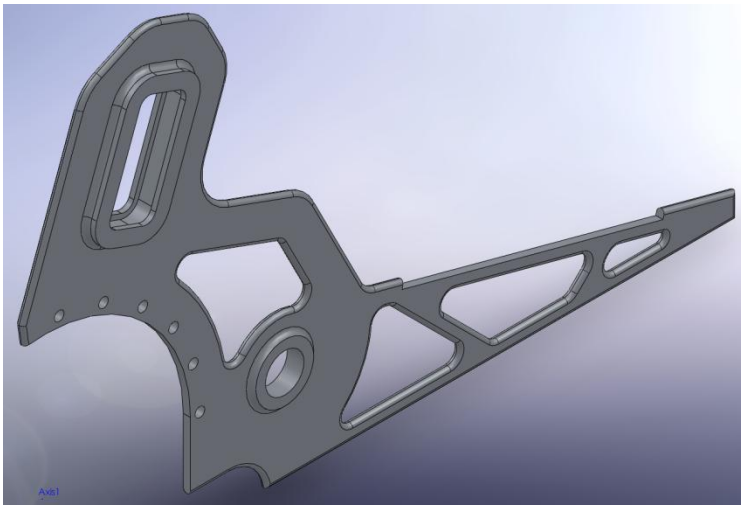

Figure 80: Second Design Iteration

The final design of the gear frame was created under all parameters listed above. The main section supports the engine higher than the previous frames and also previous years of WPI Baja. The main reason for this was by angling the engine at 15 degrees and moving it up about 4 inches, the two reductions can fit closer together and also closer underneath the engine itself. With room for and aft being at a premium and room height wise only limited by a lower center of gravity it was ideal to raise the engine and shorten the overall drive train. A slot was also designed into one of the ears allowing the entire length of the ear to support the load instead of relying solely on shear strength of the bolts. The overall dimensions of the gear frame side can be seen below.

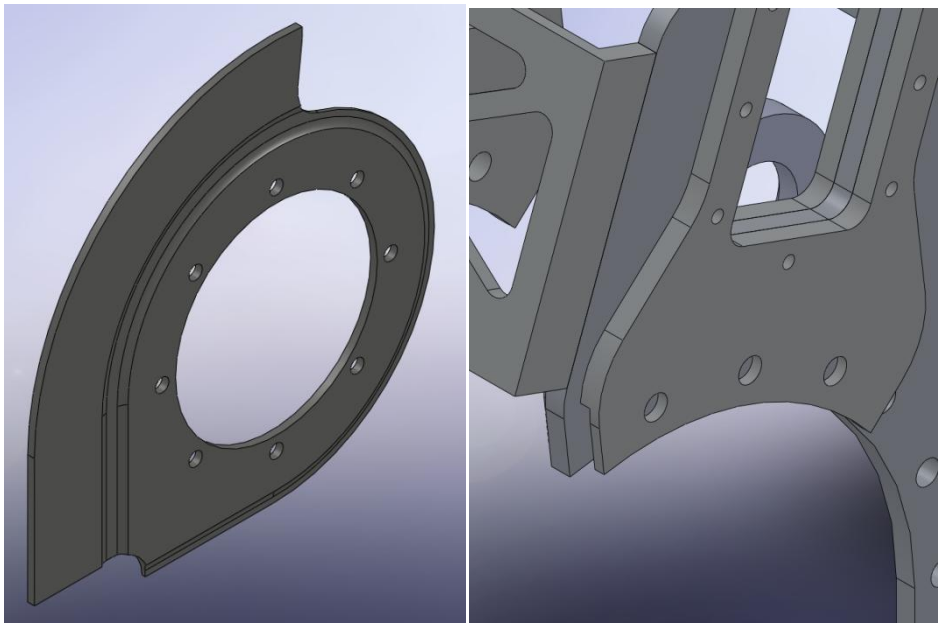

Figure 81: 4130 Tab and Slot

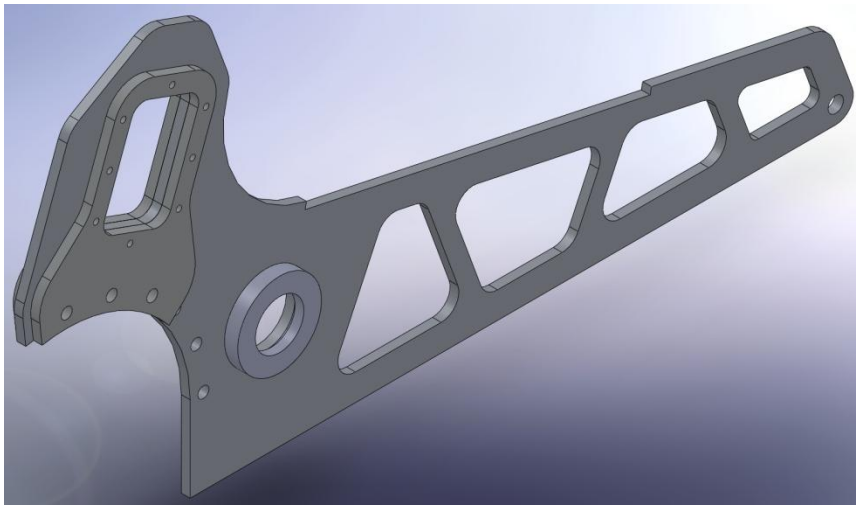

Figure 82: Final Design Iteration

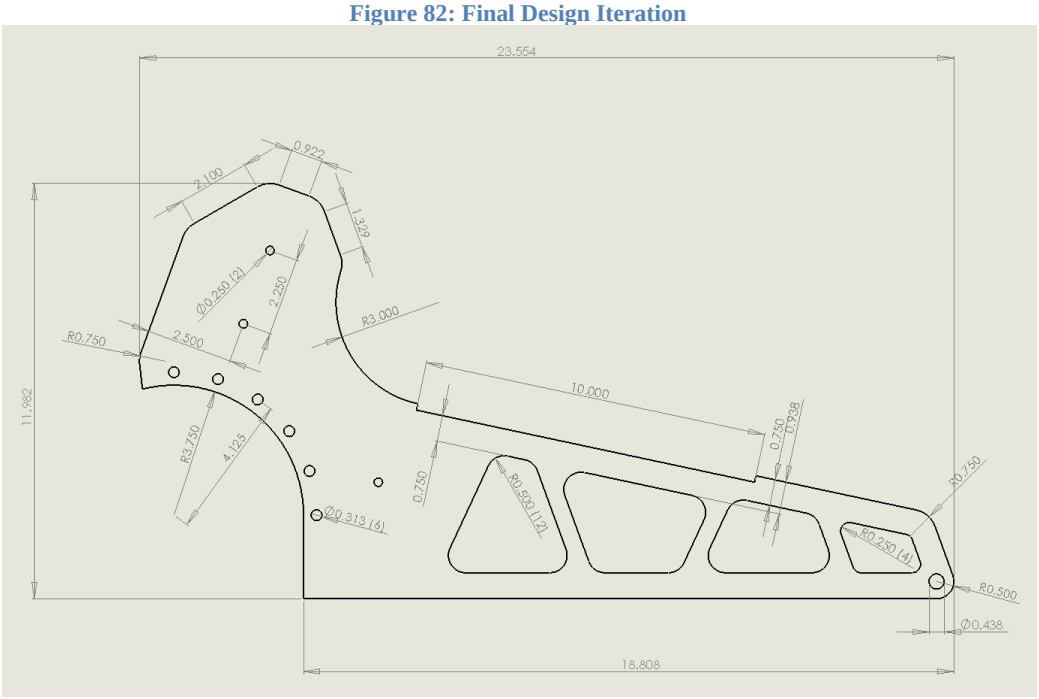

Figure 83: Gear Frame Dimensions

With the entire frame being this thick it would be heavy, however machining a 0.75 inch thick plate down would be costly and an inefficient use of machine time. This problem was solved by having the main plates be water jet cut with two, quarter inch holes in place of where the tensioner slot would be as well as one hole where the bearings for the CVT jackshaft would go. Two ‘ears’ were machined to be bolted to the water jet part which would serve as the thickness required to handle the tension load.

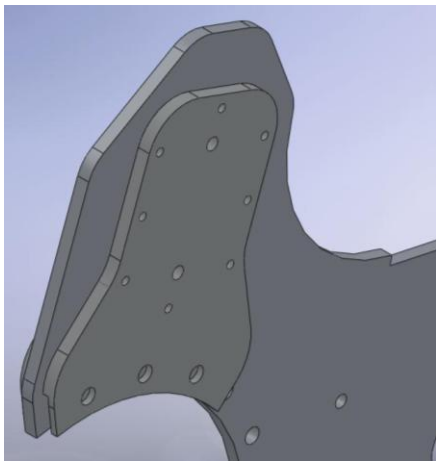

Figure 84: Machined Ear Bolted to Frame

Once each side was welded, a cross piece and engine mount were welded to the frame. For all welds 4043 weld wire was used to ensure minimal cracking in the welds during stress relieving. Proper spacing was critical for alignment and fitment within the chassis. The frame was sent out for stress relieving and tempering to bring the entire frame to T6 giving an overall ultimate tensile strength of at least 42,000 psi (290 MPa) and yield strength of at least 35,000 psi (241 MPa).

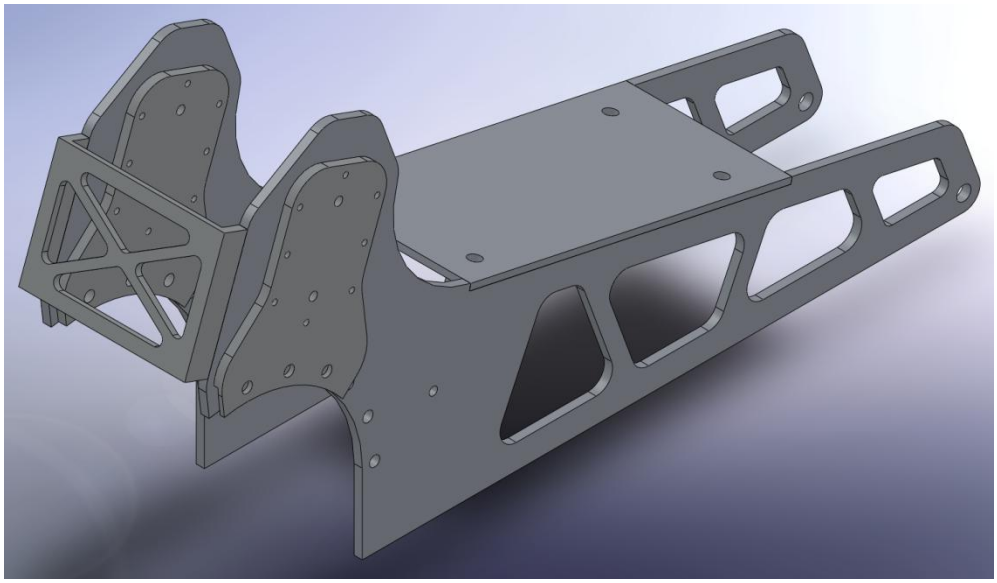

Figure 85: Gear Frame Post-Welding/ Pre-Machining

The final machining of the gear frame needed to be extremely precise to ensure that both the tensioner and the bearings would align with each side and the jack shafts would align

parallel. This was discovered to be a problem after first machining the bearing holes one at a time and having the bearings not line up. This was fixed by obtaining oversized bearings (2 inch OD over 1.625 inch OD) and machining using a 1 inch diameter by 6 inch long end mill both side were able to be cut in one fixture; allowing the bearings to be perfectly aligned. The tensioner slots were cut one at a time, the alignment was not as critical as the CVT bearings because each side has the ability to move independent of the other.

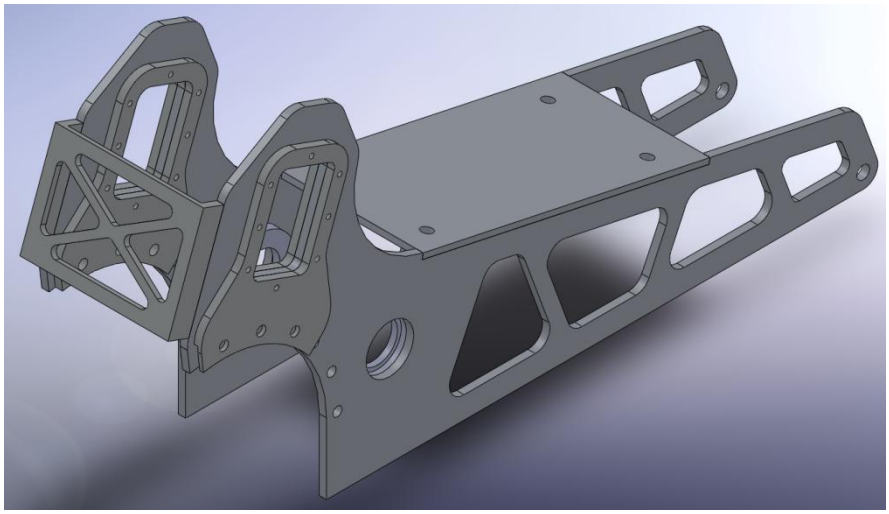

Figure 86: Final Gear Frame after Final Machining

Bearing Housing

The bearing housing for the final shaft needed to perform under the following conditions; handle a side force of 1500 lbf, light weight, built out of cheap and readily available materials, and not require heat treatment. This was accomplished by designing identical housings to go on either side of the final drive shaft and support the taper bearings. The load would be transferred into the outer bearing that would be press fit into the housing; the housing is then bolted to the inner 4130 tab that is part of the chassis. A smaller bolt pattern can be seen on the front of the hosing to allow for the grease seals to be attached. The back of the housing has a 0.625 inch radius fillet, this is to evenly distribute the loads from the flat plane that the outer bearing rest on to the rest of the chassis.

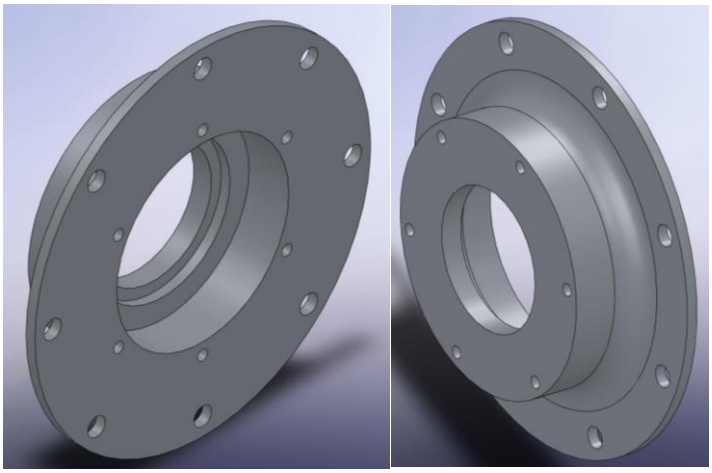

Figure 87: Bearing Housing

FEA was performed on the housing to ensure compliance with the 1500 lbf force that it would see throughout its life time. Under a purely axial loading case, the housing sees a maximum stress of 3.68 ksi, this gives the housing a safety factor of about two.

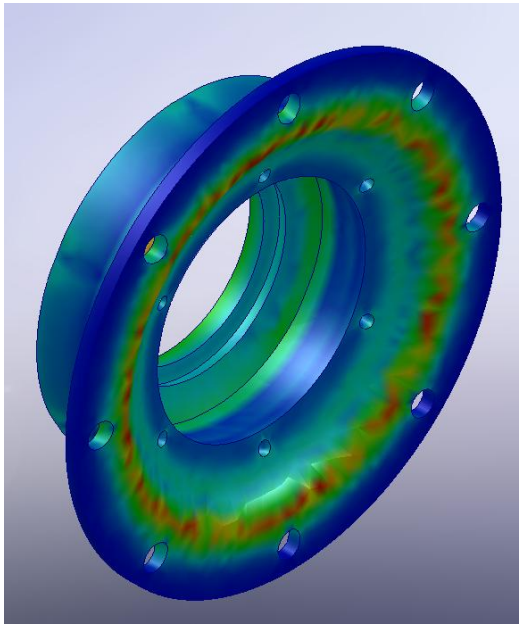

Figure 88: Bearing Housing FEA

Appendix A: Thermal Processing

Low alloy steel, AISI 4130 (tempered @ 540 C, H2O quenched)

General

Designation

Low alloy steel, AISI 4130 (tempered @ 540 C, H2O quenched)

Density		0.2818	-	0.2854	lb/in^3		
Price	*	0.2664	-	0.4138	USD/lb		

Tradenames

BSC-SR-95, British Steel plc (UK); TKS 34CRMO4, ThyssenKrupp Stahl AG (GERMANY); TKS 25CRMO4, ThyssenKrupp Stahl AG (GERMANY); A-1251, AFORA (Aceros Afora S.A.) (SPAIN); A-1250, AFORA (Aceros Afora S.A.) (SPAIN);

Mechanical

Bulk modulus		22.48	-	25.53	10^6 psi		
Compressive strength		118.9	-	145	ksi		
Elongation		13	-	21	%		
Fatigue strength at 10^7 cycles			*	58.74	-	68.17	ksi
Fracture toughness	*	39.13	-	64.61	ksi.in^1/2		
Hardness - Vickers		285	-	355	HV		
Mechanical loss coefficient		*	3.9e-4	-	4.9e-4		
Modulus of rupture		118.9	-	145	ksi		
Poisson's ratio		0.285	-	0.295			
Shape factor		27					
Shear modulus		11.17	-	12.33	10^6 psi		
Tensile strength		134.2	-	165.3	ksi		
Yield strength (elastic limit)			118.9	-	145	ksi	
Young's modulus		29.15	-	31.33	10^6 psi		

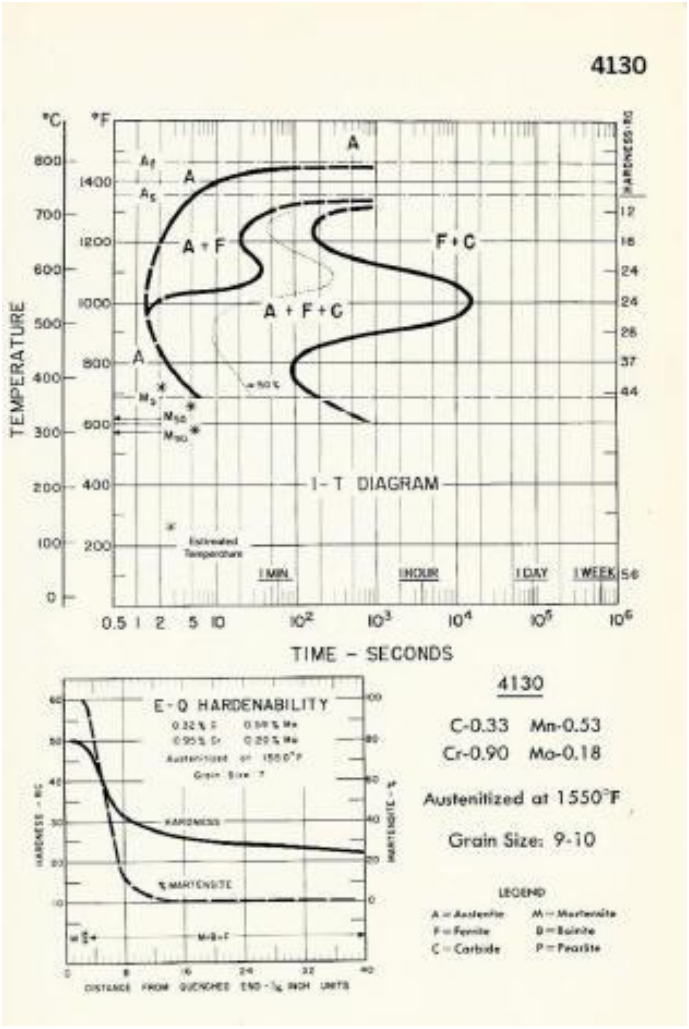

Figure 89 4130 I-T Diagram

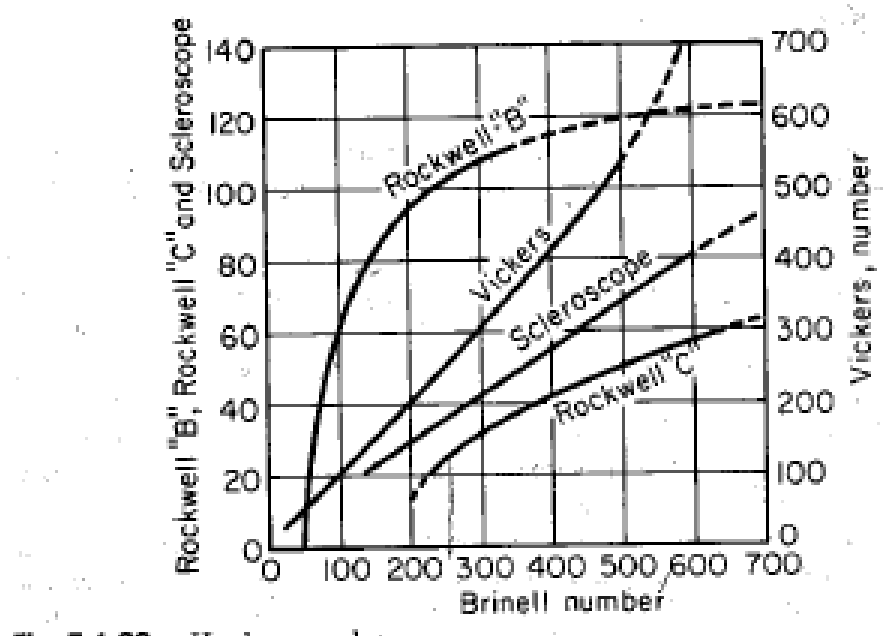

Figure 90 Material Hardness Conversion Chart

Appendix B: Input Load Determination

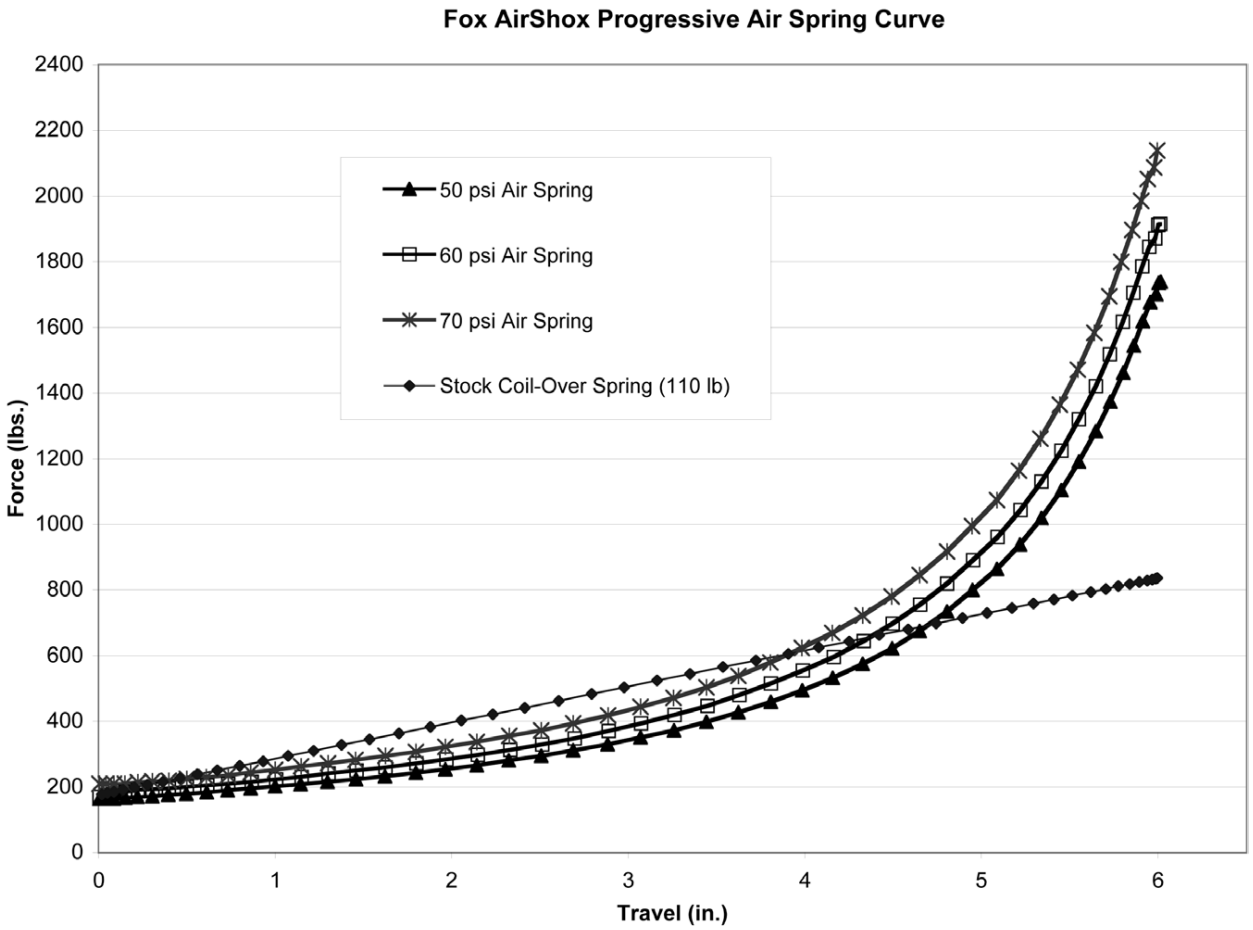

Figure 91: Fox Float 2.0 Force vs. Compression

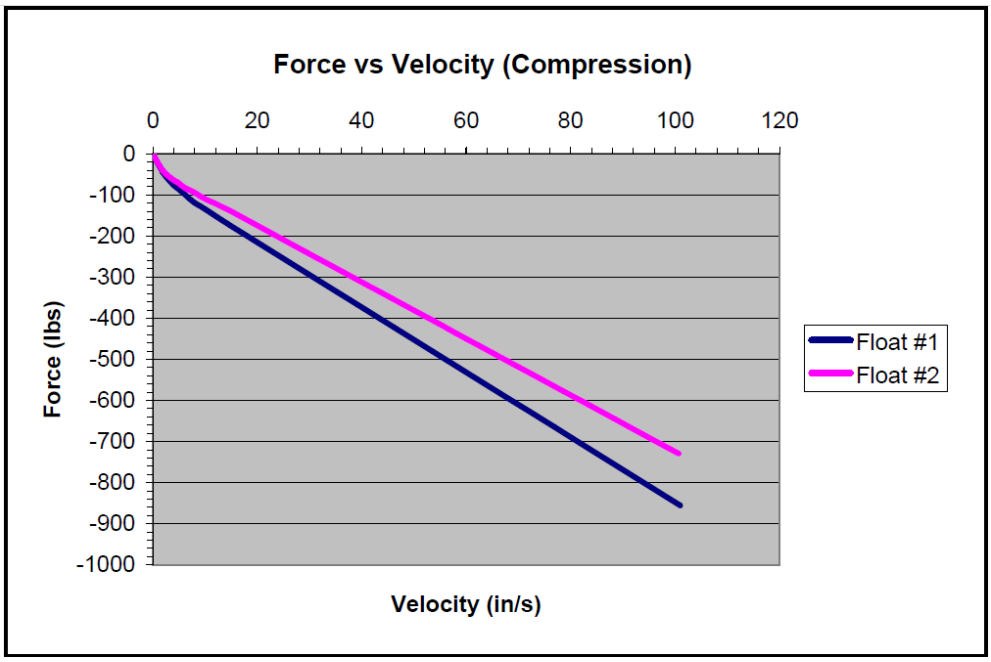

Figure 92: Fox Float 2.0 Compression Force vs. Velocity

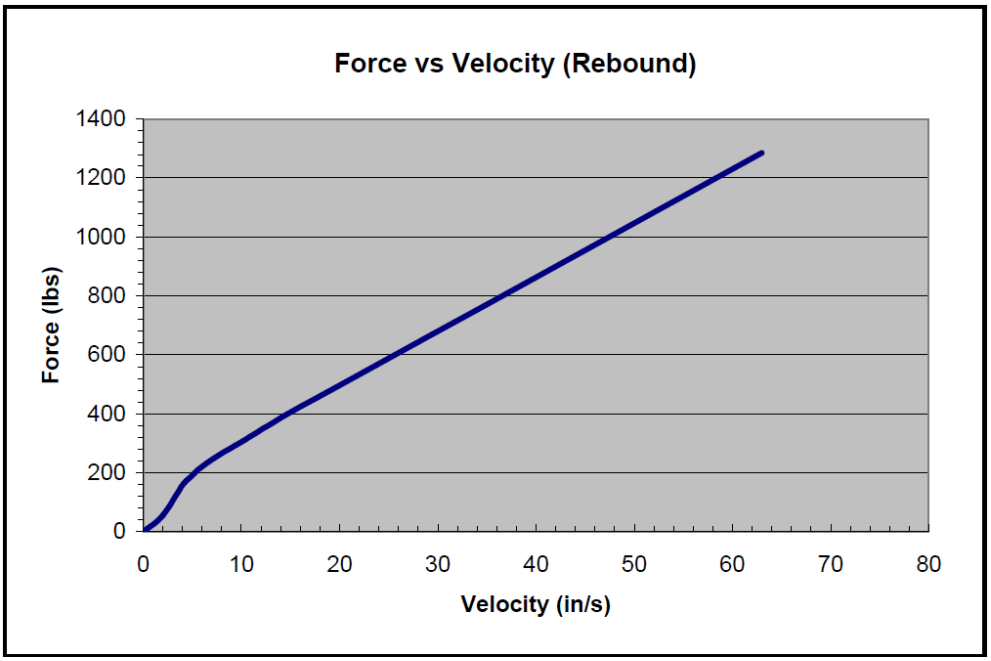

Figure 93: Fox Float 2.0 Rebound Force vs. Velocity

```
%WPI Mini Baja Suspension Simulation
%Kyle Tarry
%Last Update: 2/23/2007
%Last Modified: 2/6/2009
%----------------------------------------
%Define Inputs
dt=0.001;   %time step
V0=-18;     %initial velocity of vehicle, in ft/s
m=125;      %sprung mass of vehicle
Ka=2;     %"Effective" Spring rate in lb/in^2
Kn=3.5;     %Spring exponent (rise rate)
Kb=175;      %Spring preload (lb)
Dc=7.4;      %Damper compression slope (lb/in/s)
Dci=75;     %damper compression intercept (lb)
Dr=16.7;      %Damper rebound slope (lb/in/s)
Dri=115;     %Damper rebound intercept (lb)
T=1.0;      %total time for simulation, seconds
%x=15;       %Distance from lower shock mount to LCA pivot on chassis
%Llca=18;   %Lower control arm length

%Calculate number of iterations required
imax=T/dt;

%Calculate weight
W=m*1;   %Weight, W=m*g, g=1g.

%Initialize arrays
t=zeros(imax,1);        %time as a function of iteration number
xm=zeros(imax,1);       %position of chassis
xs=zeros(imax,1);       %position of shock body
vm=zeros(imax,1);       %velocity of chassis
```

```
vs=zeros(imax,1);       %velocity of shock body
Sf=zeros(imax,1);       %Spring force
Df=zeros(imax,1);       %Damper force
Fs=zeros(imax,1);       %Total force in shock body
Fnet=zeros(imax,1);     %net force on body
a=zeros(imax,1);        %acceleration
Keff=zeros(imax,1);     %effective spring rate
theta=zeros(imax,1);    %lower control arm angle
alpha=zeros(imax,1);    %strut angle
Rm=zeros(imax,1);       %motion ratio as a function of suspension pos.
Fnat=zeros(imax,1);     %natural frequency (undamped)
Lshock=zeros(imax,1);   %Shock length

%Initialize start values
t(1)=0;
xm(1)=0;
xs(1)=0;
vm(1)=V0*12;    %Initial velocity in inches per second
vs(1)=vm(1)/(Llca/x);
a(1)=0;
%Rm(1)=Llca/x;   %Initialize motion ratio
Rm(1)=3.1;

for i=2:imax
   t(i)=dt*(i-1);  %Time in seconds
   xm(i)=xm(i-1)+vm(i-1)*dt;   %displacement of chassis (in)
   vm(i)=vm(i-1)+a(i-1)*dt;    %velocity of chassis (in/s)
   Rm(i)=3.1;              %temporary input for constant motion ratio
   xs(i)=xm(i)/Rm(i-1);            %displacement of shock (in)
   vs(i)=vm(i)/Rm(i-1);            %velocity of shock (in/s)
```

```
        %Spring Force Calculations
        if (xs(i)<0)
            Sf(i)=abs(Ka*xs(i)^Kn)+Kb;        %Spring force (lb)
        else
            Sf(i)=0;              %Spring force is zero if car is airborne
        end

        %Damper Force Calculations
        if (xs(i)<0)          %if damper is compressed
            if (vs(i)<0)
                Df(i)=-Dc*vs(i)+Dci;        %if damper is under compression, damper force is
slope times velocity
            else
                Df(i)=-Dr*vs(i)-Dri;       %if damper is under rebound, damper force is slope
times (neg) velocity
            end
        else
            Df(i)=0;                  %If damper is uncompressed (vehicle is airborne)
        end

        Fs(i)=Df(i)+Sf(i);                  %Total axial force in damper (lb)
        Fnet(i)=Fs(i)/Rm(i-1)-W;              %Net force acting on chassis (lb)
        a(i)=Fnet(i)/m*32.2*12;               %acceleration in in/s^2 (g*ft/s*in/ft)
        Keff(i)=(Sf(i)-Sf(i-1))/(xs(i-1)-xs(i));    %effective spring rate
        %theta(i)=asind((-xm(i)-0.578*Llca)/Llca);   %Lower control arm angle
        %alpha(i)=atand((cosd(theta(i))*x-5)/(12-sind(theta(i))*x));  %damper angle
        %Rm(i)=(Llca/x/cosd(alpha(i)));  %motion ratio
        %Fnat(i)=sqrt((Keff(i)/Rm(i))/m)*1/(2*3.14159);  %Natural frequency; needs re-
formulation
        %Lshock(i)=sqrt((cosd(theta(i)*x-5))^2+(12-sind(theta(i))*x)^2); %damper length
    end
```

Appendix C: FEA Results

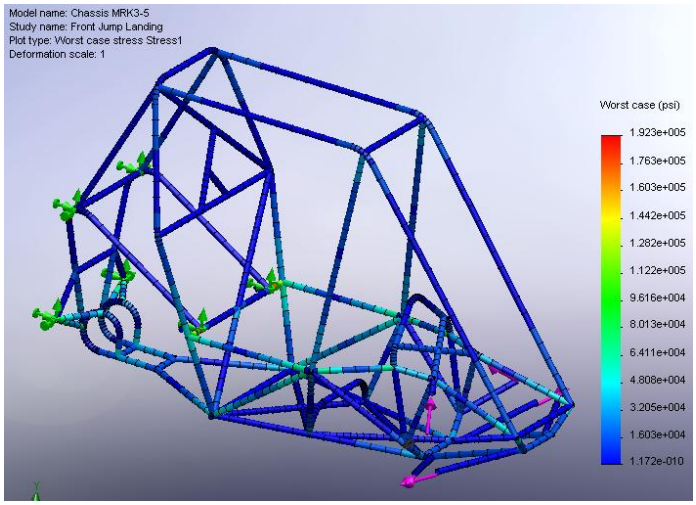

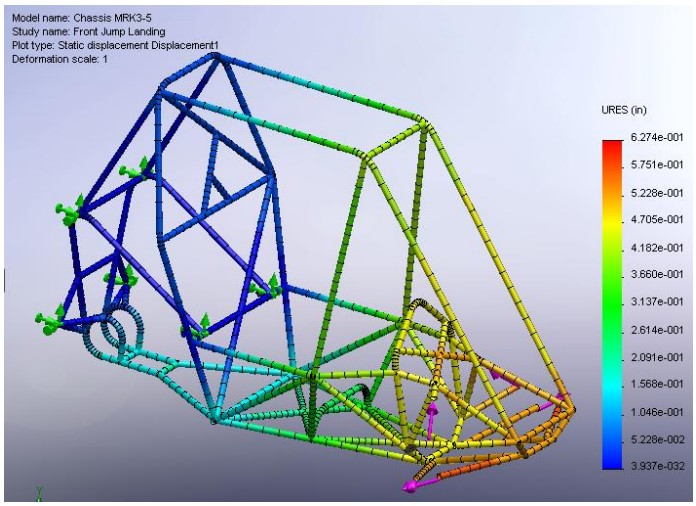

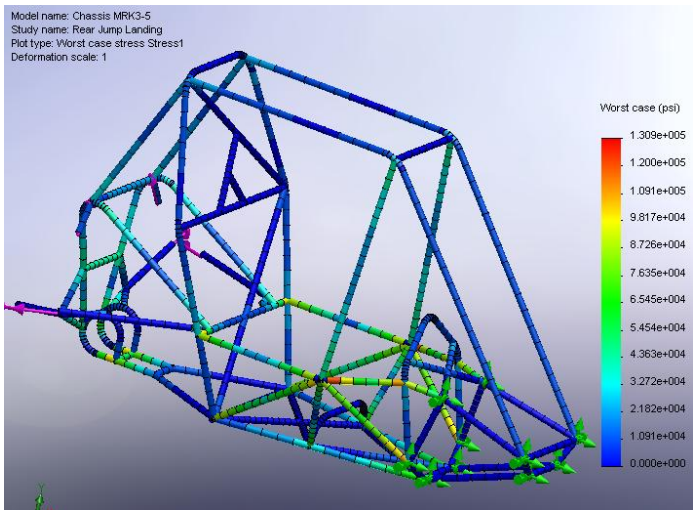

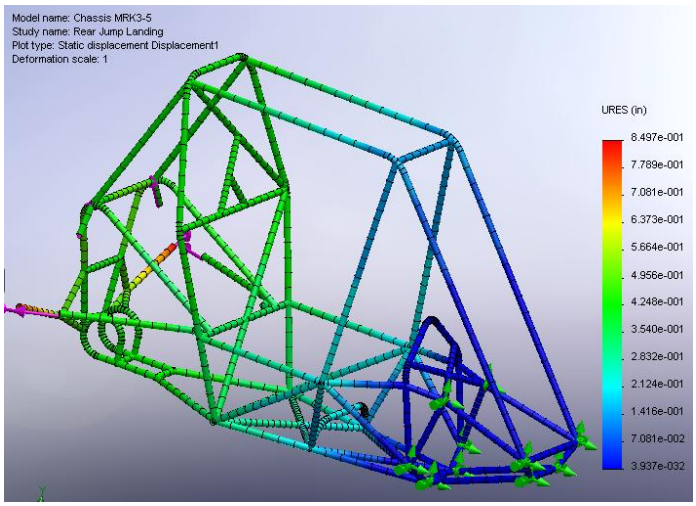
Model name: Chassis MRK3-5
Study name: Rear Jump Landing
Plot type: Static displacement Displacement1
Deformation scale: 1
URES (in)
8.497e-001
7.789e-001
7.081e-001
6.373e-001
5.664e-001
4.956e-001
4.248e-001
3.540e-001
2.832e-001
2.124e-001
1.416e-001
7.081e-002
3.937e-032

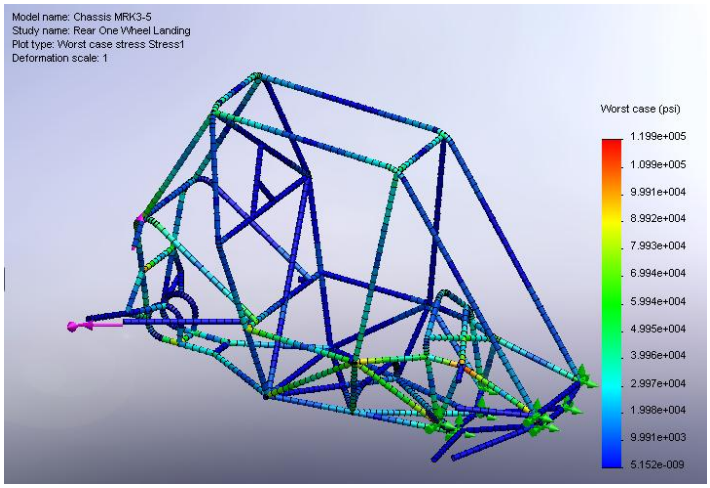
Model name: Chassis MRK3-5
Study name: Rear One Wheel Landing
Plot type: Worst case stress Stress1
Deformation scale: 1
Worst case (psi)
1.199e+005
1.099e+005
9.991e+004
8.992e+004
7.993e+004
6.994e+004
5.994e+004
4.995e+004
3.996e+004
2.997e+004
1.998e+004
9.991e+003
5.152e-009

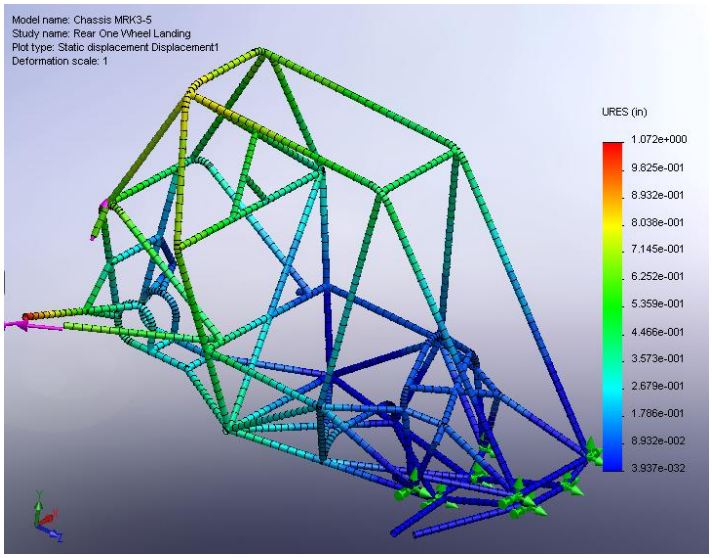
Model name: Chassis MRK3-5
Study name: Rear One Wheel Landing
Plot type: Static displacement Displacement1
Deformation scale: 1
URES (in)
1.072e+000
9.825e-001
8.932e-001
8.038e-001
7.145e-001
6.252e-001
5.359e-001
4.466e-001
3.573e-001
2.679e-001
1.786e-001
8.932e-002
3.937e-032

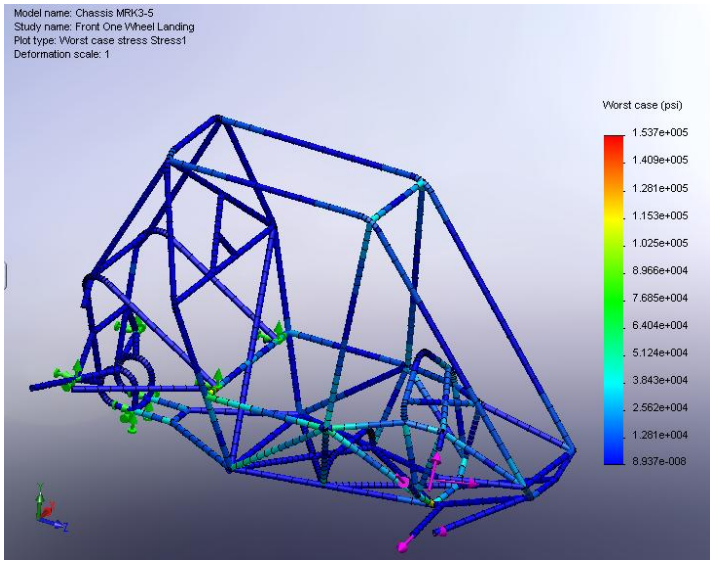
Model name: Chassis MRK3-5
Study name: Front One Wheel Landing
Plot type: Worst case stress Stress1
Deformation scale: 1
Worst case (psi)
1.537e+005
1.409e+005
1.281e+005
1.153e+005
1.025e+005
8.966e+004
7.685e+004
6.404e+004
5.124e+004
3.843e+004
2.562e+004
1.281e+004
8.937e-008

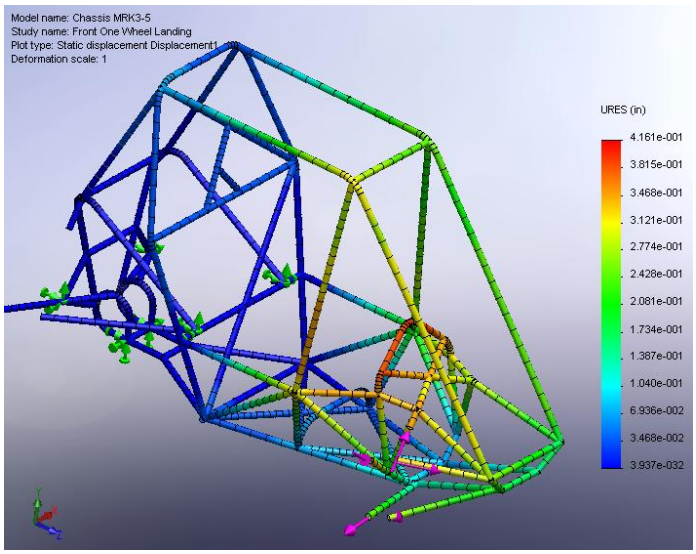
Model name: Chassis MRK3-5
Study name: Front One Wheel Landing
Plot type: Static displacement Displacement1
Deformation scale: 1
URES (in)
4.161e-001
3.815e-001
3.468e-001
3.121e-001
2.774e-001
2.428e-001
2.081e-001
1.734e-001
1.387e-001
1.040e-001
6.936e-002
3.468e-002
3.937e-032

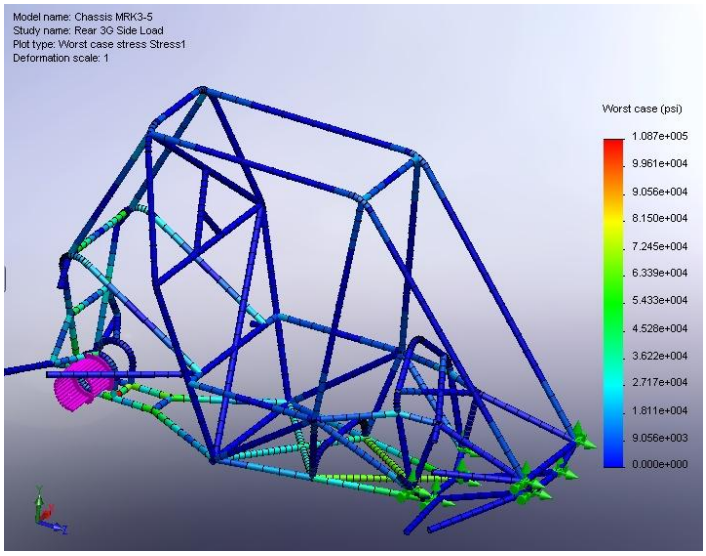
Model name: Chassis MRK3-5
Study name: Rear 3G Side Load
Plot type: Worst case stress Stress1
Deformation scale: 1
Worst case (psi)
1.087e+005
9.961e+004
9.056e+004
8.150e+004
7.245e+004
6.339e+004
5.433e+004
4.528e+004
3.622e+004
2.717e+004
1.811e+004
9.056e+003
0.000e+000

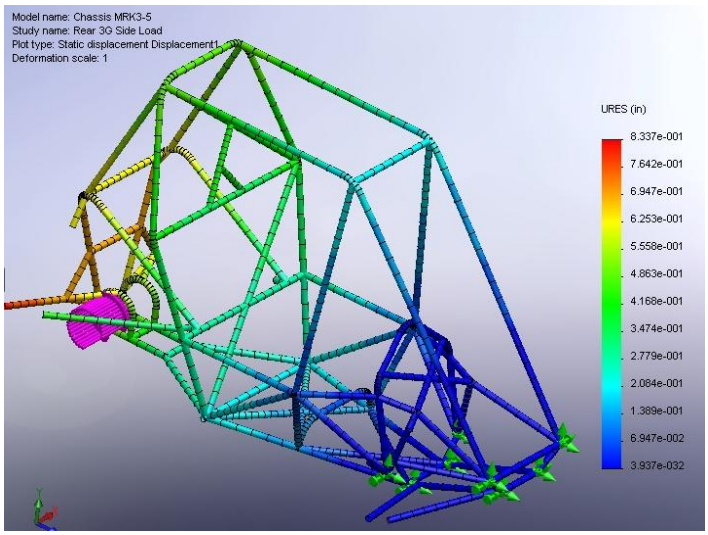
Model name: Chassis MRK3-5
Study name: Rear 3G Side Load
Plot type: Static displacement Displacement1
Deformation scale: 1
URES (in)
8.337e-001
7.642e-001
6.947e-001
6.253e-001
5.558e-001
4.863e-001
4.168e-001
3.474e-001
2.779e-001
2.084e-001
1.389e-001
6.947e-002
3.937e-032

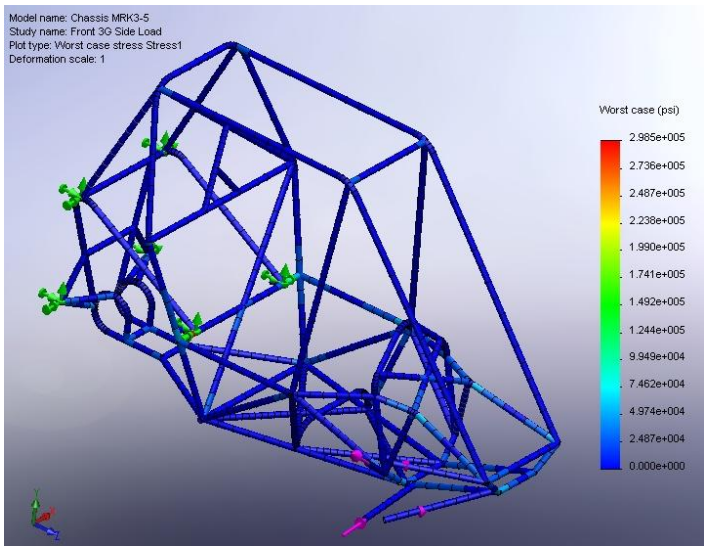
Model name: Chassis MRK3-5
Study name: Front 3G Side Load
Plot type: Worst case stress Stress1
Deformation scale: 1
Worst case (psi)
2.985e+005
2.736e+005
2.487e+005
2.238e+005
1.990e+005
1.741e+005
1.492e+005
1.244e+005
9.949e+004
7.462e+004
4.974e+004
2.487e+004
0.000e+000

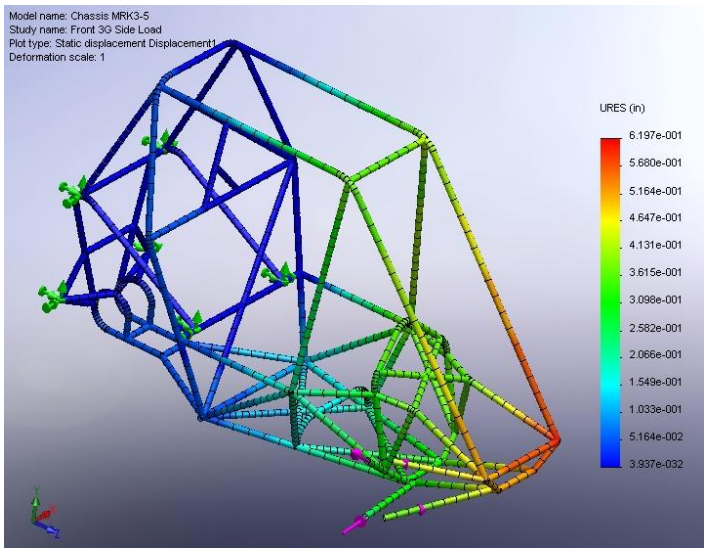
Model name: Chassis MRK3-5
Study name: Front 3G Side Load
Plot type: Static displacement Displacement1
Deformation scale: 1
URES (in)
6.197e-001
5.680e-001
5.164e-001
4.647e-001
4.131e-001
3.615e-001
3.098e-001
2.582e-001
2.066e-001
1.549e-001
1.033e-001
5.164e-002
3.937e-032

Appendix D: Stressed Panel Analysis

Cytec Thornel® P-75 Carbon Fiber/Epoxy Advanced Composite System

Physical Properties	Metric	English	Comments
Density	1.70 g/cc	0.0614 lb/in³	

Mechanical Properties	Metric	English	Comments
Tensile Strength, Ultimate	930 MPa	135000 psi	
Tensile Modulus	320 GPa	46400 ksi	
Compressive Yield Strength	440 MPa	63800 psi	
Shear Strength	55.0 MPa	7980 psi	

Thermal Properties	Metric	English	Comments
Thermal Conductivity	110 W/m-K	763 BTU-in/hr-ft²- degreesF	

Appendix E: Drive Train Calculations

$$Top\ Speed = 43\ mph = 3784\frac{feet}{minute}$$

$$D_W = 2.125'$$

$$Wheel\ RPM = \frac{Top\ Speed}{\pi * D_W} = 566.8\ RPM$$

$$CVT\ Max\ Ratio = 0.75$$

$$Engine\ Max\ RPM = 3750\ RPM$$

$$Sprocket\ RPM = \frac{3750\ RPM}{0.75} = 5000\ RPM$$

$$Final\ Reduction\ Ratio = \frac{Sprocket\ RPM}{Wheel\ RPM} = 8.82$$

$$Engine\ RPM\ at\ Max\ Power = 3250\ RPM$$

$$CVT\ Max\ Efficient\ Ratio = 1$$

$$Sprocket\ RPM = \frac{3250\ RPM}{1} = 3250\ RPM$$

$$Wheel\ RPM = \frac{3250\ RPM}{8.82} = 368.5\ RPM$$

$$Average\ Speed = 368.5\ RPM * \pi * D_W = 2459.9\frac{feet}{minute} = 27.95\ mph$$

Appendix F: Camber Vs. Steering Angle

```
clear; close; clc;

% Input intitial Kingpin Inclination = ki0

ki0 =20;

% Input Castor Angle = ca

ca =25;

% Input camber at ride height

c0 = 0;

for i = 1:51

% Input steering Input Angle inside = isia and outside = osia

isia(i) = -26 + i;

osia(i) = 26 - i;

% Calculate auxiliary steering input angle = asia
% and kingpin inclination = aki due to castor angle

asia = atand(tand(ca)/tand(ki0));

aki = atand(tand(ca)/sind(asia));

% Calculate kingpin inclination inside of bend = iki
% and outside of bend = oki

iki = atand(tand(aki)*cosd(asia-isia(i)));

oki = atand(tand(aki)*cosd(asia-osia(i)));

% Calculate camber of inside = ic and outside = oc tires

ic(i) = (ki0 + c0) - iki;

oc(i) = (ki0 + c0) - oki;
```

```
end


figure
%subplot(2,1,1)
%plot(isia, ic)

subplot(1,1,1)
plot(isia, oc)
legend('Camber Gain')
```

Color Key:	Input
	Output

Vehicle and Component Spefications						
Tire/Ground COF	Pad/Rotor COF	Vehicle Weight (lb)	Brake lever Ratio	Balance Bar Ratio (F/R)	Max line Pressure (psi)	Input Force (lbf)
0.8	0.6	600	6	0.5	1500	80

Front Brakes:				
Tire D (in)	Rotor D Front (in)	Master Cylinder D (in)	Caliper Cylinder D (in)	Weight ratio
25	6	0.5	1.2	0.4

Cylinder Ratio	Weight Per Front Wheel	Frictional Force per Front Tire	Wheel Torque	Required Friction Force on Rotor	Required Normal Force on Rotor	Required Lock Up Force	Required Line Pressure	% Over Max Input Force	% Over Max Line Pressure
0.1736	120	96	1200	400.0000	666.6667	38.5802	589.7617	-1.0736	-1.5434

Rear Brakes:					
Rear Tire D (in)	Rotor D Rear (in)	Master Cylinder D (in)	Caliper Cylinder D (in)	# of Caliper Cylinders	Weight ratio
25	6	0.5	1	2	0.6

Cylinder Ratio	Weight Per Both Wheels	Frictional Force per Both Tires	Wheel Torque	Required Friction Force on Rotor	Required Normal Force on Rotor	Required Lock Up Force	Required Line Pressure	% Over Max Input Force	% Over Max Line Pressure
0.1250	360	288.0000	3600.0000	1200.0000	2000.0000	83.3333	2547.7707	0.04	0.41125

Appendix H: Chain and Sprocket Calculations

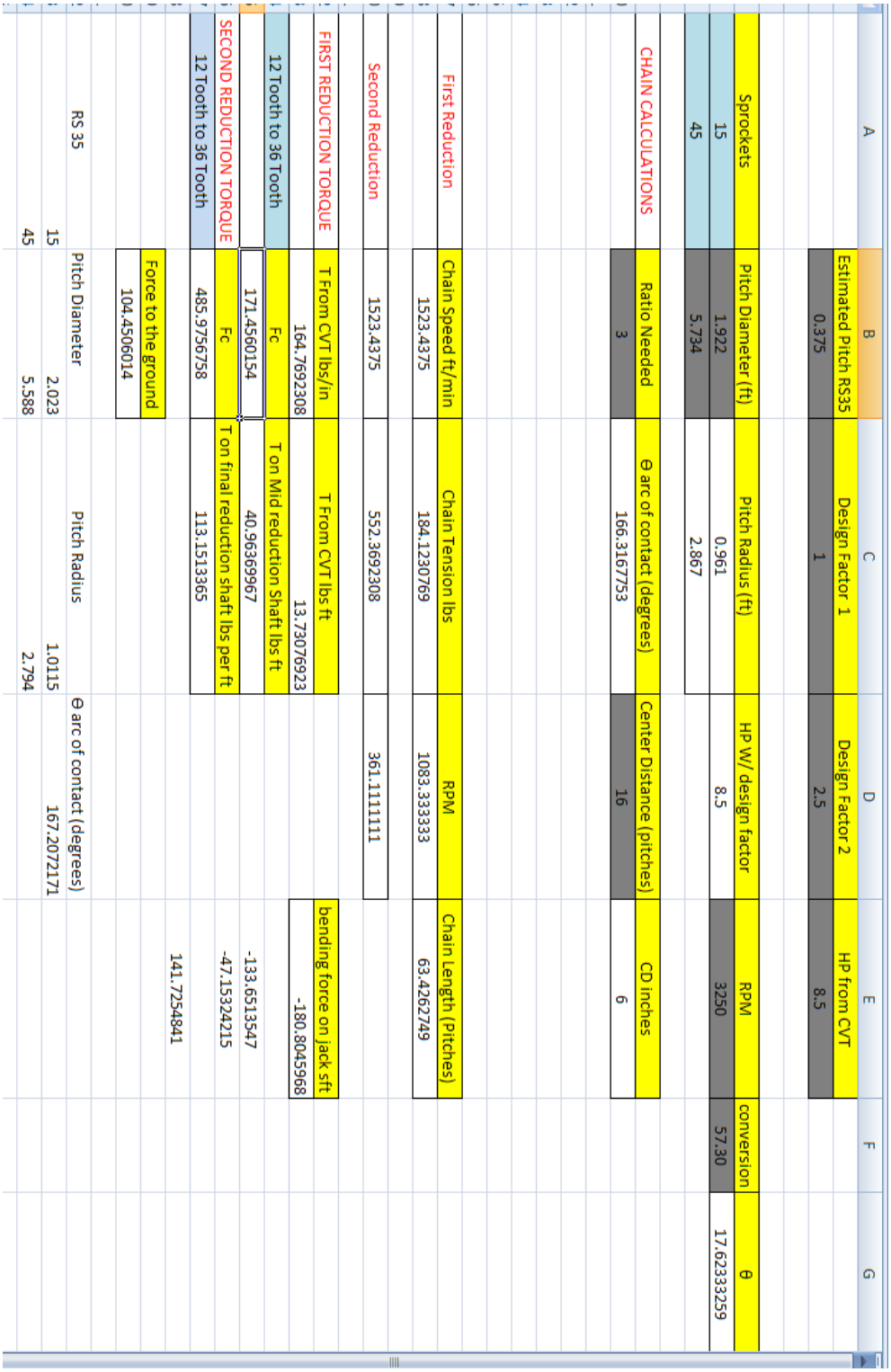

	A	B	C	D	E	F	G
		Estimated Pitch RS35	Design Factor 1	Design Factor 2	HP from CVT		
		0.375	1	2.5	8.5		
	Sprockets	Pitch Diameter (ft)	Pitch Radius (ft)	HP W/ design factor	RPM	conversion	θ
	15	1.922	0.961	8.5	3250	57.30	17.62333259
	45	5.734	2.867				
	CHAIN CALCULATIONS	Ratio Needed	Θ arc of contact (degrees)	Center Distance (pitches)	CD inches		
		3	166.3167753	16	6		
	First Reduction	Chain Speed ft/min	Chain Tension lbs	RPM	Chain Length (Pitches)		
		1523.4375	184.1230769	1083.333333	63.4262749		
	Second Reduction	1523.4375	552.3692308	361.1111111			
	FIRST REDUCTION TORQUE	T From CVT lbs/in	T From CVT lbs ft		bending force on jack sft		
		164.7692308	13.73076923		-180.8045968		
	12 Tooth to 36 Tooth	Fc	T on Mid reduction Shaft lbs ft				
		171.4560154	40.96369967		-133.6513547		
	SECOND REDUCTION TORQUE	Fc	T on final reduction shaft lbs per ft		-47.15324215		
	12 Tooth to 36 Tooth	485.9756758	113.1513365		141.7254841		
		Force to the ground					
		104.4506014					
		RS 35	Pitch Diameter	Pitch Radius	Θ arc of contact (degrees)		
		15	2.023	1.0115	167.2072171		
		45	5.588	2.794			

Appendix I: Brake Disc Thermal Analysis

	Energy Generated (lbf-in)	Temperature Increase (Farenheit)			
	489176.8838	99.9044707			
Joules	55269.56656				
	Force on Disk (lbf)				
	1200				
	Disk diameter (in)	Brake Pad Radius (in)	Brake Circumference (in)	Heating volume correction 2	Heating volume (in^3)
	6	2.5	15.70796327		15.34990062
	Disk thickness (in)				
	0.25				
	Caliper area (in^2)	Caliper Hegiht (in)			
	3	1.954410048			
	rotational start speed (rpm)		Speed (mph)	Tire Dia(feet)	
	461.3624836		35	2.125	
	rotational stop speed (rpm)				
	0				
	Time of deceleration (s)				
	15				
	Coefficient of friction				
	0.45				
	Cp break disc (BTU/lb-F)	ft-lbf/lb-F	in-lbf/lb-F		
	0.12	93.6	1123.2		
	Break Disc Density (lb/in^3)	Brake Heating mass (lb)			
	0.284	4.359371776			

Works Cited

Carroll Smith; (1984). Engineer to Win: The Essential Guide to Racing Car Materials Technology Or How to Build Winners Which Don't Break, Published by MotorBooks/MBI Publishing Company

G.K. Batchelor. (1999). An introduction to fluid dynamics

George E. Totten, Maurice A. H. Howes; (1997). Steel Heat Treatment Handbook; Published by Marcel Dekker

Georgia State University. (2008). *Hyperphysics*.http://hyperphysics.phy-astr.gsu.edu/hbase/airfri.html

Heat Treaters Guide: Standard Practice and Procedure for Steel, eds.
P.M.Unterweiser, H.E.Boyer and J.J.Kubbs,
ASM, Metals Park, Ohio, (1982). (UCD PSL: TN751.H4 1982

J. Reimpell & H. Stoll. (1996). The automotive chassis: Engineering principles

J.Y. Wong, P. D. (1978). *Theory of ground vehicles*

Julian Happian-Smith (Ed.). (2002). An introduction to modern vehicle design

Kraftfahrtechnisches taschenbuch. english. automotive handbook / [editor in chief, horst bauer; edictorial staff, karl-heinz dietsche, jurgen cripin, folkhart dinkler] variant title: Bosch automotive handbook primary material: Book subject(s): Automobiles--design and construction--handbooks, manuals, etc.

Krauss, G; (1990). "Steels: Heat Treatment and Processing Principles"; ASM International

Lindeburg,Michael R.Other Author(s): Professional Engineering Registration Program. Mechanical engineering reference manual / michael R. lindeburg. primary material: Book subject(s): Mechanical engineering--problems, exercises, etc.

Matex Products, I. (2008). *Planetary gears.*, (2008). from http://www.matexgears.com/

Maurice Olley, William F. Milliken and Douglas L. Milliken. (2002). *The automotive chassis: Engineering principles*

Roberto Lot. (2004). A motorcylce tire model for dynamic simulations: Theoretical and experimental aspects.

Sindo Kou; (2003). Welding Metallurgy; Published by John Wiley and Sons

Wikipedia. *Castor angle.*, (2008). from http://en.wikipedia.org/wiki/Castor_angle

Yankee Publishing Inc. (2008). *Weather history for U.S. and Canada - the old farmer's almanac.*, 2008, from http://www.almanac.com/weatherhistory/index.php